NASA TECHNICAL NOTE

NASA TN D-1971

NASA TN D-1971

WIND-TUNNEL MEASUREMENTS OF PERFORMANCE, BLADE MOTIONS, AND BLADE AIR LOADS FOR TANDEM-ROTOR CONFIGURATIONS WITH AND WITHOUT OVERLAP

by Robert J. Huston
Langley Research Center
Langley Station, Hampton, Va.

NATIONAL AERONAUTICS AND SPACE ADMINISTRATION • WASHINGTON, D.C. • OCTOBER 1963

TECHNICAL NOTE D-1971

WIND-TUNNEL MEASUREMENTS OF PERFORMANCE, BLADE MOTIONS, AND BLADE AIR LOADS FOR TANDEM-ROTOR CONFIGURATIONS WITH AND WITHOUT OVERLAP

By Robert J. Huston

Langley Research Center
Langley Station, Hampton, Va.

NATIONAL AERONAUTICS AND SPACE ADMINISTRATION

NATIONAL AERONAUTICS AND SPACE ADMINISTRATION

TECHNICAL NOTE D-1971

WIND-TUNNEL MEASUREMENTS OF PERFORMANCE, BLADE MOTIONS, AND BLADE AIR LOADS FOR TANDEM-ROTOR CONFIGURATIONS WITH AND WITHOUT OVERLAP

By Robert J. Huston

SUMMARY

Results of an investigation in the Langley full-scale tunnel of the performance, blade motions, and instantaneous blade air loads are presented for two tandem-rotor configurations for a range of tip-speed ratios from 0 to 0.28. The results indicate that the induced power requirements of tandem-rotor helicopters are generally predictable on the basis of the span loading of the blade-swept area. Interference effects on lateral rotor tilt, at transition tip-speed ratios contribute yaw-trim changes with speed, aside from yaw-trim changes due to unequal torque to the front and rear rotors. Air-loads measurements on the rear rotors of the tandem configurations indicate that the vortices generated by the blades of the front rotor significantly affect the azimuth variation of the air loads on the rear rotor.

INTRODUCTION

The aerodynamic performance of a helicopter with tandem rotors is affected by mutual interference between rotors. This mutual interference results in an unequal distribution of specific power (horsepower per pound of thrust) between rotors and affects blade motions and blade loads.

Investigations of the power requirements of tandem rotors have been made for some specific conditions (refs. 1 to 4). The flow field of tandem rotors has been studied both theoretically and experimentally (refs. 4 to 8) with regard to predicting the interference power increments, blade motions, and stability effects. The results presented in this report are intended to supplement and extend the previously published information.

The present paper presents measured power and blade motions for both rotors of two tandem-rotor configurations (nonoverlapped and highly overlapped) over a range of tip-speed ratios from 0 to 0.28. Presented as an appendix are measured blade loads (at five spanwise stations on the rear rotor) for each of the conditions investigated.

SYMBOLS

a_0 constant term in Fourier series that expresses β; hence, rotor coning angle, deg

a_1 coefficient of $-\cos \psi$ in expression for β; hence, longitudinal tilt of rotor cone with respect to axis of no feathering, positive for rearward tilt, deg

a_2 coefficient of $-\cos 2\psi$ in expression for β; positive for upward flapping at $\psi = 90^\circ$ and 270°, deg

A_0 mean blade pitch angle at three-quarter radii, deg

b_1 coefficient of $-\sin \psi$ in expression for β; hence, lateral tilt of rotor cone with respect to axis of no feathering, positive for tilt toward advancing side, deg

b_2 coefficient of $-\sin 2\psi$ in expression for β; positive for upward flapping at $\psi = 0^\circ$ and 180°, deg

$C_{P,i}$ induced power coefficient, $\dfrac{\text{Induced power}}{\pi R^2 \rho (\Omega R)^3}$

C_T rotor thrust coefficient, $\dfrac{\text{Thrust}}{\pi R^2 \rho (\Omega R)^2}$

f equivalent flat-plate area representing propulsive force, based on unit coefficient, $\dfrac{\text{Propulsive force}}{\text{Free-stream dynamic pressure}}$, sq ft

l instantaneous section lift, lb

l_0 steady term in Fourier series for section lift, lb/in.

l_n coefficient of $\cos(n\psi + \Phi_n)$ in series for section lift, lb/in.

L instantaneous total blade lift, lb

L_0 steady term in Fourier series for total blade lift, lb

L_n coefficient of $\cos(n\psi + \Phi_n)$ in series for total blade lift, lb

n harmonic order

q free-stream dynamic pressure, lb/sq ft

r radial distance to blade element, ft

R blade radius measured from center of rotation, ft

V free-stream velocity, ft/sec

x distance between rotor shafts, ft

α rotor tip-path angle of attack; angle between projection in plane of symmetry of shaft axis and line perpendicular to flight path, positive rearward, deg

β blade flapping angle, with respect to axis of no feathering at particular azimuth position $\left(\beta = a_0 - a_1 \cos \psi - b_1 \sin \psi - a_2 \cos 2\psi - b_2 \sin 2\psi \ . \ . \ .\right)$

μ tip-speed ratio, $\frac{V \cos \alpha}{\Omega R}$

ρ mass density of air, slugs/cu ft

φ_n phase angle, with respect to zero azimuth, of amplitude of nth harmonic of section lift, deg

Φ_n phase angle, with respect to zero azimuth, of amplitude of nth harmonic of total blade lift, deg

χ wake skew angle, deg

ψ blade azimuth angle measured from downwind position in direction of rotation, deg

Ω rotor angular velocity, radians/sec

APPARATUS AND TESTS

The tests were conducted in the Langley full-scale tunnel which is fully described in reference 9.

The rotor configurations tested are shown in figure 1. The rotors, in all cases, were identical in planform with a radius of 7.625 feet, a constant chord of 1.16 feet, and an NACA 0012 airfoil section. The solidity was 0.0968. The blades were mounted on teetering hubs with zero built-in coning.

For the tandem configurations, the rotor blades were phased 90° apart. As viewed from above, the front rotor rotated clockwise and the rear rotor, counterclockwise. The spacing between hubs was varied to give an overlapped configuration ($x/R = 1.23$) and a nonoverlapped configuration ($x/R = 2.03$). A large ground board was mounted 2.04 radii below the rotors.

The thrust and torque of each rotor were measured independently by using strain-gage instrumentation located in each rotor support. Blade-flapping and blade-feathering motions, with respect to the rotor shaft, were sensed by strain gages and recorded on an oscillograph. Blade flapping with respect to axis of no feathering, was determined from these measurements. The overall accuracies of the data are estimated to be as follows:

Thrust	±9 lb or 2%
Torque	±4 ft-lb or 1%
Rotor tip speed	±1 fps or 0.2%
Flapping and feathering motions	±0.25 deg

All tests were conducted at a tip speed of approximately 500 fps, which corresponds to a tip Reynolds number of 3.7×10^6 in hovering. The rotors were always trimmed for zero flapping with respect to the shaft; thus both rotors of the tandem configurations were maintained in the same plane. The rotors on the tandem configurations were maintained at the same thrust. (Thrust, in this case, is defined as the force along the shaft axes.)

The measured power requirements of all rotors were adjusted to zero parasite drag on the basis of the measured longitudinal forces on the entire model; that is, the power was corrected for the longitudinal components of the rotor resultant force. These longitudinal, or propulsive forces, were corrected for rotor-off tares. The power correction was calculated as the power required to produce the propulsive force at the test airspeed. For the power requirements of the individual rotors of the tandem configurations, the power correction was equally divided between the two rotors.

Calculations of the jet-boundary effects, according to reference 10, indicated that only at the lowest forward-flight speed was the correction significant with respect to the accuracy of the data. At the lowest forward-flight speed ($\mu = 0.075$), the angle-of-attack correction for the nonoverlapped tandem was determined to be 0.8°. However, considering the individual rotors, the correction for the front rotor was 0.06° while that for the rear rotor was 1.4°. Because of this ambiguity, the data, even for this tip-speed ratio, are not corrected for jet-boundary effects.

The forward-flight results presented in this investigation were obtained by using the same tandem-rotor model as that used to obtain the hovering results of reference 2.

RESULTS AND DISCUSSION

The comparisons of performance and blade motions between single rotor and multirotor configurations, included in this paper, are intended to aid in identifying interference effects. It must be clearly understood that the comparison of the aerodynamic efficiency of the configurations, on the basis of the presented power-required curves, assumes a specific set of conditions. These conditions will not be compatible in a series of configurations (single and multirotor) all

designed for the same mission. The important consideration is that the ingredients of a power-required curve for the different configurations be shown to be predictable.

Power Requirements

The level-flight power requirements of the two tandem configurations and the single-rotor configuration are presented in figure 2 as nondimensional power-to-thrust ratio for a range of tip-speed ratios. (This ratio is, for the single rotor, the more familiar ratio of power coefficient to thrust coefficient.) The results presented are for zero parasite drag and at constant thrust per rotor ($C_T = 0.0043$ for each rotor, matched within the accuracy of the measurements), hence keeping the mean blade load constant throughout the speed range. The hovering performance and blade motions were obtained from reference 2.

Hovering.- It is noted that the nonoverlapped tandem ($x/R = 2.03$) requires the same specific power (power per pound of thrust) as the single rotor in hovering. In contrast, the overlapped tandem ($x/R = 1.23$), at the same mean blade load, requires about 8 percent more total power, which (assuming all the increase to be in the induced portion of the power) corresponds to about 13 percent more induced power. Of this 13 percent, about $7\frac{1}{2}$ percent can be attributed to the increased disk loading based on the swept area of the overlapped tandem. The remaining $5\frac{1}{2}$-percent increase in induced power must be attributed to flow interference within the overlapped area. Had the disk loading been equal to that of the nonoverlapped tandem, this $5\frac{1}{2}$-percent increase in induced power would have represented a total power increase of about $3\frac{1}{2}$ percent. It is shown in reference 2 that the twin-rotor hovering-power requirements (including the effect of interference) can be adequately predicted by either the methods of reference 4 or 5.

Forward flight.- In forward flight, the specific power required by the rear rotor of both configurations exhibits a substantial increase between hovering and a tip-speed ratio of 0.075. This increase results in the total specific power, at this tip-speed ratio, being nearly the same as that in hovering. Another interesting result is that the total specific power of the overlapped configuration ($x/R = 1.23$), at the higher tip-speed ratios, becomes nearly equal to (actually slightly less than) the specific power requirements of the nonoverlapped configuration ($x/R = 2.03$). Considering that the swept-area disk loading of the overlapped configuration is 15.6 percent greater than that of the nonoverlapped configuration (since front and rear rotors carried the same thrust in all cases), this fact appears to contrast with normal expectations. The flow studies of reference 6 indicate that the explanation for these results appears to lie in the flow field experienced by the rear rotor of tandem configurations. This flow field apparently results in an increase in the induced power requirements on the rear rotor.

One method suggested for predicting the induced power requirements of the rear rotor of a tandem is to determine the mean value of the induced velocity of the front rotor acting upon the rear rotor (from charts such as those given in ref. 11), and to add this velocity to the rear-rotor induced velocity to determine the induced-plus-interference power requirements. The results of such a computation are given in figure 3(a) for the rear rotor of the nonoverlapped configuration. The computations were made with due regard for the effect of the interference velocity on the rear-rotor induced velocity. The experimental induced-power data (shown by the symbols) were determined by assigning the tandem configurations the same profile power-to-thrust losses as the single rotor for, logically, any real change in the profile power of one rotor due to the proximity of a second rotor should be attributed to interference. It is seen from figure 3(a) that the computation seriously underestimates the actual rear-rotor induced-plus-interference power requirements.

Another method is suggested by the theory that predicts the induced power requirements of a single-rotor helicopter. The induced power requirements of a single-rotor helicopter can be reduced to

$$\frac{C_{p,i}}{C_T} = \frac{\mu(\text{Lift})}{\pi q(\text{Span})^2} \tag{1}$$

for certain limits of angle of attack and tip-speed ratio. The same result is obtained from simple wing theory by considering the span loading. This result suggests a comparison of the measured induced and interference power to an induced power calculated on the basis of the span loading of the configuration. Inasmuch as the exact expression for the induced power of a single rotor machine is:

$$\frac{C_{p,i}}{C_T} = \frac{\mu(\text{Lift})}{\pi q(\text{Span})^2}\left(\frac{\sin \chi}{\cos^3 \alpha}\right) \tag{2}$$

it appears that equation (2) is a more useful equation for general use.

The results of calculations made by using equation (2) to predict the induced power requirements are given in figure 3(b) for the two tandem-rotor configurations. Inasmuch as the lift and dynamic pressure are the same for both configurations, at the same tip-speed ratio, the two configurations have the same calculated induced power. The experimental data agree reasonably well with the calculated performance. The results indicate that the power requirements of tandem-rotor helicopters, with longitudinal spacing between the two limits of this investigation, can be adequately predicted by this method.

The distribution of power between the front and rear rotors appears to be predictable by assigning the front rotor the induced power requirements of a single rotor and assigning the rear-rotor induced power requirements three times that of a single rotor (fig. 3(a)). The average induced power of the tandem configurations, with such a division of power, is as predicted by the span loading.

Blade Motions

Measured first-harmonic blade flapping, over the tip-speed range, is presented in figure 4. There appears to be little net interference effect between rotors, or effect of longitudinal spacing, on the longitudinal tilt (a_1 flapping) of the tandem configurations. The longitudinal tilt of the tandem-rotor configurations does show a slightly steeper slope with tip-speed ratio than that of the single rotor.

The significant interference effects on lateral tilt (b_1 flapping) of the rotors on the tandem configuration occur below a tip-speed ratio of 0.2. This can be noted by comparing the front and rear rotor flapping of the tandem configurations with that of the single rotor. The b_1 flapping of the single rotor is the result of blade coning (involving blade bending) and the self-induced time-average longitudinal variation of induced velocity across the rotor.

The b_1 flapping of the front rotor of the nonoverlapped tandem is only slightly affected by the rear rotor. This effect is greatest in hovering and at tip-speed ratios above transition speeds (μ = 0.04 to 0.08). However, the front rotor lateral flapping of the overlapped tandem is substantially larger than that of the single rotor, below a tip-speed ratio of 0.2, and has approximately the same magnitude as the b_1 flapping of the nonoverlapped tandem at the higher tip-speed ratios. The lateral flapping of the rear rotors of both tandems is reduced substantially, at low tip-speed ratios, from that of the single rotor. The primary result of the tandem-rotor interference effects on lateral tilt is to contribute changes in yaw trim with speed, aside from yaw-trim changes due to unequal torque to front and rear rotors.

Three sources for the interference effects on b_1 flapping are possible. First is the interference contribution to the time-average longitudinal variation of induced velocity across the rotor. Estimates of this effect, based on the charts of reference 11, indicate that this effect increases b_1 flapping for the front rotor of the overlapped tandem, and decreases the b_1 flapping for the rear rotors of the tandem configurations. In addition, the predicted b_1 flapping, due to the longitudinal variation of induced velocity, would be a maximum in the transition region (μ = 0.04 to 0.08) with negligible lateral tilt contributed at the higher tip-speed ratios. However, while the predicted trends agree with the trends of the measured data, the magnitude of the predicted b_1 flapping is inadequate to account for the flapping interference.

The second and third sources of the interference effects on the lateral tilt of the tandem rotors are the result of interference effects on steady-state blade coning (a_0) and second harmonic flapping (a_2). (Both a_0 and a_2, for the teetering rotor used in this investigation, occur as blade bending.) Changes in a_0 and a_2 on the tandem rotors, differing from those resulting on the single rotor, result in an interference-induced change in the lateral tilt of the rotors. The effect of a_0 and a_2 on lateral tilt increases with tip-speed ratio but would be negligible in hovering. Because the large interference effects on lateral flapping appear in hovering and throughout the transition region (where

the effect of a_0 and a_2 on b_1 is small), the principal source of the effect is attributed to the interference contribution to the time-average longitudinal variation of induced velocity across the rotors.

The blade collective pitch required to obtain constant thrust per rotor is given in figure 5 for all configurations investigated. The corresponding rotor tip-path-plane angle of attack and resulting total propulsive force, in square feet of drag area, are also given in figure 5. The propulsive force of the tandem configurations would be expected to be twice that of the single rotor; however, the data of figure 5 indicate that the procedure used in setting the test conditions resulted in somewhat greater than twice the propulsive force.

Air Loads

The rear-rotor air loads, for all conditions previously discussed, are presented in the appendix. The air-loads data are included to provide designers of tandem-rotor helicopters with quantitative measurements of the exciting forces on a rotor blade operating in the wake of an adjacent rotor. This information is required for a rational analysis of sources of vibration excitation, thereby leading to a structural design free of dynamic and fatigue problems.

The pressure measurements indicate an additional complication to the problem of predicting theoretical air loads for tandem-rotor helicopters. It is shown, experimentally and theoretically in references 12 and 13, that the variation of air loads around the azimuth, for a single-rotor helicopter, is affected by the relative location of the blades with respect to previously generated vortices from adjacent blades. Limited examination, in the light of the results of reference 12, indicates that rear-rotor air loads are more strongly affected by vortices generated by the front rotor than by vortices generated by the adjacent blade of the same rotor, at least for the conditions of this investigation. The effect of the forward rotor can be determined by comparing, at the same tip-speed ratio, the single-rotor air loads of reference 14 with the air loads of this investigation. This effect, as a function of the amount of overlap, can be studied from comparisons of the section loading, blade loading, and the harmonic analysis of the air loads of the two tandem configurations.

CONCLUDING REMARKS

The results of a wind-tunnel investigation with two tandem-rotor configurations, with equal thrust per rotor, indicate that the induced power requirements of tandem-rotor helicopters are generally predictable on the basis of the span loading of the configuration.

The effect of mutual interference on blade flapping is largest at high tip-speed ratios for longitudinal tilt but is largest at transition tip-speed ratios for lateral tilt. The interference effects on lateral tilt will contribute yaw-trim changes with speed, aside from yaw-trim changes due to unequal torque to the front and rear rotors.

The results of the air-loads measurements on the rear rotor of the tandem configurations indicate that the vortices generated by the blades of the front rotor significantly affect the azimuth variation of the rear-rotor air loads.

Langley Research Center,
National Aeronautics and Space Administration,
Langley Station, Hampton, Va., July 10, 1963.

APPENDIX

AERODYNAMIC LOADING ON THE REAR ROTOR OF THE TANDEM CONFIGURATIONS

EQUIPMENT

The equipment used in this investigation to measure the azimuth variation of the air loads is essentially the same as that used in references 14 and 15. The equipment is described in detail in the aforementioned references but is reviewed briefly here.

Rotor Blades

One blade of the two-bladed teetering rotor is instrumented to measure differential pressures between the upper and lower surfaces at 10 chordwise locations at each of 5 spanwise stations. Figure 6 is a sketch of the instrumented blade showing the principal dimensions and the pressure-orifice locations.

Pressure-Pickup Installation

The pressure pickups used are miniature electrical pressure gages (ref. 16) of a variable-inductance type. The overall frequency response for the pressure pickup-recording oscillograph system was determined to be flat to about 60 cycles per second, the sixth harmonic of rotor speed. There was a time lag in the system, independent of frequency, which amounted to 8° of azimuth.

Due to the limited number of sliprings available, simultaneous readings of all 50 pressure pickups were not possible. Therefore, with the use of a stepping switch, stations 1, 2, and 3 (at $r/R = 0.31$, 0.56, and 0.75, respectively) were recorded and then stations 3, 4, and 5 (at $r/R = 0.75$, 0.85, and 0.95, respectively) were recorded. Station 3 was thus recorded twice at each test condition as a check of the repeatability of the data and the compatibility of the inboard pressure measurements with the outboard pressure measurements. The second measurement of station 3 air loads is presented in the data as a flagged symbol.

TEST PROCEDURE AND DATA REDUCTION

Test conditions were set to the desired thrust per rotor and zero flapping, with respect to the rotor shaft, with model tare forces being taken into account. The shaft angles were predetermined for each test point in attempting to hold a constant representative flat-plate area.

The output of each pressure gage was recorded on an oscillograph and read at 48 points per revolution. The readings for corresponding points for

10 revolutions were averaged and recorded on automatic punch cards. Automatic computing machines then converted this average to a pressure differential and summed the output at each spanwise station to give the section loading. The section loading was then harmonically analyzed to give the amplitude and phase angle, with respect to zero azimuth, of each harmonic of loading. A correction for the time lag in the instrumentation described previously was then introduced. The values of section loading, when plotted against radius, were manually integrated to give total blade lift at 24 points per revolution. These data were then harmonically analyzed to give the amplitude and phase angle of each harmonic of total blade lift.

PRESENTATION OF RESULTS

Harmonic Analysis

The results of the harmonic analysis of the section blade lift and the total blade lift are given in tables I to IV. The section lift is presented as the first six harmonic terms in the harmonic series

$$l = l_0 + \sum_{n=1}^{n} l_n \cos(n\psi + \varphi_n)$$

The total blade lift is presented as the first six harmonic terms in the harmonic series

$$L = L_0 + \sum_{n=1}^{n} L_n \cos(n\psi + \Phi_n)$$

In order to make comparisons between different span stations and/or test conditions of the magnitude of the harmonics, the section lift is presented as a percentage of the steady-state mean blade loading $\left(\text{percent } L_0/R\right)$ as determined from the pressure measurements. In a similar manner, the harmonics of the total blade load are presented as a percent of the steady-state blade lift $\left(\text{percent } L_0\right)$.

Section Loading

The variation of section aerodynamic loading with azimuth is presented in figures 7 to 11 for the five radial stations. The data are presented in the following order:

Figure

Total Blade Lift

The variation of total blade lift with azimuth is presented in figures 12 to 16 in the following order:

Figure

REFERENCES

1. Dingeldein, Richard C.: Wind-Tunnel Studies of the Performance of Multirotor Configurations. NACA TN 3236, 1954.

2. Sweet, George E.: Hovering Measurements for Twin-Rotor Configurations With and Without Overlap. NASA TN D-534, 1960.

3. Halliday, A. S., and Cox, D. K.: Wind Tunnel Experiments on a Model of a Tandem Rotor Helicopter. C. P. No. 517, British A.R.C., 1961.

4. Stepniewski, W. Z.: A Simplified Approach to the Aerodynamic Rotor Interference of Tandem Helicopters. Proc. Second Annual Western Forum, American Helicopter Soc., Inc., Sept. 21 and 22, 1955, pp. 71-90.

5. Heyson, Harry H.: An Evaluation of Linearized Vortex Theory As Applied to Single and Multiple Rotors Hovering In and Out of Ground Effect. NASA TN D-43, 1959.

6. Heyson, Harry H.: Preliminary Results From Flow-Field Measurements Around Single and Tandem Rotors in the Langley Full-Scale Tunnel. NACA TN 3242, 1954.

7. Cheeseman, I. C.: A Method of Calculating the Effect of One Helicopter Rotor Upon Another. C. P. No. 406, British A.R.C., 1958.

8. Bramwell, A. R. S.: Part I - The Longitudinal Stability and Control of the Tandem-Rotor Helicopter. R. & M. No. 3223, British A.R.C., 1961, pp. 1-69.

9. DeFrance, Smith J.: The N.A.C.A. Full-Scale Wind Tunnel. NACA Rep. 459, 1933.

10. Heyson, Harry H.: Linearized Theory of Wind-Tunnel Jet-Boundary Corrections and Ground Effect for VTOL-STOL Aircraft. NASA TR R-124, 1962.

11. Jewel, Joseph W., Jr., and Heyson, Harry H.: Charts of the Induced Velocities Near a Lifting Rotor. NASA MEMO 4-15-59L, 1959.

12. Scheiman, James, and Ludi, LeRoy H.: Qualitative Evaluation of Effect of Helicopter Rotor-Blade Tip Vortex on Blade Airloads. NASA TN D-1637, 1963.

13. Castles, Walter, Jr., and Durham, Howard L., Jr.: Tables for Computing the Instantaneous Velocities Induced at the Blade Axes of a Lifting Rotor in Forward Flight by the Skewed Helical Wake Vortices and a Method for Calculating the Resultant Blade Air Loads. Contract No. Nonr 991(05), Eng. Exp. Station, Ga. Inst. Tech., June 1962.

14. Rabbott, John P., Jr., and Churchill, Gary B.: Experimental Investigation of the Aerodynamic Loading on a Helicopter Rotor Blade in Forward Flight. NACA RM L56I07, 1956.

15. Rabbott, John P., Jr.: Static-Thrust Measurements of the Aerodynamic Loading on a Helicopter Rotor Blade. NACA TN 3688, 1956.

16. Patterson, John L.: A Miniature Electrical Pressure Gage Utilizing a Stretched Flat Diaphragm. NACA TN 2659, 1952.

TABLE I.- HARMONIC ANALYSIS OF MEASURED SECTION LOADING

AND TOTAL BLADE LIFT IN HOVERING

n	r/R = 0.31		r/R = 0.56		r/R = 0.75		r/R = 0.75 (repeat)		r/R = 0.85		r/R = 0.95		Total blade lift	
	l_n, percent $\frac{L_o}{R}$	ϕ_n, deg	l_n, percent $\frac{L_o}{R}$	ϕ_n, deg	l_n, percent $\frac{L_o}{R}$	ϕ_n, deg	l_n, percent $\frac{L_o}{R}$	ϕ_n, deg	l_n, percent $\frac{L_o}{R}$	ϕ_n, deg	l_n, percent $\frac{L_o}{R}$	ϕ_n, deg	L_n, percent L_o	Φ_n, deg
x/R = 2.03; L_o = 168.4 lb														
0	28.5	---	88.5	---	167.9	---	164.4	---	252.2	---	274.0	---	100.0	---
1	4.7	195	7.3	189	8.5	174	7.3	173	5.9	15	37.7	338	.5	245
2	3.8	34	6.2	68	6.3	96	7.7	87	12.5	111	26.3	106	7.8	88
3	3.1	312	2.0	329	5.6	13	6.0	340	18.7	336	14.1	338	6.1	338
4	1.1	148	1.1	7	2.8	353	.4	147	5.4	182	9.4	182	.6	160
5	2.0	56	.6	34	2.2	307	1.5	299	3.9	5	9.2	72	1.6	33
6	.6	290	.6	130	.2	54	2.7	60	4.8	51	5.2	140	1.7	136
x/R = 2.03; L_o = 232.0 lb														
0	27.2	---	96.0	---	180.1	---	176.9	---	249.6	---	246.2	---	100.0	---
1	5.4	203	9.1	205	8.3	171	3.6	116	7.1	334	16.7	319	3.9	221
2	2.1	99	5.2	137	6.6	144	6.0	143	9.3	156	12.5	139	3.3	146
3	1.3	5	2.8	313	7.9	333	5.8	328	17.0	329	16.5	309	5.6	319
4	.5	218	2.2	167	2.9	132	1.9	342	2.1	218	8.3	171	1.6	173
5	1.3	79	1.7	62	.5	260	1.0	45	5.7	13	10.7	17	1.2	22
6	.6	302	.7	189	2.6	335	2.0	19	2.1	3	.9	125	.7	265
x/R = 1.23; L_o = 131.2 lb														
0	20.6	---	85.8	---	192.1	---	191.6	---	299.2	---			100.0	---
1	9.5	37	8.3	55	21.0	169	15.6	169	5.0	161			7.3	94
2	16.1	137	16.6	152	27.8	146	24.9	127	44.0	123			16.5	139
3	11.5	299	9.5	307	5.5	6	6.9	46	16.5	28			6.3	344
4	6.1	88	4.6	349	17.6	335	20.4	329	32.4	312			8.1	329
5	4.4	230	6.2	126	23.2	138	18.8	139	35.7	119			11.6	141
6	1.4	346	4.2	279	12.3	295	13.1	300	23.9	299			7.8	312
x/R = 1.23; L_o = 185.1 lb														
0	23.2	---	78.9	---	200.8	---	198.4	---	281.4	---			100.0	---
1	6.4	48	6.8	65	18.5	164	17.5	183	8.1	154			6.1	108
2	12.7	146	15.4	156	22.2	154	28.0	152	34.5	149			15.2	148
3	9.6	310	7.7	304	11.0	338	1.5	332	3.3	259			4.6	300
4	3.7	119	2.4	321	15.8	305	16.1	341	18.2	338			6.1	331
5	1.2	190	4.4	110	20.4	117	15.6	129	28.0	111			8.7	115
6	2.7	349	3.4	297	12.2	315	9.9	283	16.5	264			3.8	280

TABLE II.- HARMONIC ANALYSIS OF MEASURED SECTION LOADING

AND TOTAL BLADE LIFT IN FORWARD FLIGHT

[x/R = 2.03]

n	r/R = 0.31		r/R = 0.56		r/R = 0.75		r/R = 0.75 (repeat)		r/R = 0.85		r/R = 0.95		Total blade lift	
	l_n, percent $\frac{L_o}{R}$	ϕ_n, deg	l_n, percent $\frac{L_o}{R}$	ϕ_n, deg	l_n, percent $\frac{L_o}{R}$	ϕ_n, deg	l_n, percent $\frac{L_o}{R}$	ϕ_n, deg	l_n, percent $\frac{L_o}{R}$	ϕ_n, deg	l_n, percent $\frac{L_o}{R}$	ϕ_n, deg	L_n, percent L_o	Φ_n, deg
	$\mu = 0.075$; $L_o = 181.2$ lb													
0	14.3	---	103.3	---	212.5	---	206.9	---	262.7	---			100.0	---
1	17.9	356	20.0	16	4.6	271	4.0	281	13.4	205			7.8	349
2	7.9	35	12.9	13	16.6	13	16.7	27	19.4	75			8.4	31
3	4.3	261	.5	181	9.8	20	7.4	27	10.6	22			1.7	359
4	3.6	153	3.4	159	3.6	278	4.6	252	13.0	273			3.3	238
5	1.9	50	1.5	188	3.4	197	3.3	202	1.2	146			1.9	164
6	1.4	265	.8	142	5.3	81	6.1	97	9.9	94			2.0	58
	$\mu = 0.10$; $L_o = 183.6$ lb													
0	19.2	---	104.9	---	209.9	---	210.1	---	277.3	---	160.1	---	100.0	---
1	18.7	21	28.2	13	1.6	56	1.1	140	13.6	190	23.2	228	8.2	3
2	9.5	26	26.3	359	34.8	355	36.6	350	13.0	19	45.1	101	15.4	17
3	.8	191	3.8	217	5.9	9	10.8	7	18.4	4	8.0	285	2.4	341
4	1.9	145	.6	276	6.0	329	5.7	324	22.0	306	16.7	305	4.2	305
5	1.0	76	1.8	143	4.4	222	5.7	258	2.5	219	12.3	128	1.3	96
6	.7	161	1.7	185	8.6	117	8.0	102	18.8	98	22.6	140	3.6	123
	$\mu = 0.14$; $L_o = 171.5$ lb													
0	17.7	---	120.0	---	228.6	---	232.8	---	281.6	---	80.0	---	100.0	---
1	17.2	5	24.1	14	12.3	58	8.2	78	6.9	274	24.9	256	8.8	2
2	15.3	8	34.4	348	48.8	333	52.0	335	15.0	349	52.0	121	17.5	354
3	1.2	316	6.5	317	27.1	331	24.9	325	39.8	342	13.9	311	10.0	325
4	2.2	81	7.8	255	8.1	238	9.1	286	18.5	282	32.6	210	5.6	236
5	4.2	30	.7	40	6.3	217	8.9	224	19.0	228	17.3	211	5.3	236
6	1.2	23	3.5	227	11.4	255	9.0	265	15.1	118	41.2	158	5.4	156
	$\mu = 0.19$; $L_o = 195.8$ lb													
0	22.0	---	108.9	---	196.1	---	201.6	---	243.4	---	205.7	---	100.0	---
1	16.9	40	17.3	50	9.2	297	5.8	318	27.9	330	18.4	289	8.3	13
2	10.1	358	46.2	357	62.6	342	55.3	346	27.6	350	11.0	240	23.3	353
3	6.3	132	15.7	62	33.1	16	22.6	3	39.4	341	32.3	348	13.0	15
4	1.7	118	2.0	124	7.3	14	9.6	325	6.1	349	14.4	307	1.8	297
5	1.6	98	1.7	142	.8	44	2.4	195	17.0	288	15.1	270	1.4	281
6	1.7	78	1.0	58	9.3	143	8.4	179	22.6	124	20.8	116	4.7	120
	$\mu = 0.24$; $L_o = 189.3$ lb													
0	19.0	---	117.3	---	189.8	---	197.7	---	253.1	---	205.8	---	100.0	---
1	10.6	77	19.0	101	30.6	331	27.9	353	53.6	333	29.9	298	10.1	6
2	12.6	342	50.1	344	52.5	345	45.5	344	32.6	5	14.2	50	24.3	348
3	12.2	140	15.8	103	32.1	14	27.3	16	38.2	349	30.1	346	9.0	25
4	2.4	138	3.0	255	9.1	110	6.7	136	10.8	108	.6	275	3.1	98
5	5.2	62	2.3	104	15.0	331	15.9	334	19.7	314	14.8	293	5.2	328
6	3.1	117	3.7	189	19.0	149	21.9	143	17.1	133	6.4	123	5.2	138
	$\mu = 0.28$; $L_o = 176.5$ lb													
0	17.3	---	127.9	---	203.0	---	195.0	---	262.9	---	153.6	---	100.0	---
1	11.9	108	28.2	111	48.5	336	42.8	338	58.0	335	9.1	300	10.5	21
2	25.6	326	65.7	327	70.6	330	50.9	318	39.7	324	15.1	41	32.9	329
3	17.9	131	18.1	81	50.5	353	52.0	323	69.3	314	40.7	310	13.8	348
4	4.9	183	9.8	180	22.9	124	14.0	81	18.2	71	8.8	73	5.8	116
5	5.0	47	4.1	203	15.6	333	13.4	311	16.8	300	3.6	233	2.8	309
6	4.4	91	4.5	209	14.8	133	9.2	140	5.8	159	11.7	224	3.0	154

TABLE III.- HARMONIC ANALYSIS OF MEASURED SECTION LOADING AND TOTAL BLADE LIFT IN FORWARD FLIGHT FOR SPECIAL CONDITIONS

[x/R = 2.03; μ = 0.19]

n	r/R = 0.31		r/R = 0.56		r/R = 0.75		r/R = 0.75 (repeat)		r/R = 0.85		r/R = 0.95		Total blade lift	
	l_n, percent $\frac{L_o}{R}$	ϕ_n, deg	l_n, percent $\frac{L_o}{R}$	ϕ_n, deg	l_n, percent $\frac{L_o}{R}$	ϕ_n, deg	l_n, percent $\frac{L_o}{R}$	ϕ_n, deg	l_n, percent $\frac{L_o}{R}$	ϕ_n, deg	l_n, percent $\frac{L_o}{R}$	ϕ_n, deg	L_n, percent L_o	Φ_n, deg
Disk loading = 6 lb/sq ft; L_o = 234.9 lb														
0	23.1	---	118.1	---	212.1	---	207.6	---	233.7	---	187.2	---	100.0	---
1	16.4	36	12.3	41	6.1	337	5.3	327	26.7	340	13.0	293	10.2	7
2	13.3	349	47.3	349	48.9	335	43.0	341	18.8	343	10.7	129	22.4	346
3	7.0	121	10.0	38	26.7	348	20.3	345	34.1	331	28.1	337	9.4	357
4	2.8	130	2.3	322	10.8	330	5.8	334	2.2	134	6.4	286	1.4	334
5	2.6	133	1.3	217	1.9	312	3.3	174	14.6	283	14.6	279	2.0	263
6	1.5	113	2.0	332	9.2	192	8.9	187	17.3	125	15.1	118	3.7	151
Disk loading = 3 lb/sq ft; L_o = 100.5 lb														
0	4.1	---	128.4	---	224.6	---			277.1	---	109.0	---	100.0	---
1	13.0	355	15.7	71	2.1	224			36.9	322	14.0	28	8.7	353
2	16.5	24	47.3	359	59.1	348			43.8	23	61.1	53	30.2	9
3	8.3	134	14.7	72	30.8	25			34.1	10	31.1	12	14.2	40
4	6.1	107	2.6	170	9.8	296			13.3	135	10.5	219	3.4	186
5	5.3	68	2.5	82	5.3	181			37.4	283	6.5	271	3.4	288
6	2.7	42	2.5	21	10.5	170			5.4	127	18.3	139	4.2	129
Yaw angle = 10°; L_o = 192.3 lb														
0	18.4	---	107.4	---	208.7	---	210.2	---	257.7	---	204.7	---	100.0	---
1	19.3	62	15.5	75	7.2	257	8.4	303	21.2	353	3.2	351	9.7	45
2	8.2	39	24.1	38	16.1	65	23.7	58	26.6	114	31.5	121	12.4	65
3	7.2	186	15.7	84	48.5	59	47.8	77	48.7	35	37.5	23	17.0	58
4	2.8	168	6.2	314	18.3	318	20.0	297	5.1	210	7.8	173	4.0	271
5	2.7	184	4.2	218	8.8	174	3.6	174	12.2	323	14.9	326	1.9	255
6	2.2	190	6.3	141	10.0	228	9.0	233	11.8	197	10.5	186	4.8	185

TABLE IV.- HARMONIC ANALYSIS OF MEASURED SECTION LOADING

AND TOTAL BLADE LIFT IN FORWARD FLIGHT

[x/R = 1.23]

n	r/R = 0.31		r/R = 0.56		r/R = 0.75		r/R = 0.75 (repeat)		r/R = 0.85		r/R = 0.95		Total blade lift	
	l_n, percent $\frac{L_o}{R}$	ϕ_n, deg	l_n, percent $\frac{L_o}{R}$	ϕ_n, deg	l_n, percent $\frac{L_o}{R}$	ϕ_n, deg	l_n, percent $\frac{L_o}{R}$	ϕ_n, deg	l_n, percent $\frac{L_o}{R}$	ϕ_n, deg	l_n, percent $\frac{L_o}{R}$	ϕ_n, deg	L_n, percent L_o	Φ_n, deg
$\mu = 0.075$; $L_o = 167.3$ lb														
0	10.9	---	111.1	---	225.1	---	227.4	---	417.5	---	89.3	---	100.0	---
1	36.2	8	36.5	10	3.7	306	6.2	282	18.4	214	17.7	80	29.2	18
2	3.4	69	20.8	350	48.6	335	48.8	331	24.8	19	12.8	354	15.6	353
3	5.3	254	9.0	196	31.5	148	28.5	142	95.3	149	43.0	148	15.8	196
4	3.8	57	10.6	335	25.1	330	21.9	338	137.8	311	59.5	313	10.9	348
5	4.0	150	3.2	140	4.8	157	7.0	153	31.1	131	7.1	96	5.6	338
6	3.4	252	4.7	216	6.8	192	6.6	185	38.6	132	18.9	108	6.5	162
$\mu = 0.10$; $L_o = 182.7$ lb														
0	11.6	---	107.5	---	200.2	---	203.8	---	276.6	---	214.3	---	100.0	---
1	33.5	13	38.5	9	1.6	0	2.1	322	12.8	215	15.3	189	16.2	8
2	8.8	40	34.1	347	73.3	336	71.2	35	51.9	325	12.4	35	25.1	346
3	2.6	336	6.3	205	23.4	145	24.8	142	34.0	119	56.3	143	10.3	149
4	4.7	39	9.6	325	23.0	330	18.8	333	41.1	312	103.4	306	18.1	328
5	5.1	131	2.9	113	6.6	147	7.6	139	10.0	179	13.3	105	4.0	91
6	3.6	210	3.9	203	7.2	210	7.1	203	18.2	121	31.8	114	5.9	140
$\mu = 0.14$; $L_o = 178.4$ lb														
0	18.5	---	123.5	---	217.5	---	216.7	---	272.7	---	146.9	---	100.0	---
1	30.9	21	34.4	21	11.4	14	10.6	5	13.4	250	7.2	350	14.8	16
2	12.9	47	43.4	253	79.7	339	80.9	341	63.6	334	16.8	52	31.1	351
3	.5	14	7.2	186	5.2	152	8.2	138	26.4	88	49.6	147	10.3	134
4	7.9	32	15.8	315	27.5	293	26.3	296	57.7	301	139.7	307	26.8	308
5	7.0	99	4.4	100	10.5	100	8.5	96	13.7	151	23.4	160	6.2	110
6	3.3	178	6.4	183	11.3	195	13.0	204	27.5	157	43.6	116	11.4	155
$\mu = 0.19$; $L_o = 194.0$ lb														
0	15.7	---	113.9	---	198.8	---	197.0	---	248.8	---	215.8	---	100.0	---
1	25.1	24	22.1	47	9.5	334	10.0	352	8.2	340	13.0	215	10.5	35
2	8.9	36	48.2	347	64.1	330	58.9	331	55.3	326	19.0	332	26.8	337
3	2.7	184	10.7	108	8.0	62	5.6	99	5.6	112	17.0	117	5.2	156
4	8.4	357	12.6	317	26.2	297	25.2	303	34.7	296	57.6	304	16.3	315
5	9.0	74	10.8	53	9.2	82	8.1	97	8.2	103	9.5	177	7.4	98
6	4.5	148	7.8	153	15.4	167	15.2	177	16.4	177	18.4	153	8.0	167
$\mu = 0.24$; $L_o = 194.6$ lb														
0	17.3	---	116.2	---	198.4	---	200.0	---	248.9	---	200.0	---	100.0	---
1	21.0	30	26.6	70	17.2	329	15.6	344	23.2	327	7.5	298	12.6	35
2	7.8	21	49.9	350	60.8	344	58.8	342	56.3	343	31.1	359	28.1	344
3	11.7	194	18.2	113	20.4	94	20.6	93	14.4	85	17.2	132	8.0	120
4	11.7	340	12.4	309	19.9	332	15.3	329	17.7	324	37.8	315	13.3	328
5	10.3	68	15.1	44	12.6	66	12.4	65	8.8	105	10.2	127	9.5	80
6	6.1	139	12.2	132	21.3	161	22.6	158	17.6	153	14.3	164	9.0	159
$\mu = 0.28$; $L_o = 165.4$ lb														
0	9.9	---	130.5	---	236.6	---	214.2	---	278.3	---	110.1	---	100.0	---
1	25.3	43	33.8	70	33.2	343	29.1	338	41.1	322	43.0	336	21.2	20
2	22.4	324	67.3	340	92.1	343	90.6	338	82.9	336	57.5	1	46.5	340
3	28.8	160	20.1	115	20.7	80	15.3	82	10.2	100	49.1	171	15.2	136
4	8.5	326	17.4	282	16.6	345	16.6	336	22.6	326	81.5	319	17.4	322
5	12.7	18	16.2	17	12.7	54	15.1	33	12.3	47	5.5	99	7.2	37
6	13.3	155	14.3	129	16.0	144	15.9	123	12.2	119	22.8	93	9.3	143

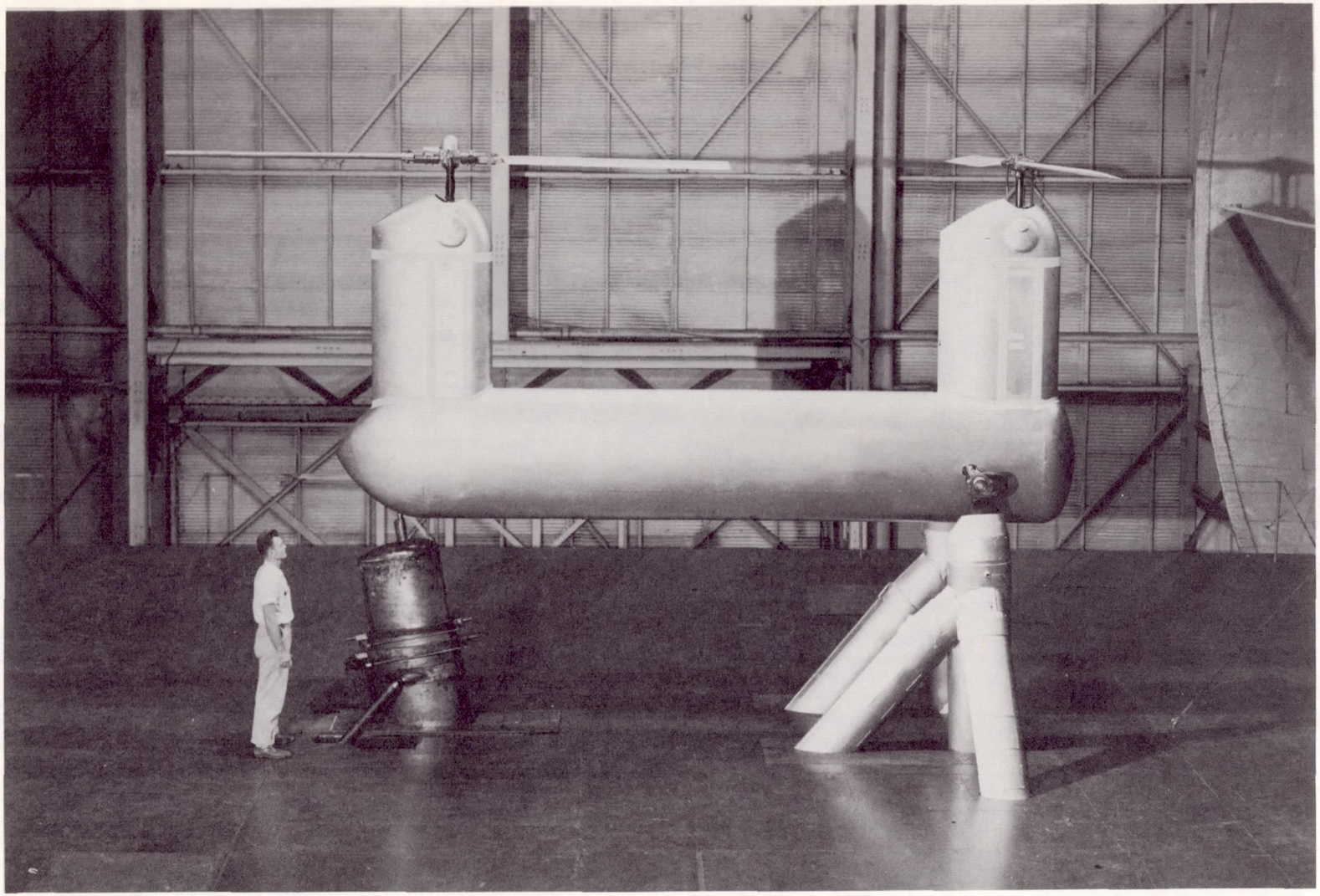

(a) Nonoverlapped tandem. x/R = 2.03. L-95189

Figure 1.- Helicopter model in Langley full-scale tunnel.

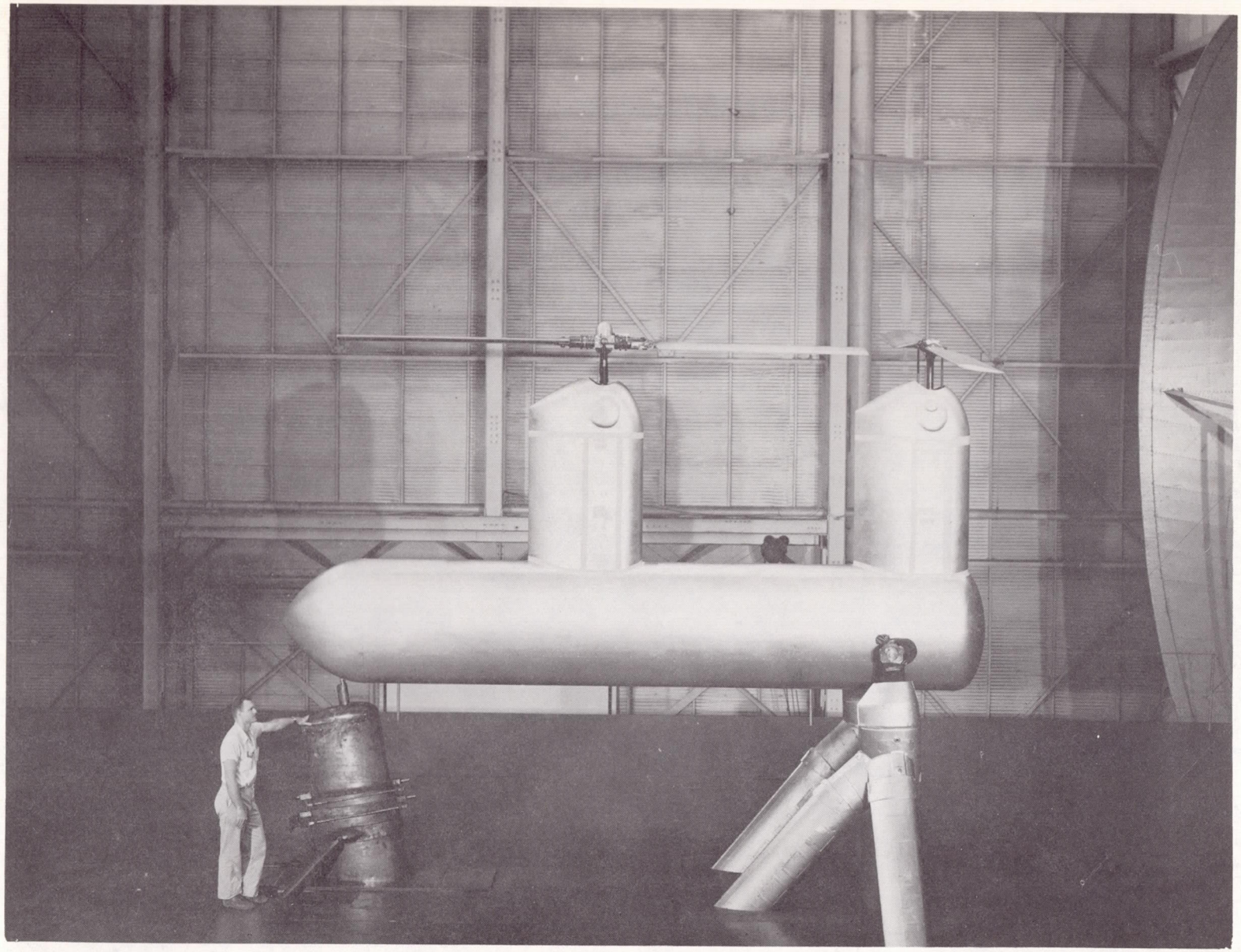

(b) Overlapped tandem. x/R = 1.23. L-95399

Figure 1.- Continued.

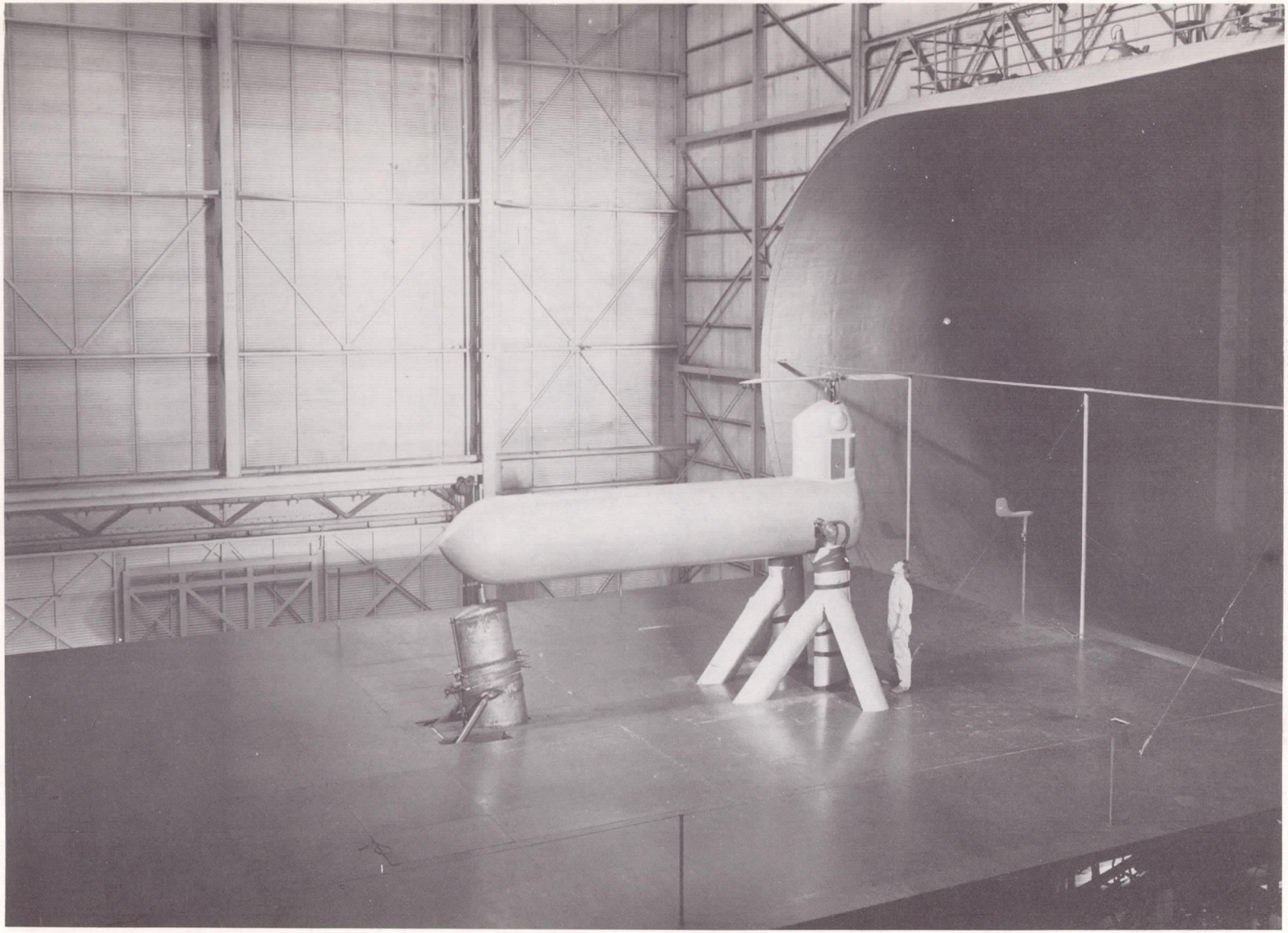

(c) Single rotor. L-57-2389

Figure 1.- Concluded.

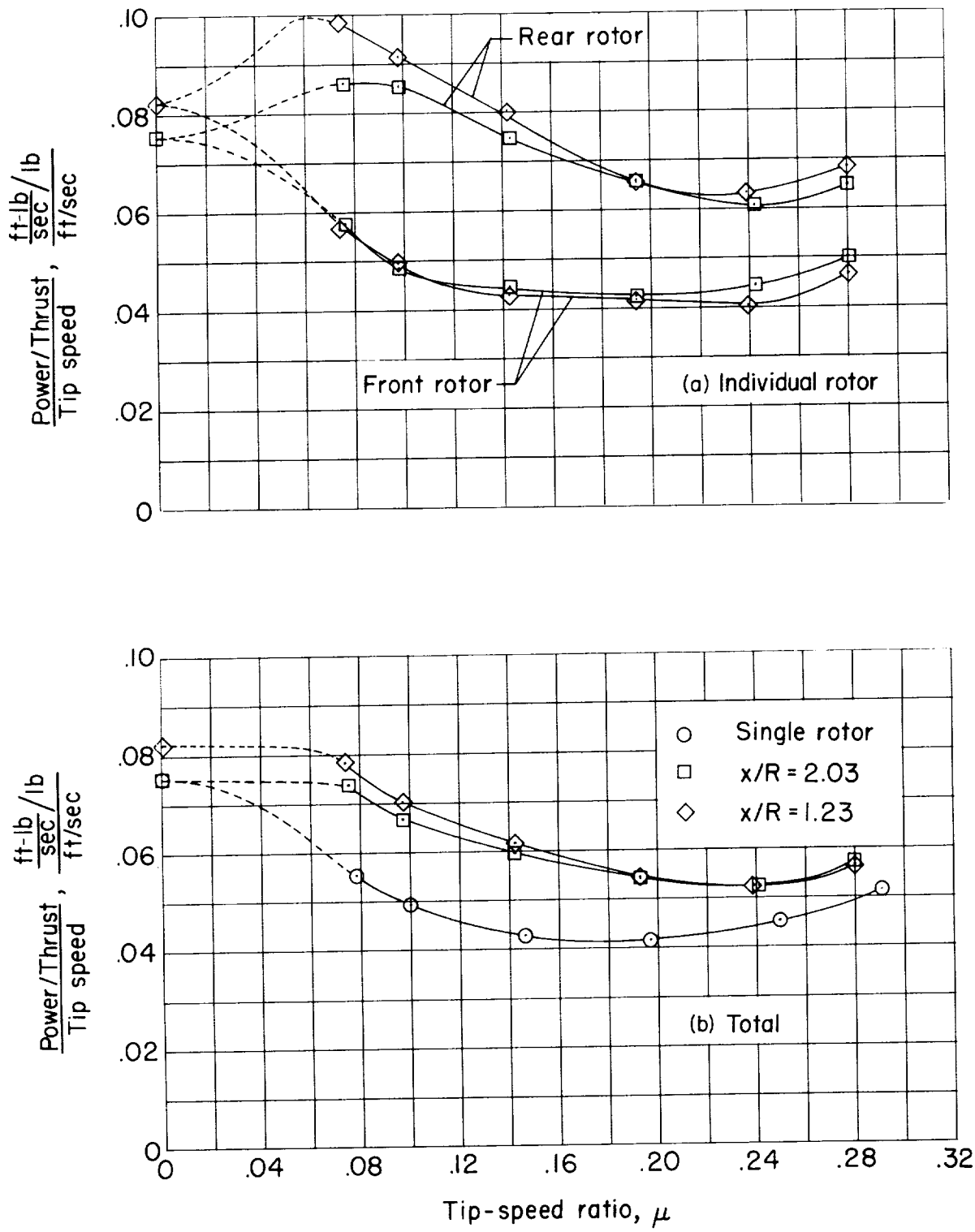

Figure 2.- Level-flight power requirements of tandem- and single-rotor configurations. C_T = 0.0043 (each rotor); zero parasite drag; hovering points from reference 2.

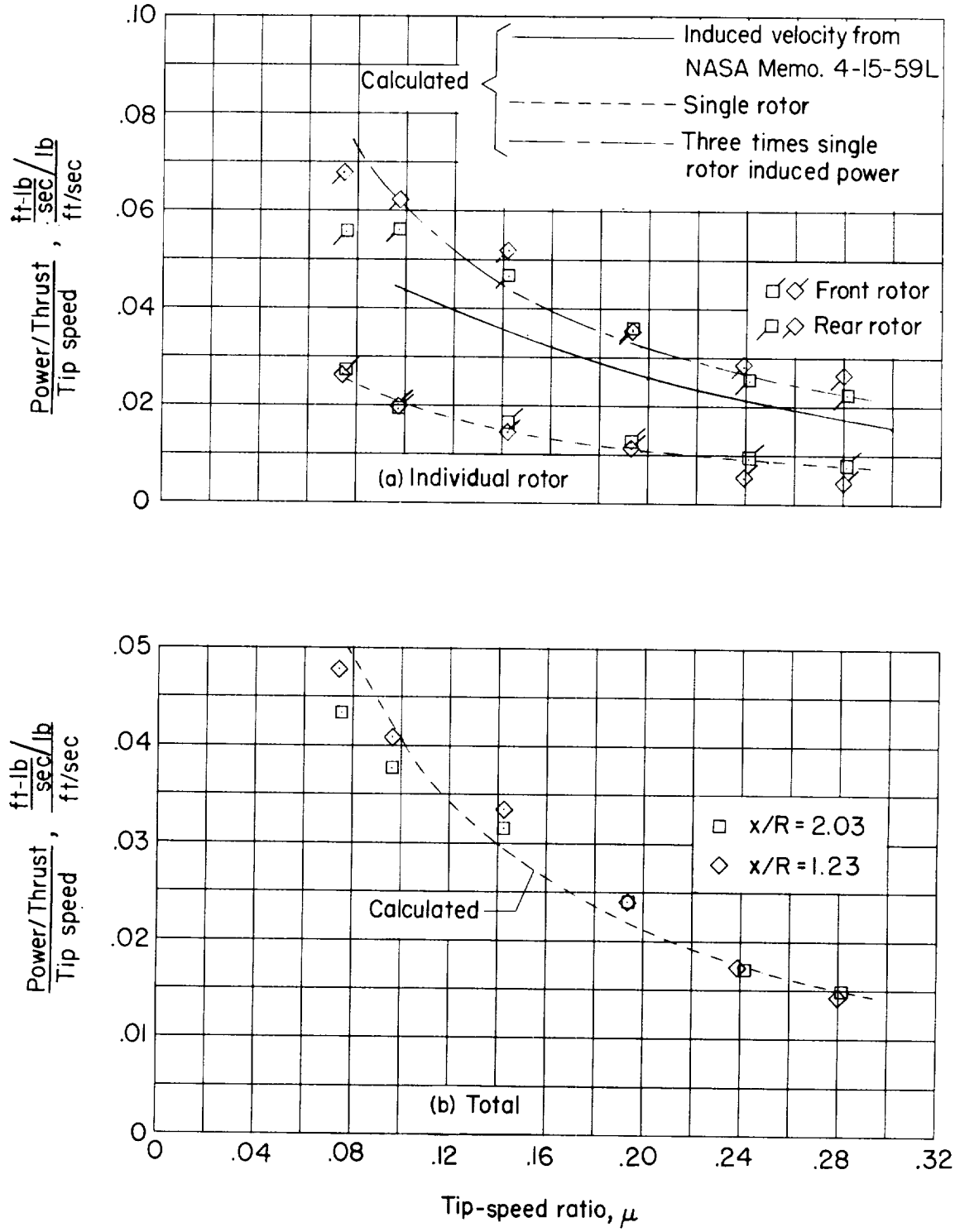

Figure 3.- Induced-plus-interference power requirements of tandem configurations. C_T = 0.0043 (each rotor).

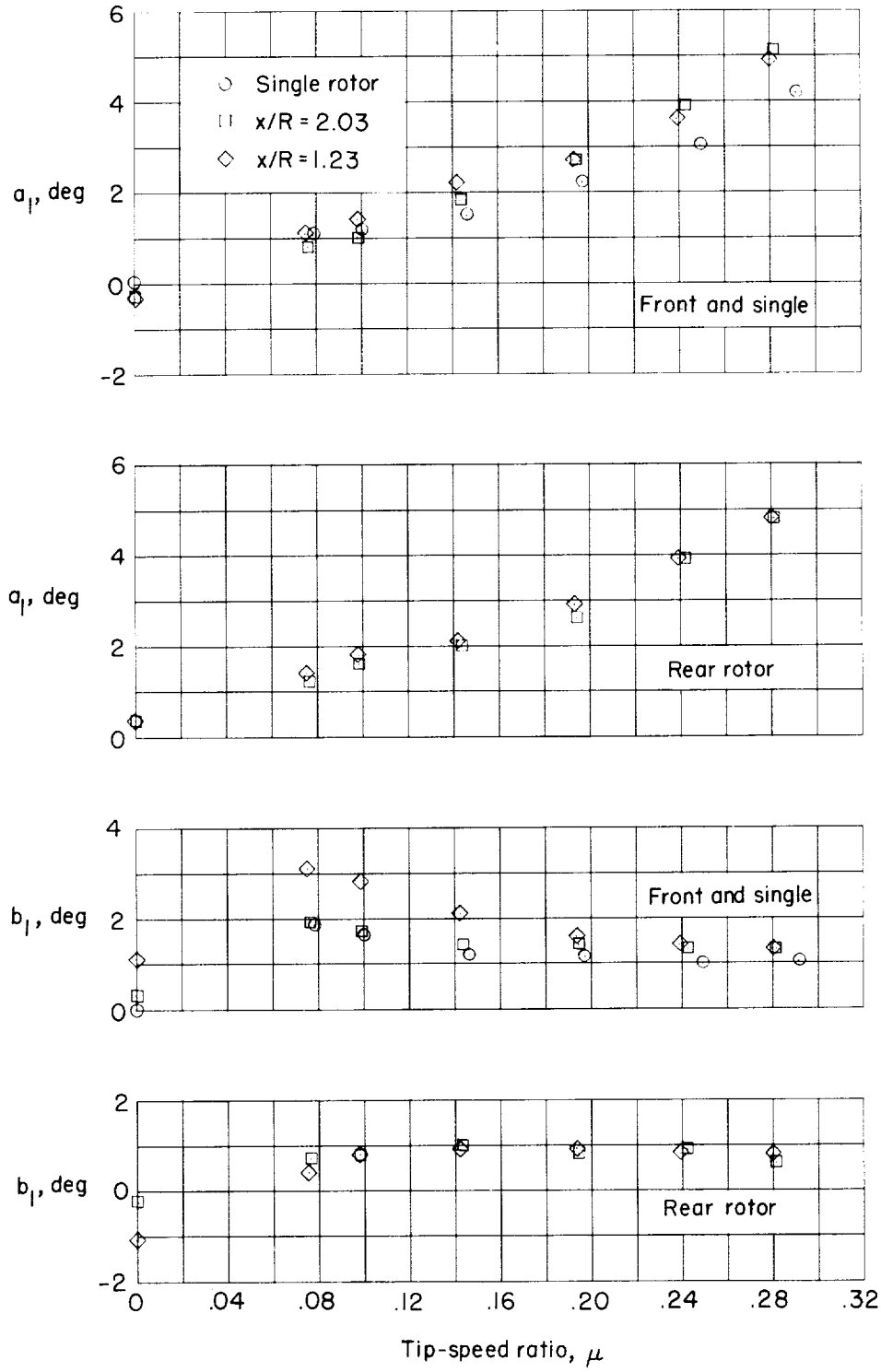

Figure 4.- Longitudinal and lateral flapping of tandem- and single-rotor configurations. C_T = 0.0043 (each rotor); hovering points from reference 2.

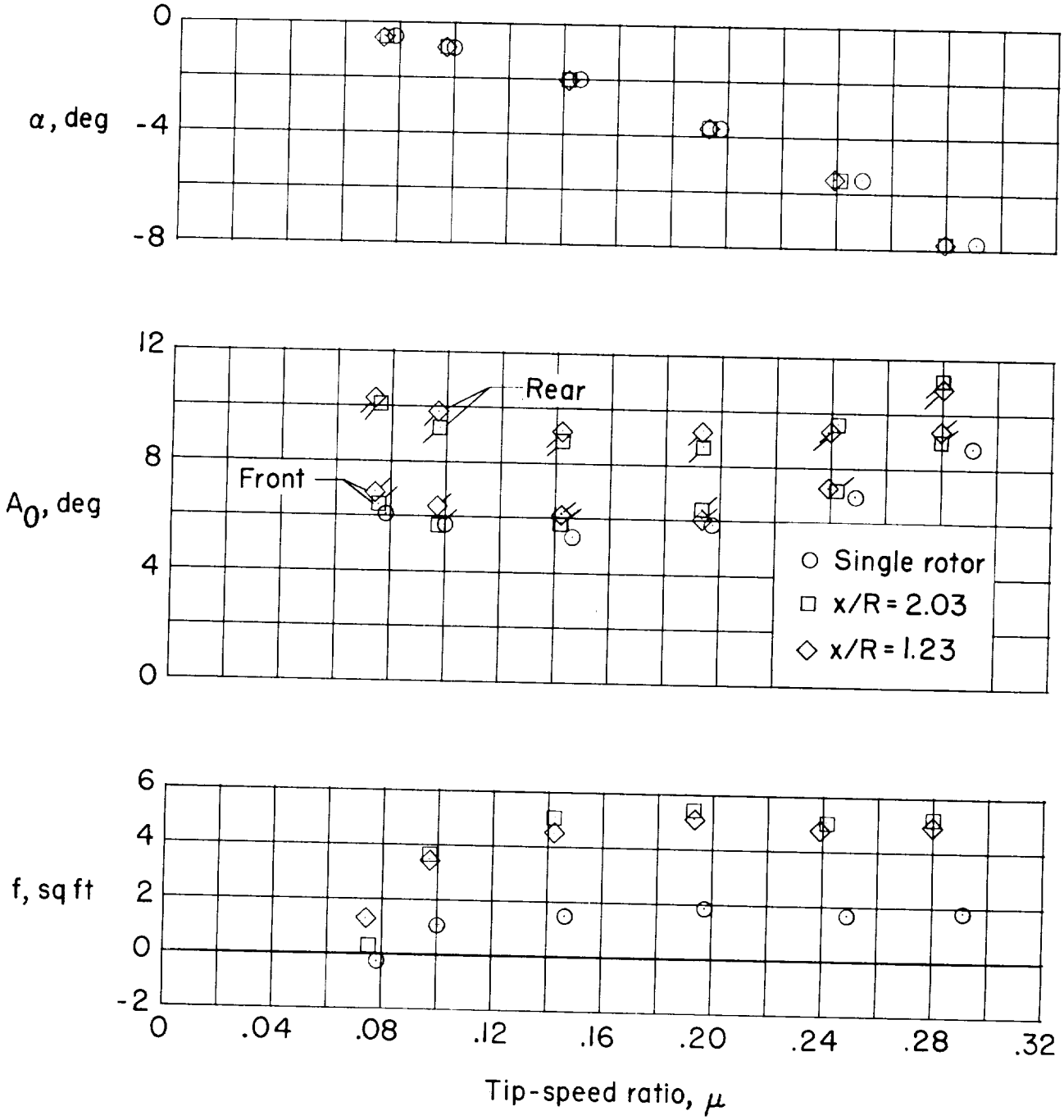

Figure 5.- Tip-path-plane angle of attack, mean blade pitch, and propulsive-force flat-plate area for tandem- and single-rotor configurations.

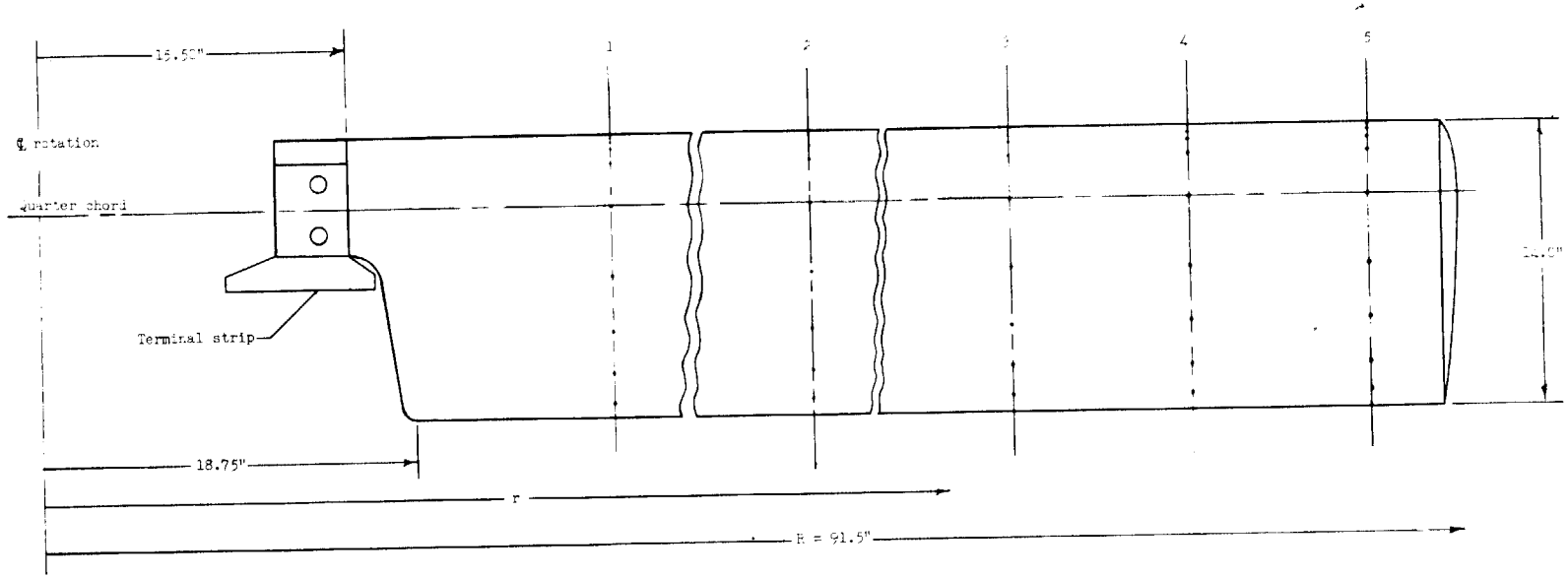

Chordwise station	Percent chord,
1	0.5
2	1.0
3	2.5
4	5.0
5	10.0
6	25.0
7	50.0
8	70.0
9	85.0
10	95.0

Radial station	r/R
1	0.33
2	.5
3	.75
4	.85
5	.95

Figure 6.- Blade layout showing location of pressure orifices. Airfoil section, NACA 0012; rotor solidity, 0.097.

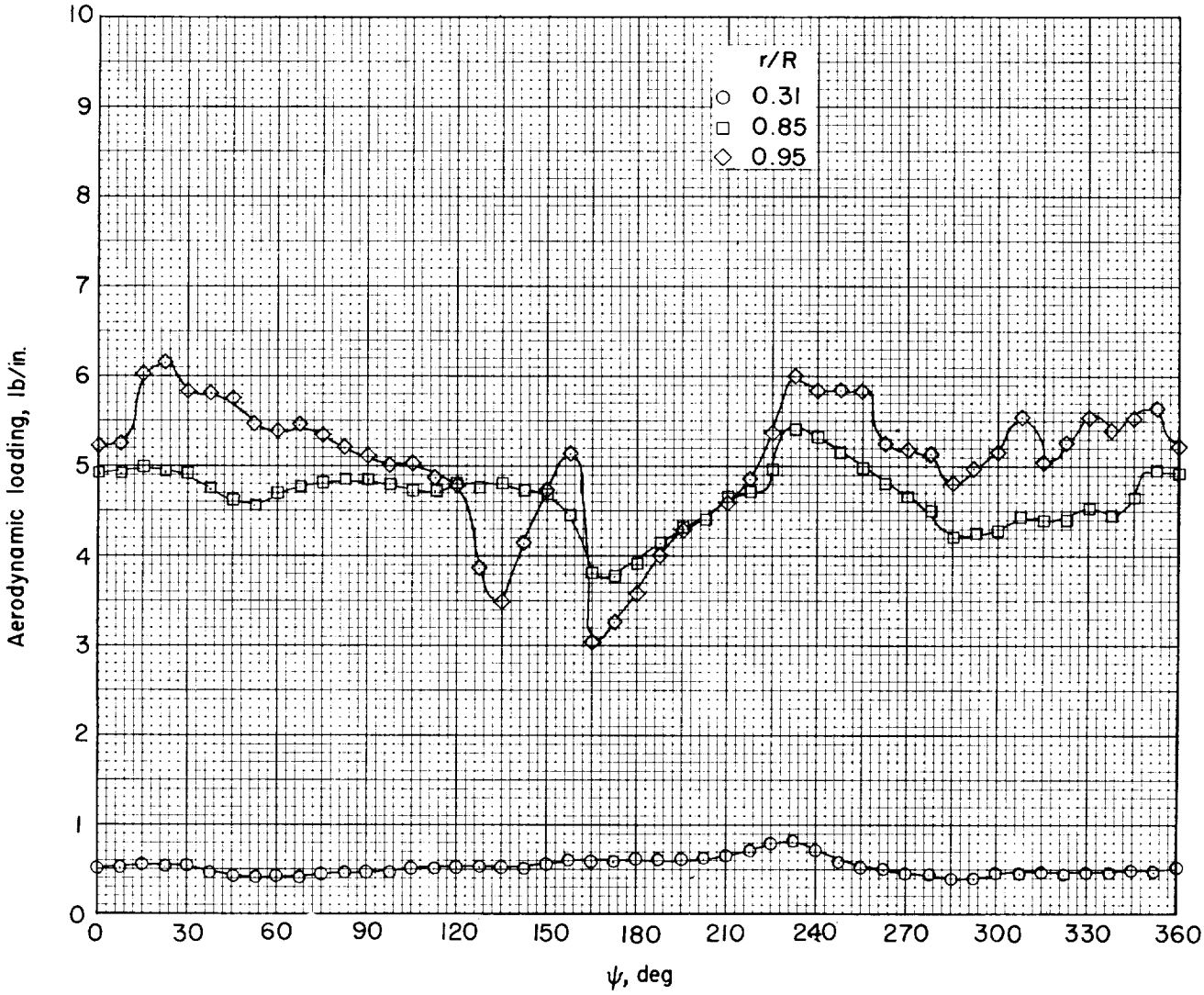

(a) L_0 = 168.4 lb.

Figure 7.- Variation of section aerodynamic loading with azimuth at various spanwise stations for rear rotor of nonoverlapped rotor system. x/R = 2.03; hovering.

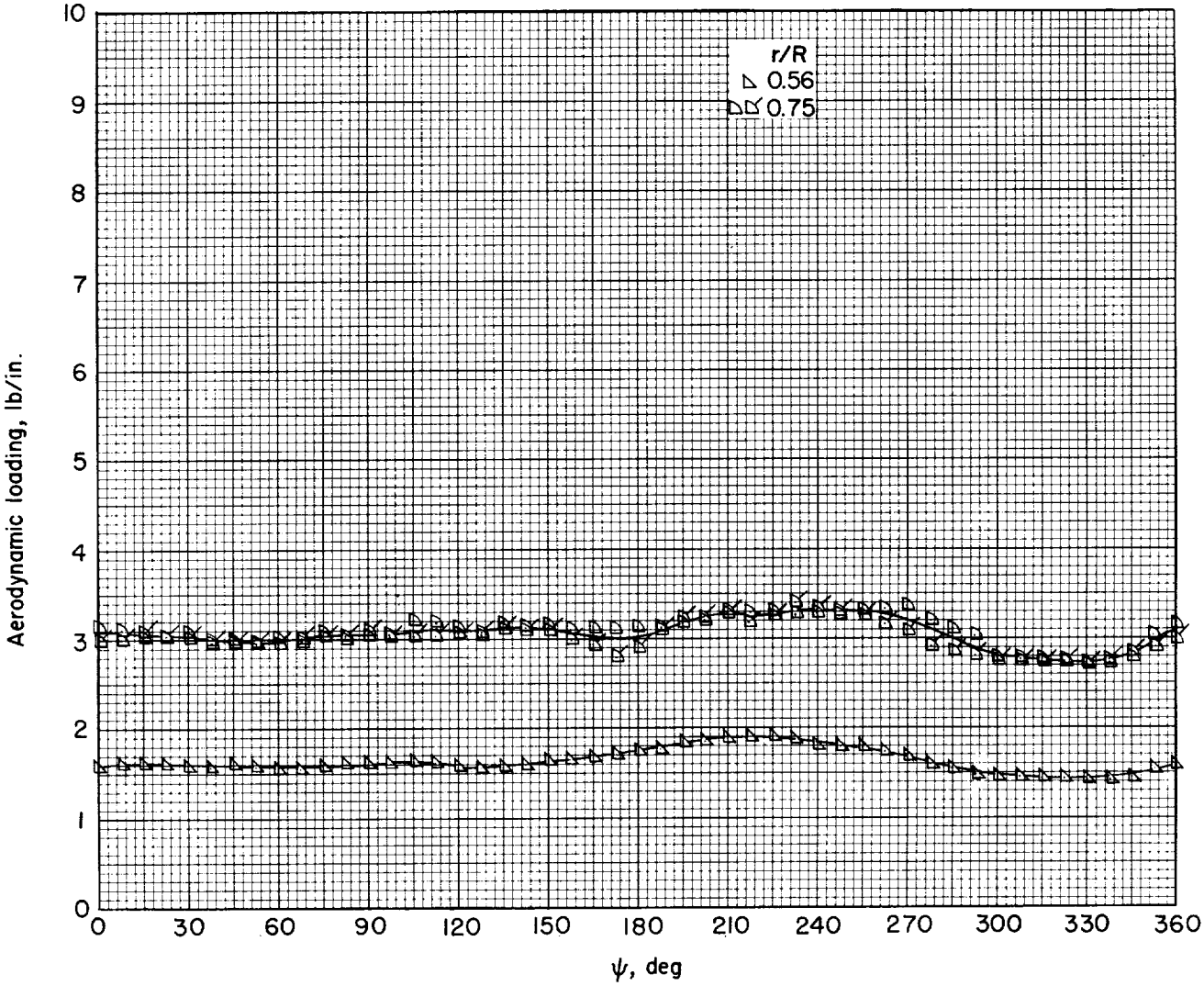

(a) Concluded.

Figure 7.- Continued.

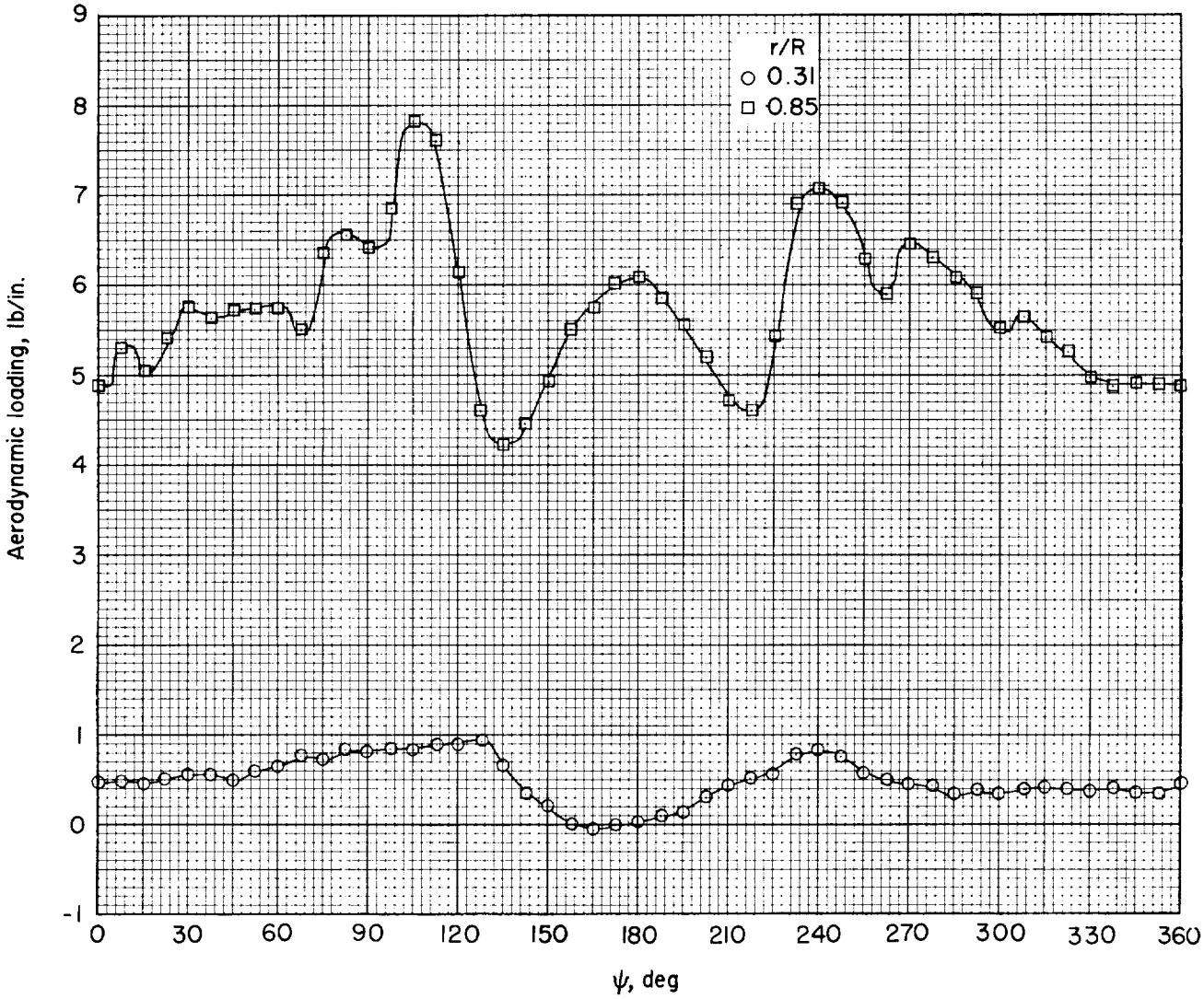

(b) L_0 = 232.0 lb.

Figure 7.- Continued.

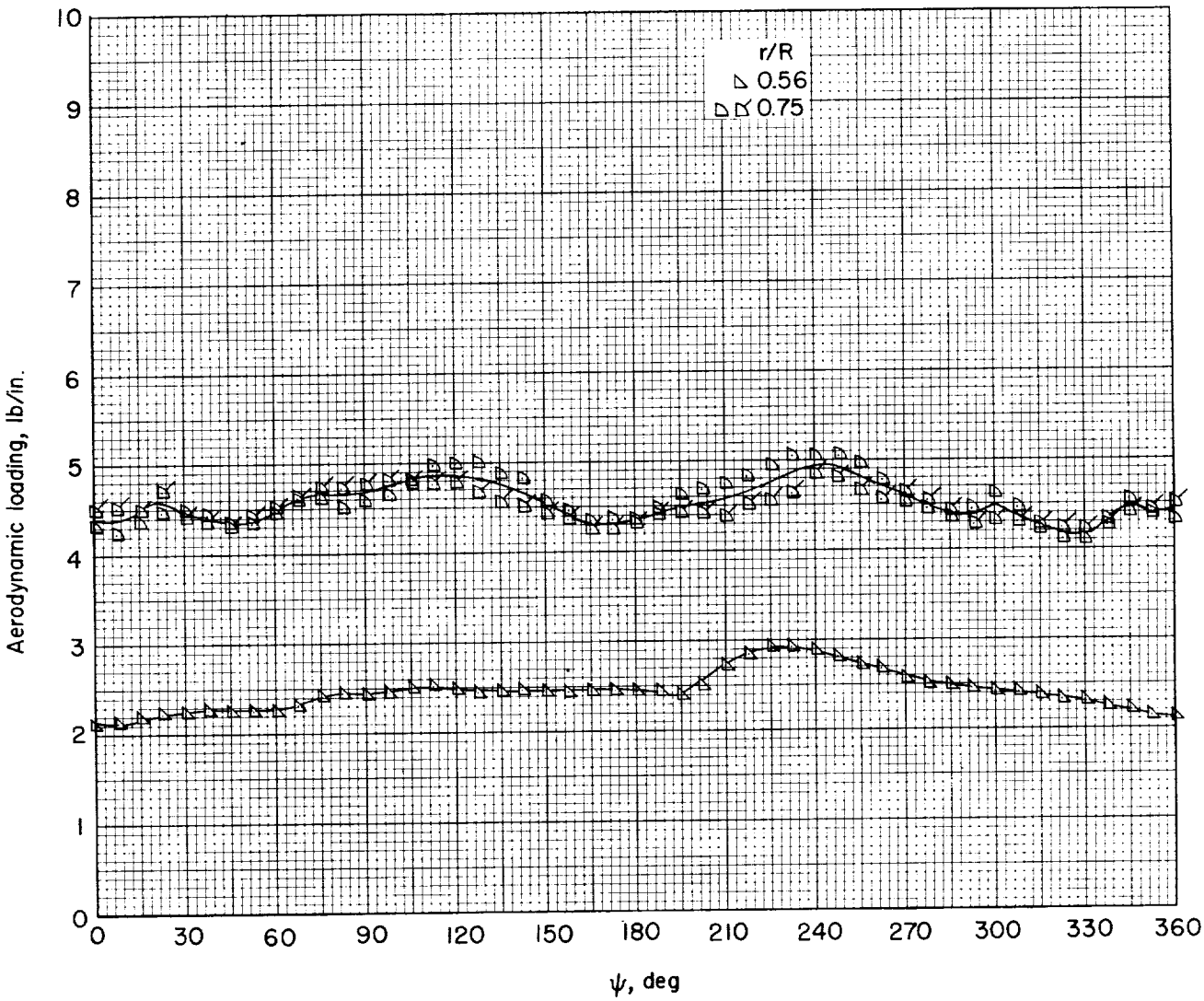

(b) Concluded.

Figure 7.- Concluded.

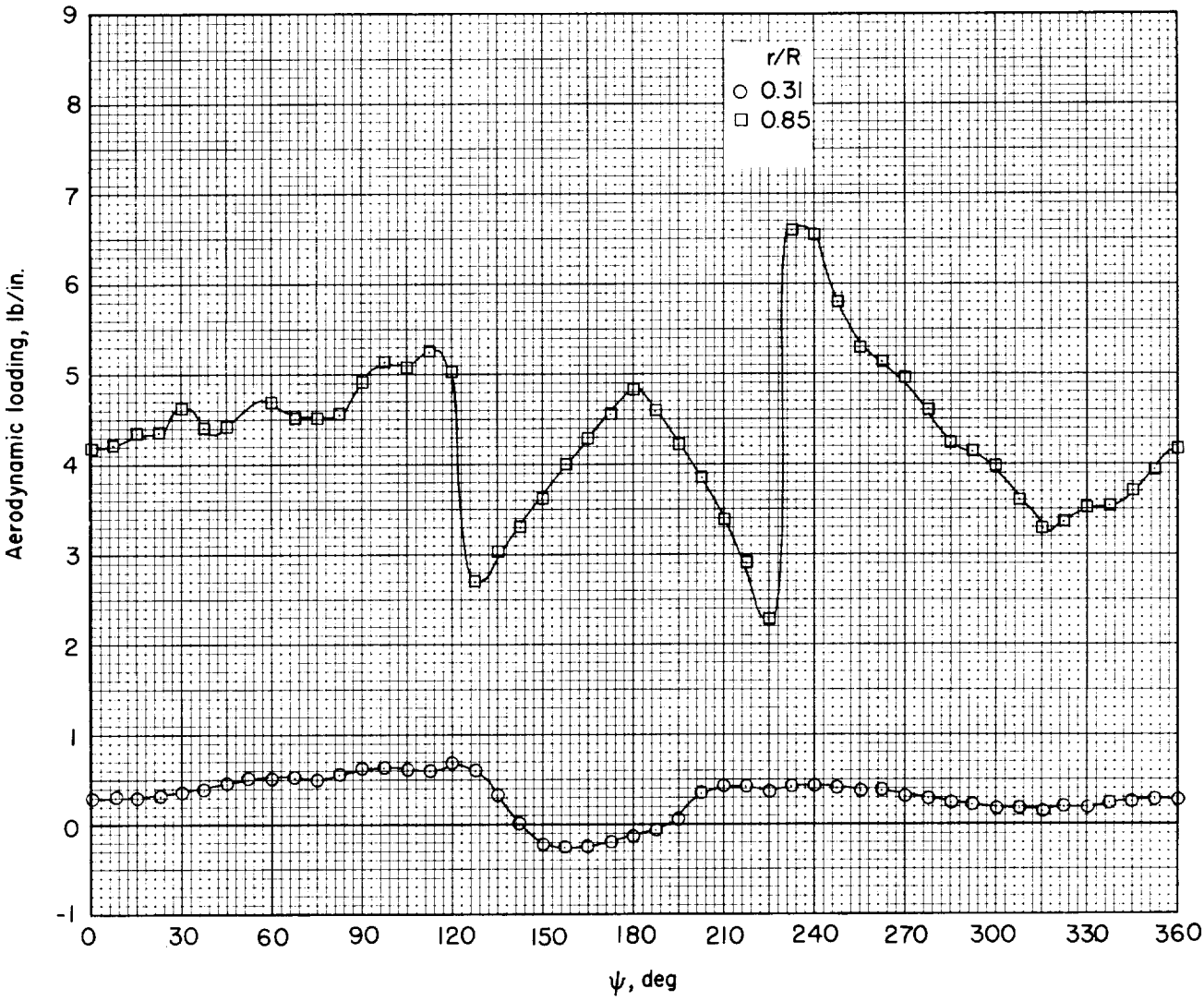

(a) L_0 = 131.2 lb.

Figure 8.- Variation of section aerodynamic loading with azimuth at various spanwise stations for rear rotor at overlapped rotor system. x/R = 1.23; hovering.

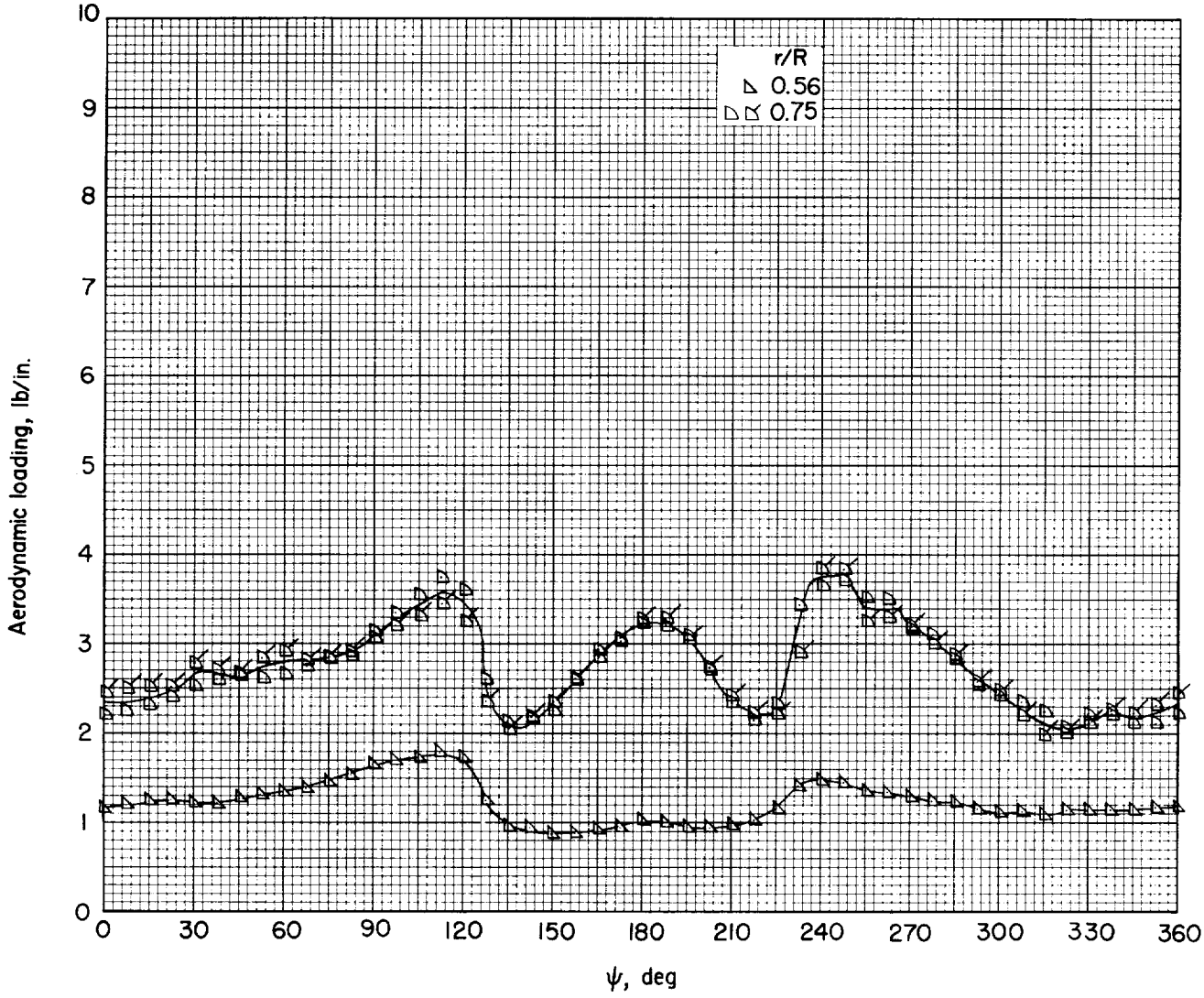

(a) Concluded.

Figure 8.- Continued.

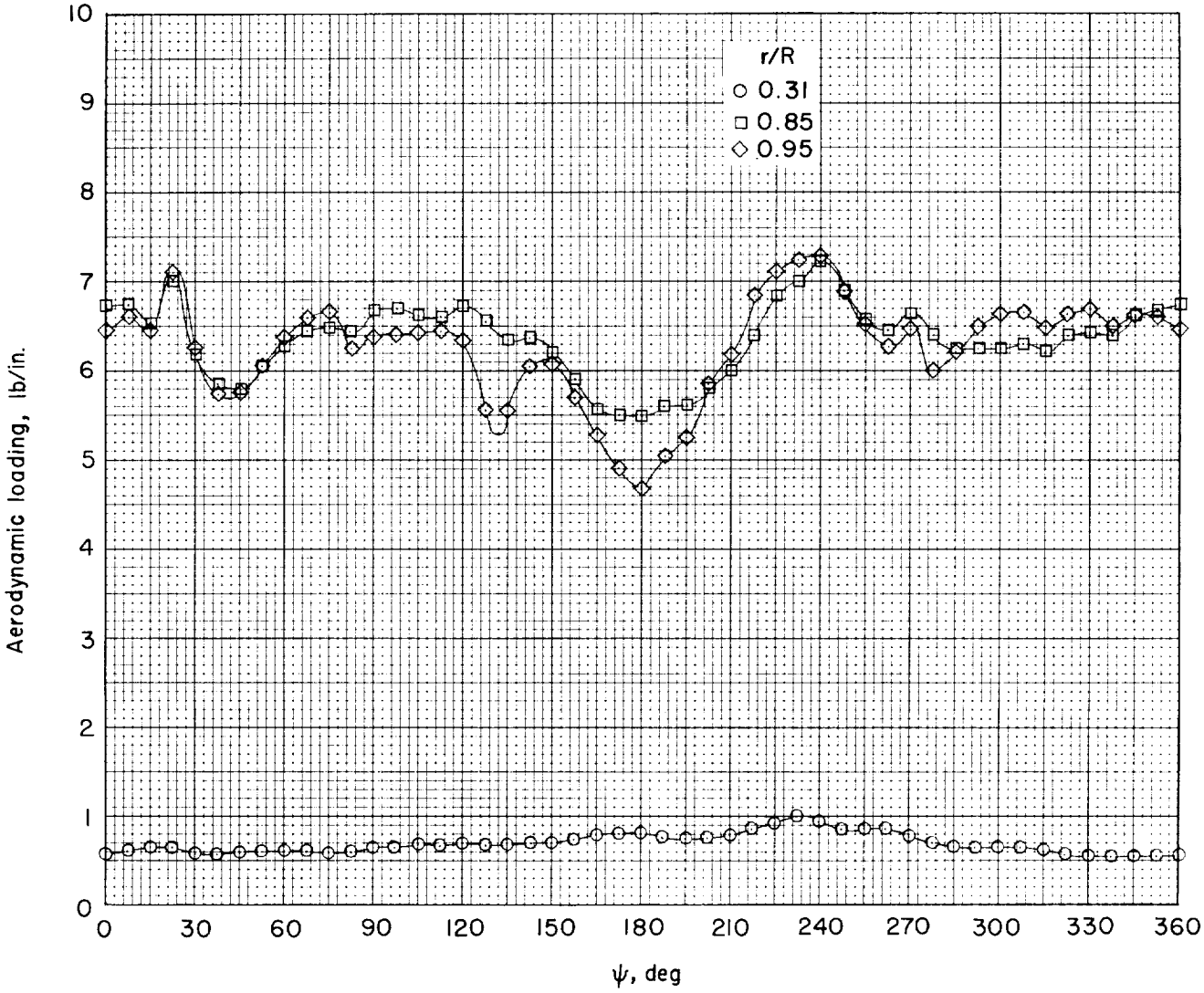

(b) L_0 = 185.1 lb.

Figure 8.- Continued.

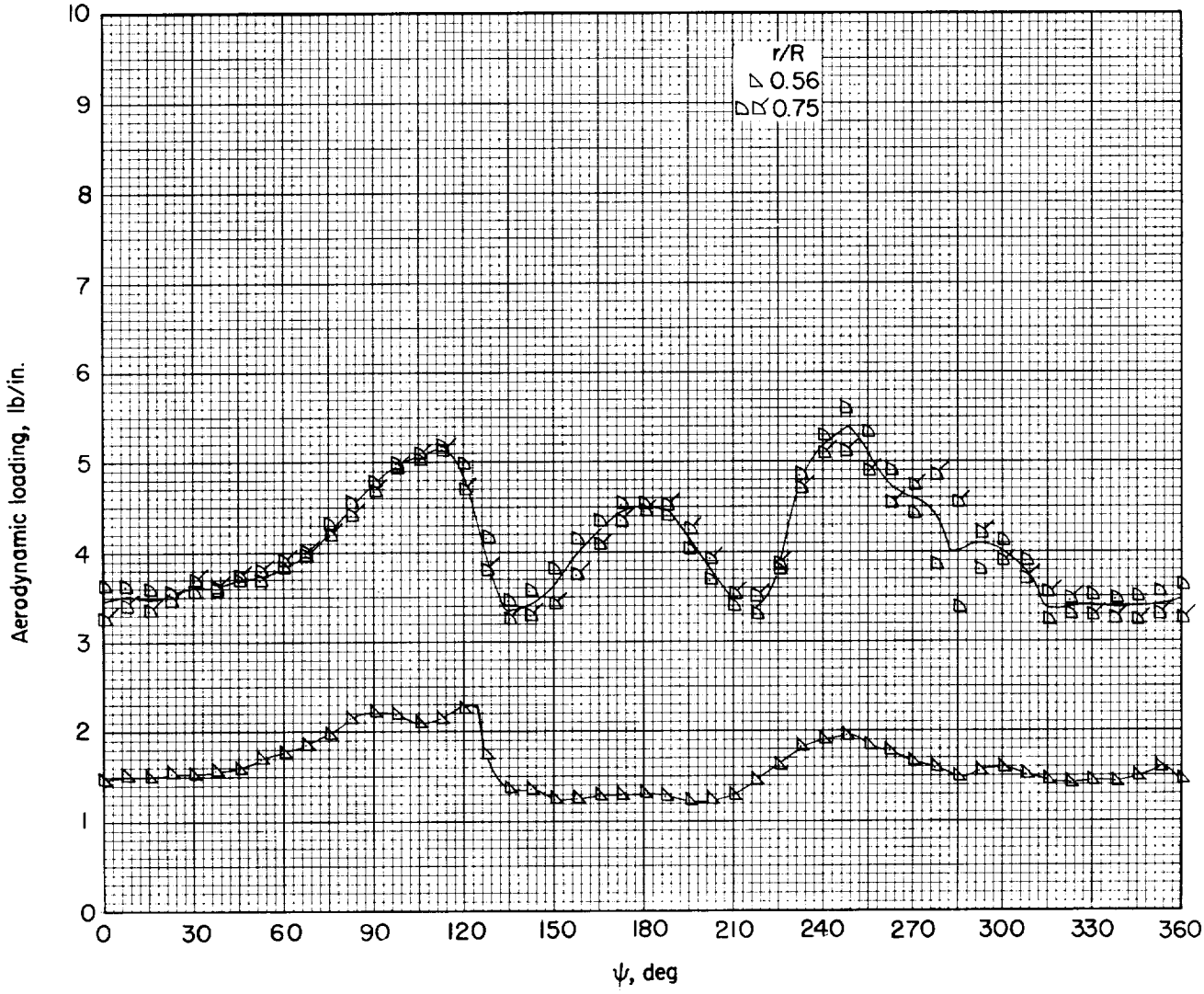

(b) Concluded.

Figure 8.- Concluded.

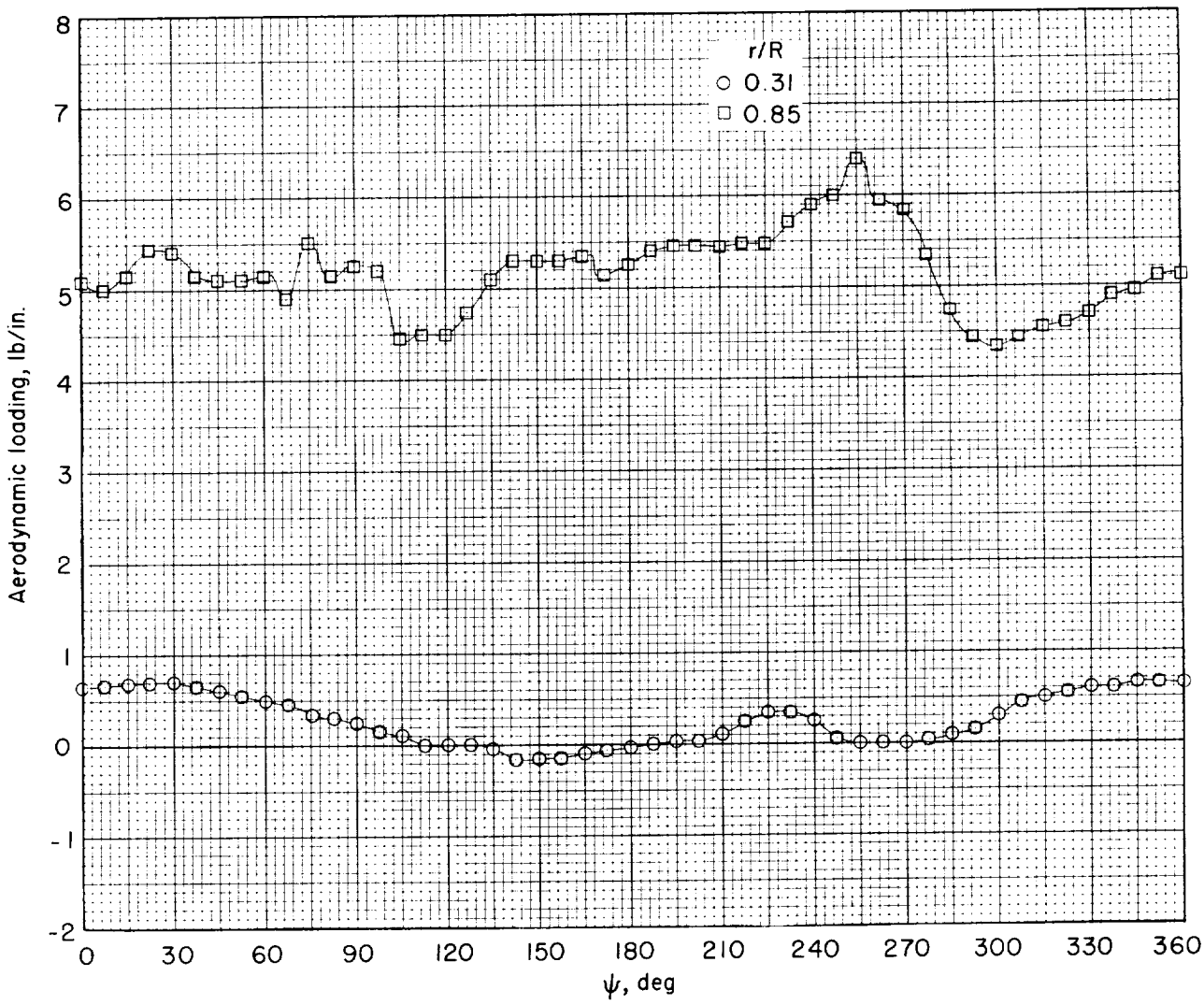

(a) $\mu = 0.075$.

Figure 9.- Variation of section aerodynamic loading with azimuth at various spanwise stations for rear rotor of nonoverlapped rotor system. x/R = 2.03.

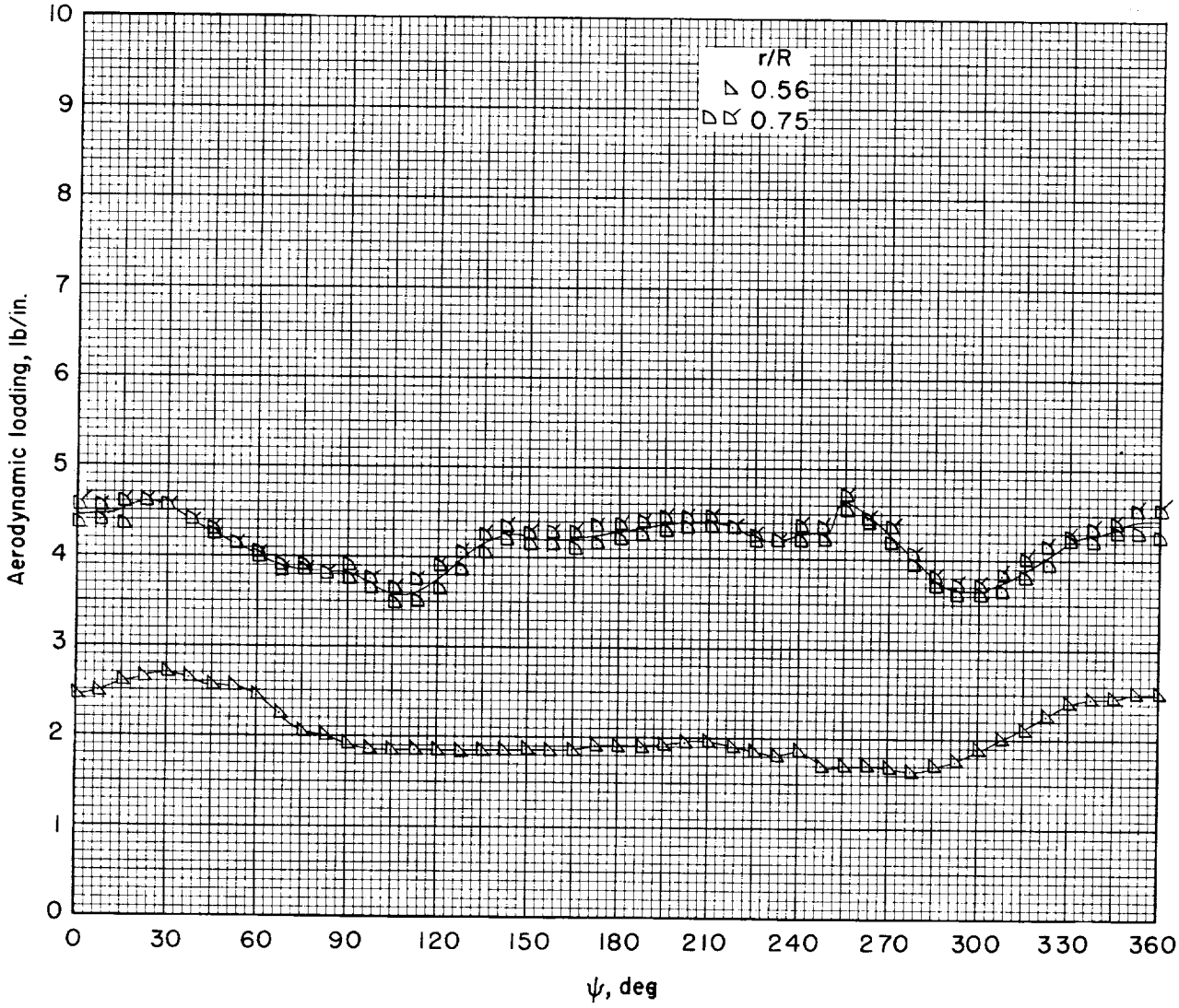

(a) Concluded.

Figure 9.- Continued.

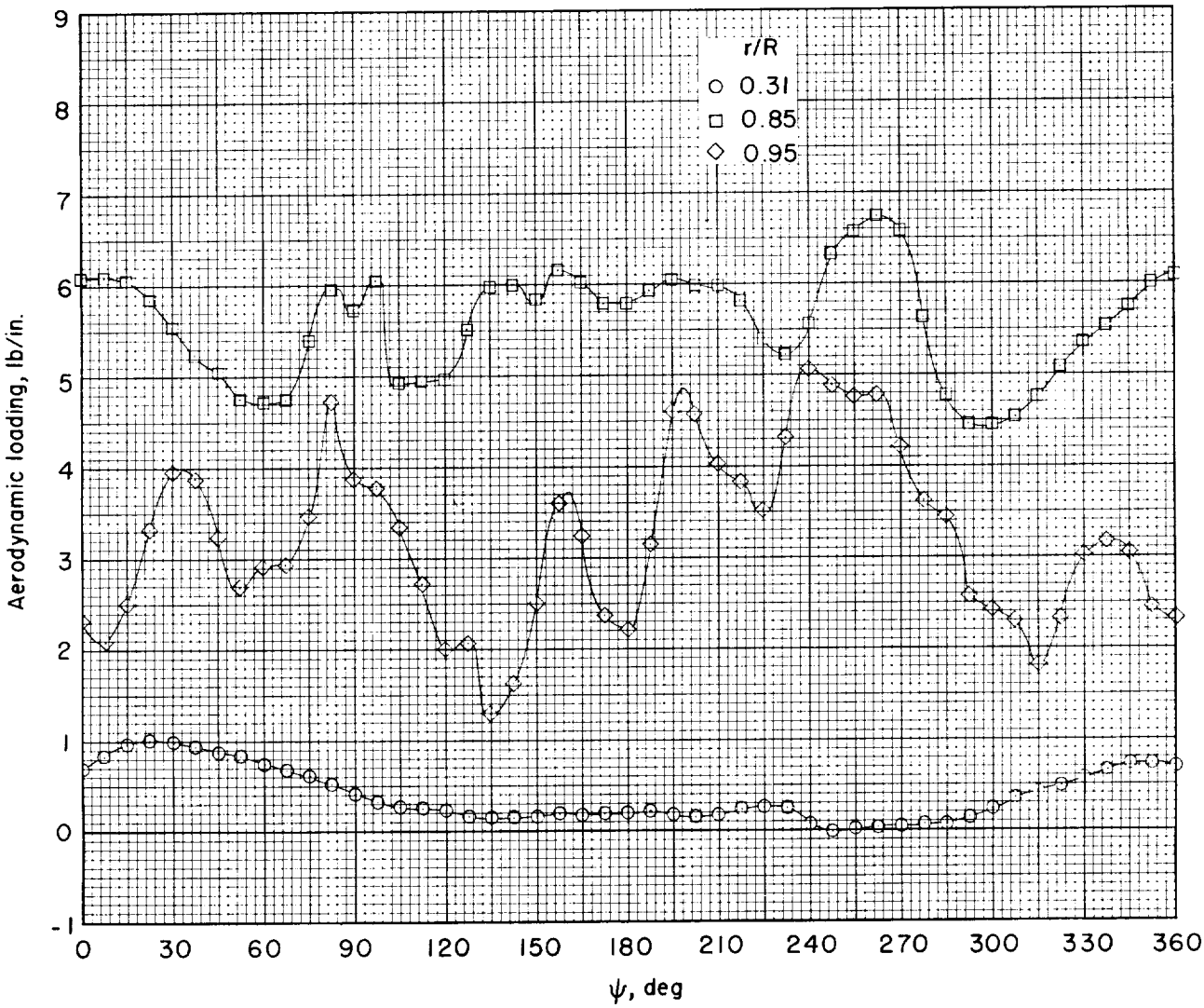

(b) $\mu = 0.10$.

Figure 9.- Continued.

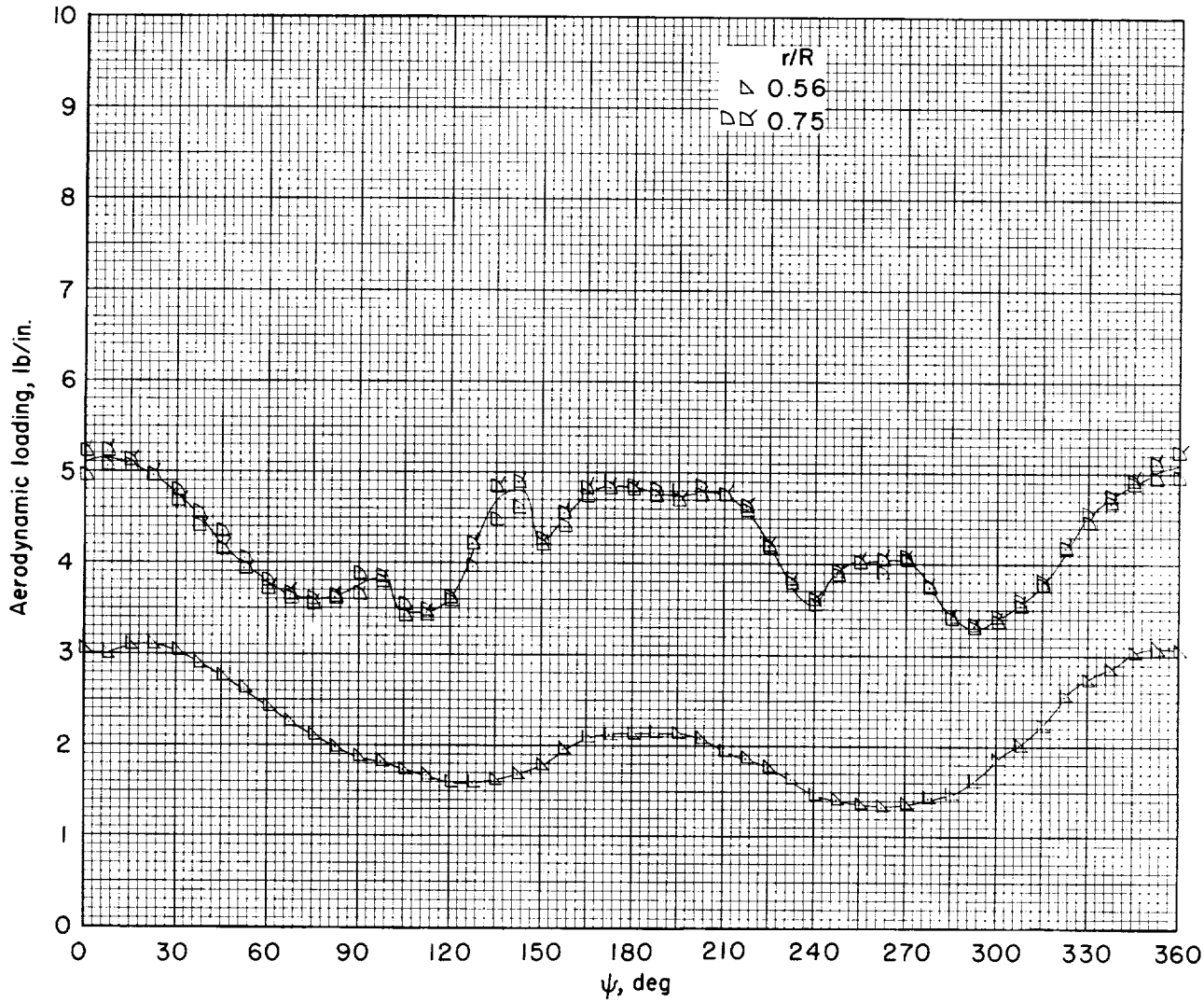

(b) Concluded.

Figure 9.- Continued.

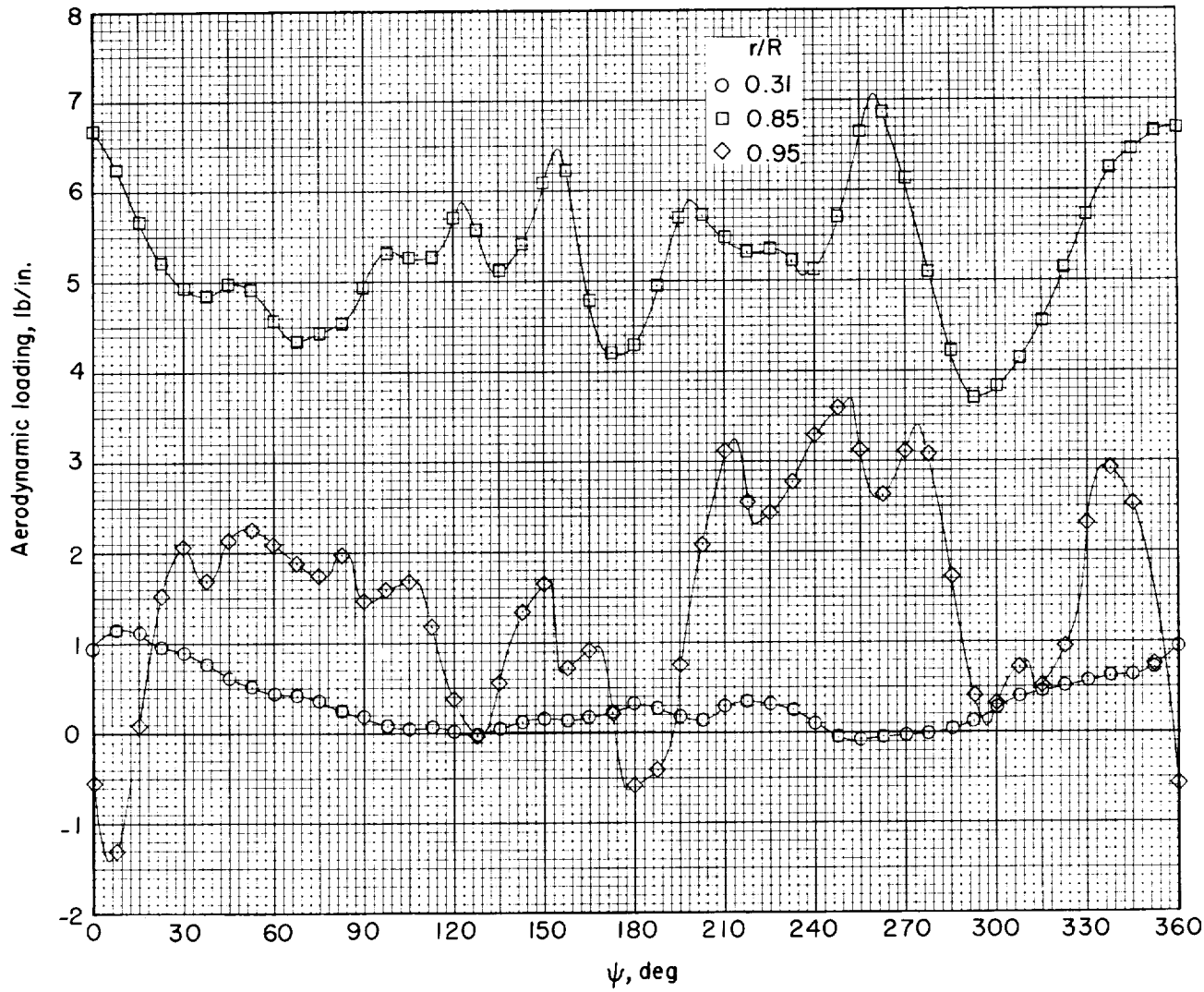

(c) $\mu = 0.14$.

Figure 9.- Continued.

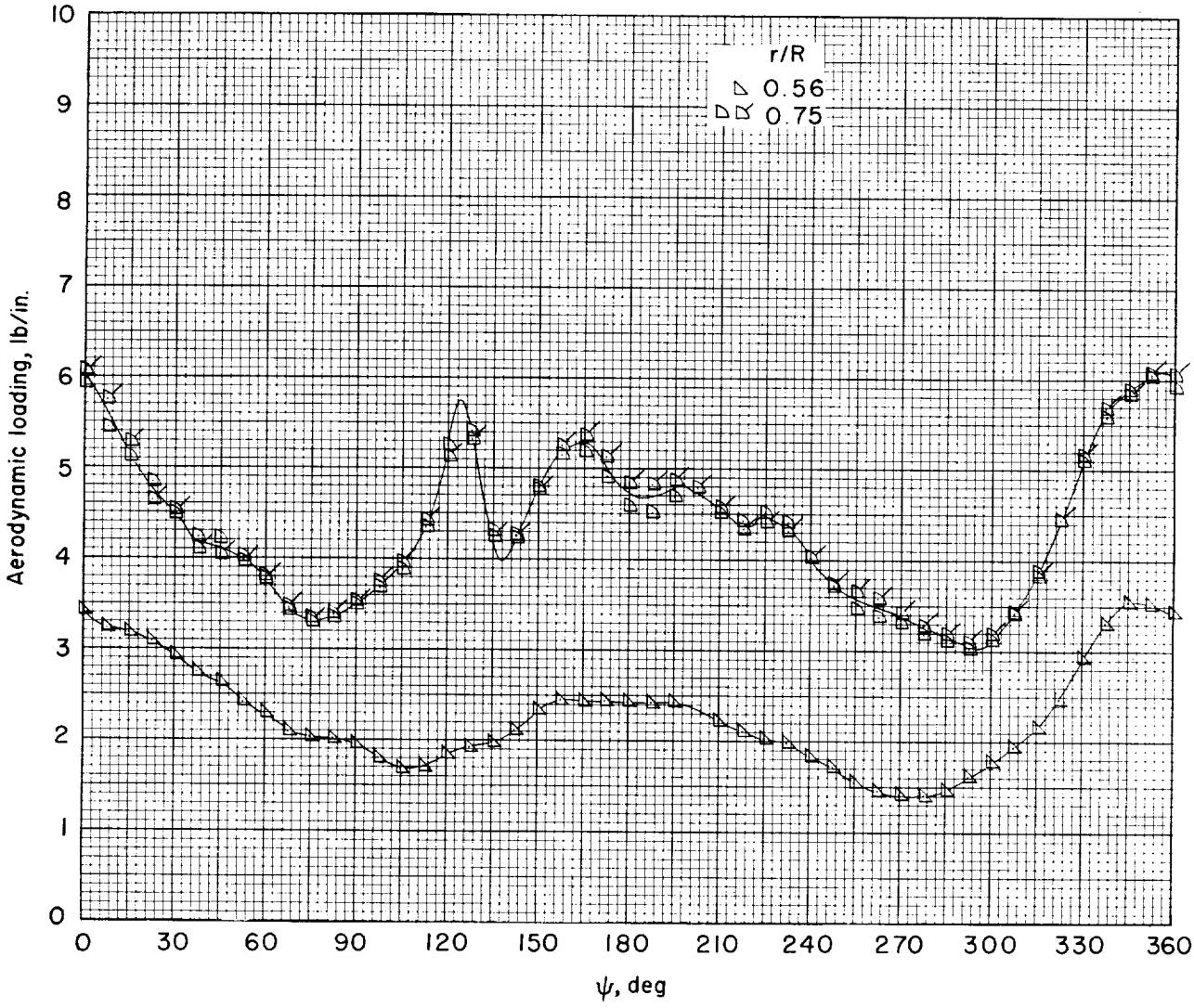

(c) Concluded.

Figure 9.- Continued.

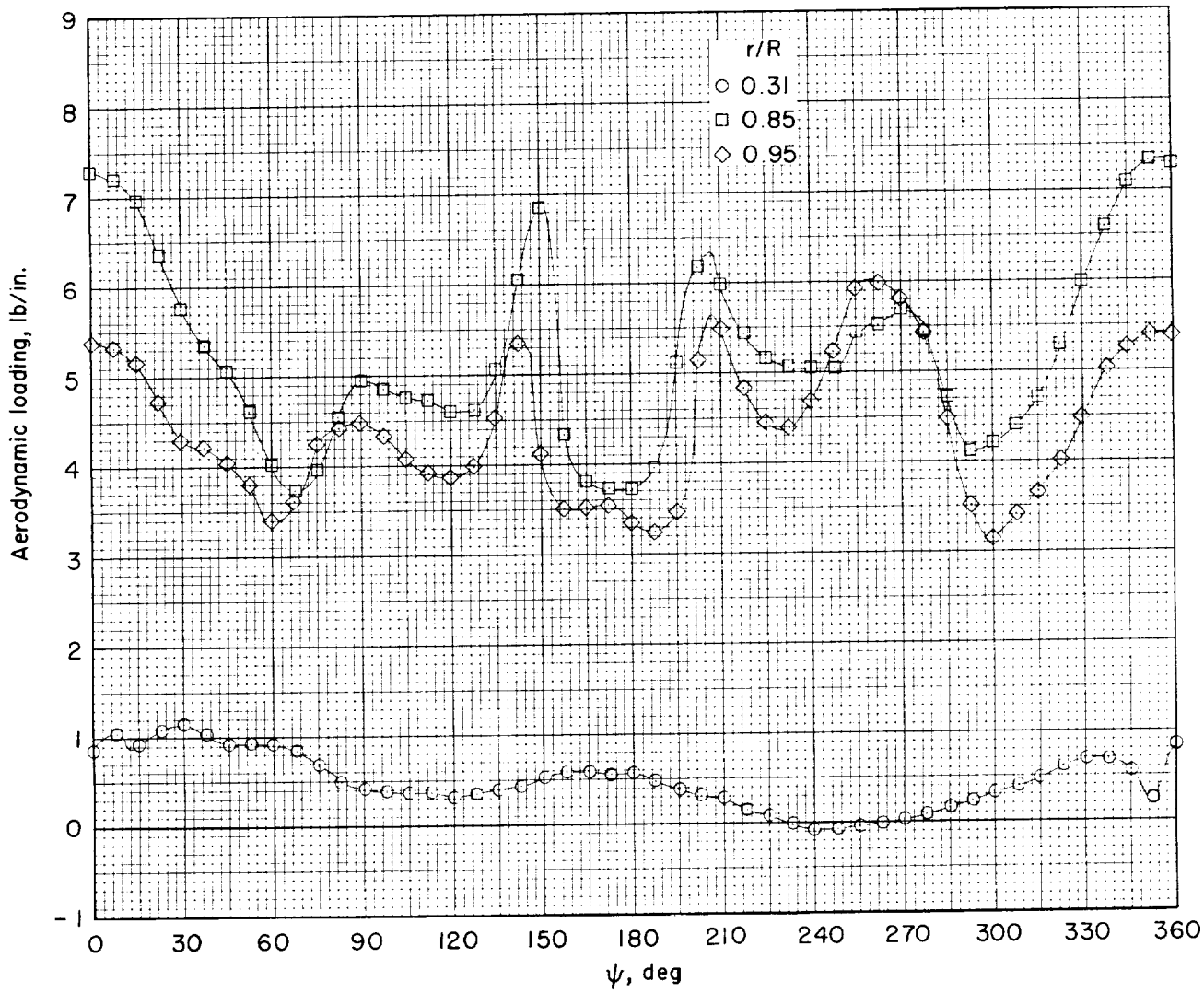

(d) $\mu = 0.19$.

Figure 9.- Continued.

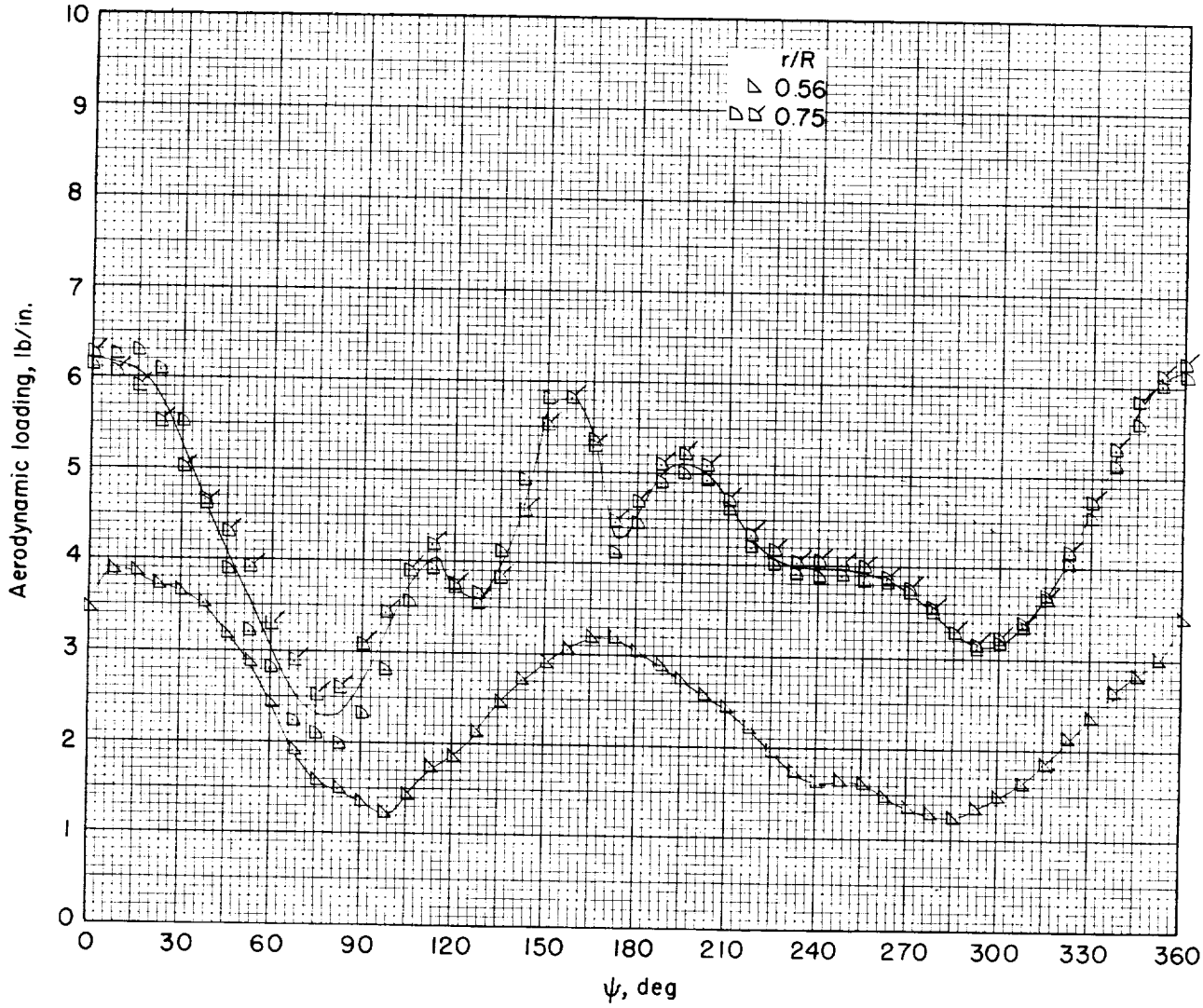

(d) Concluded.

Figure 9.- Continued.

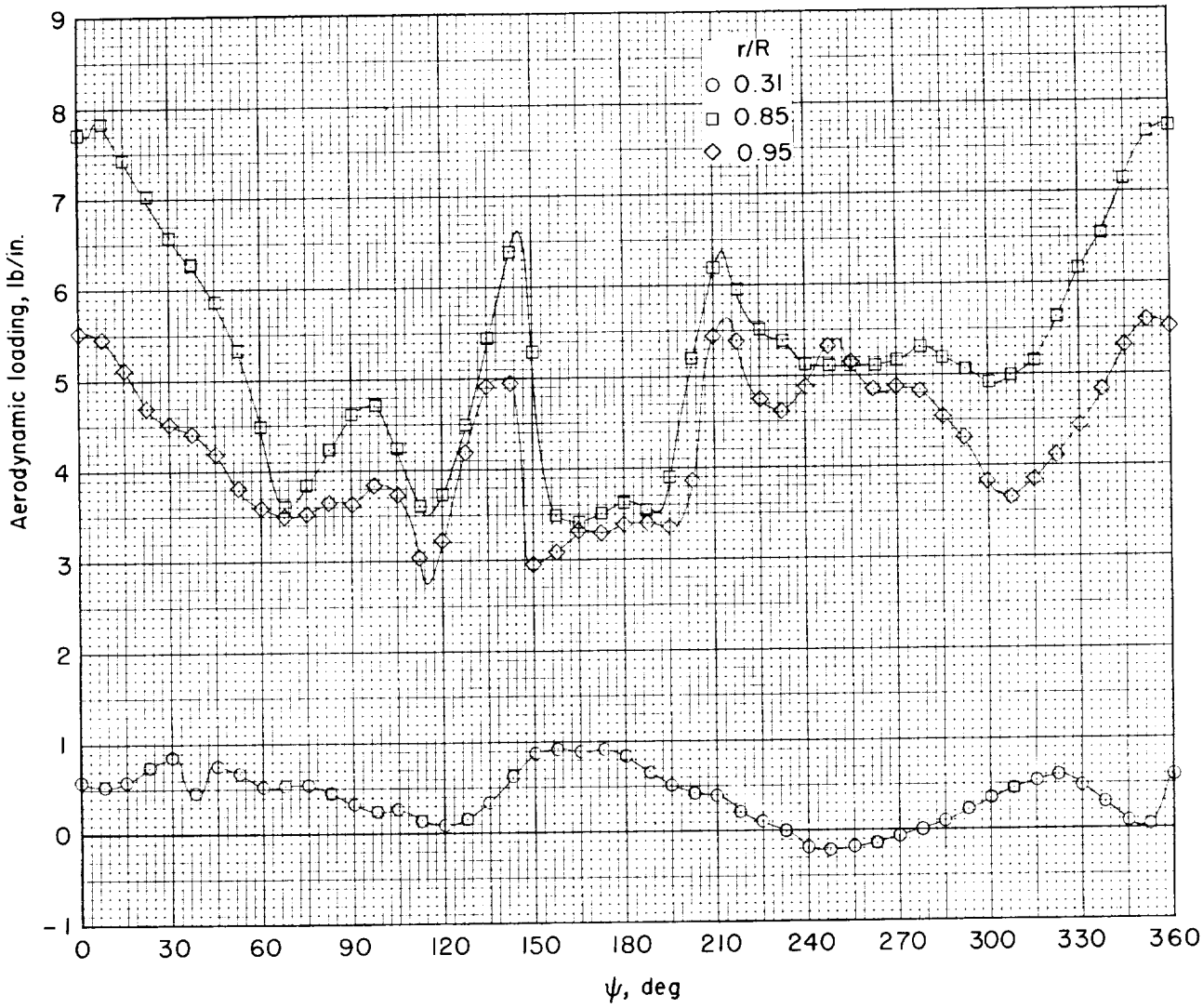

(e) $\mu = 0.24$.

Figure 9.- Continued.

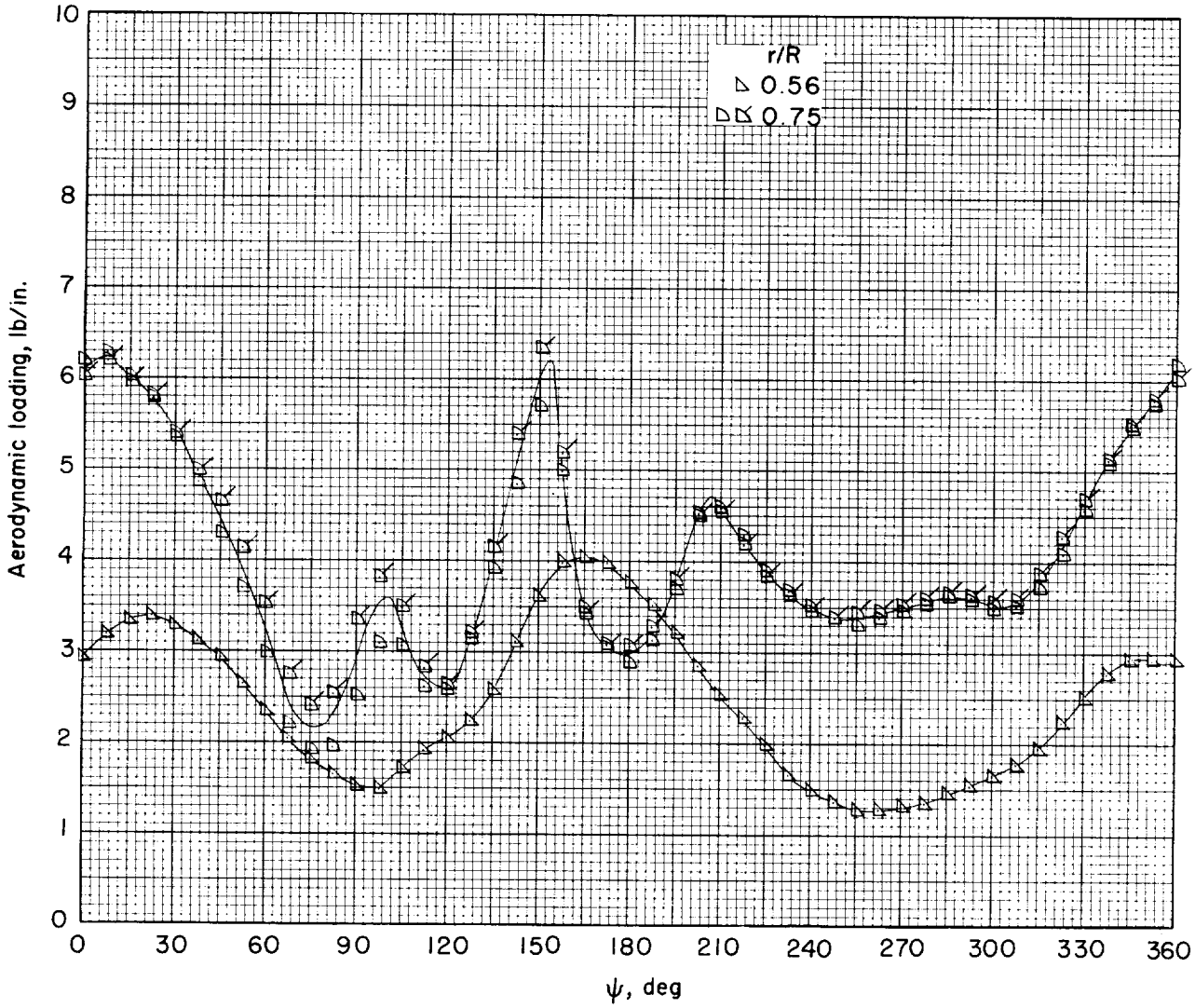

(e) Concluded.

Figure 9.- Continued.

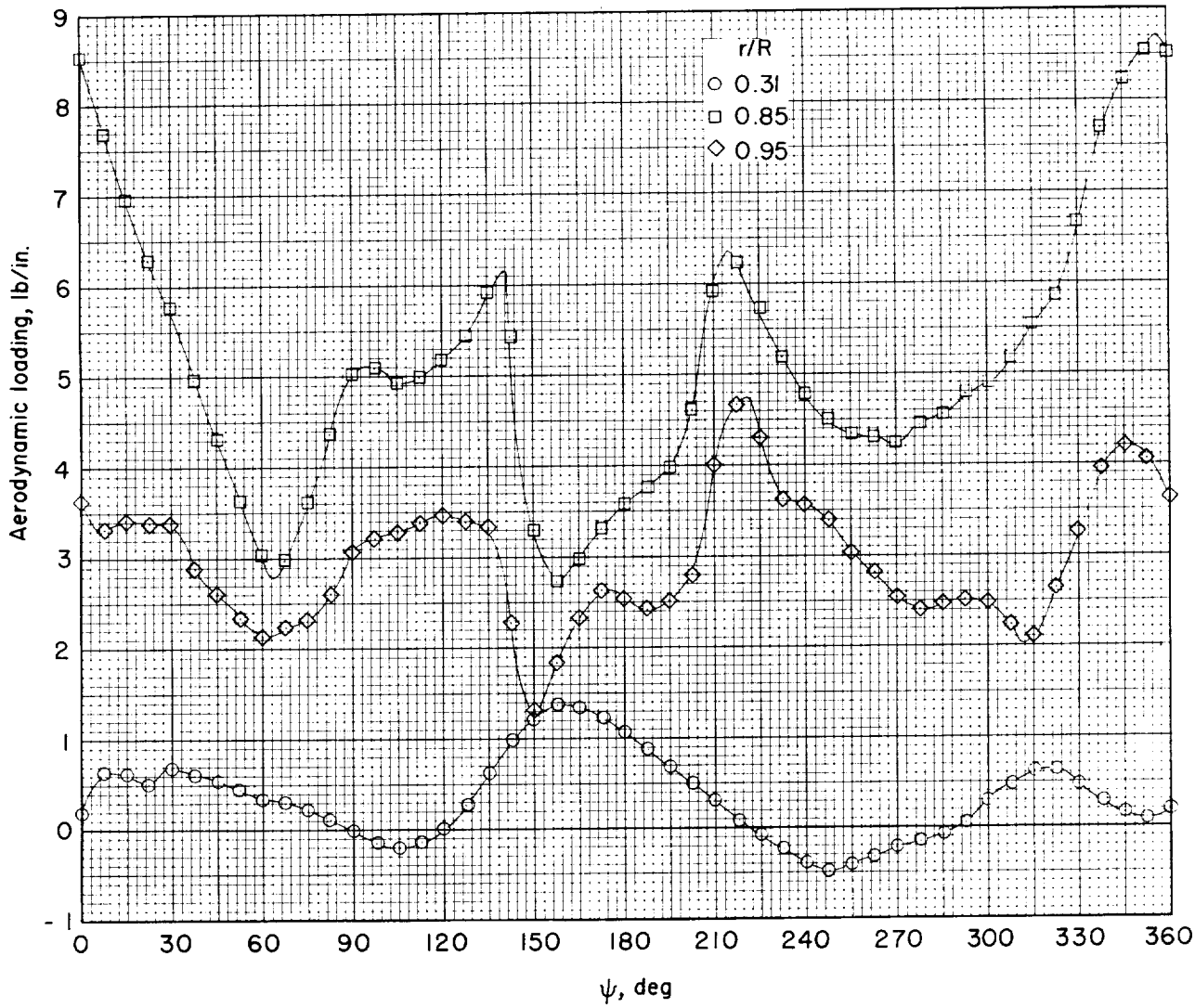

(f) $\mu = 0.28$.

Figure 9.- Continued.

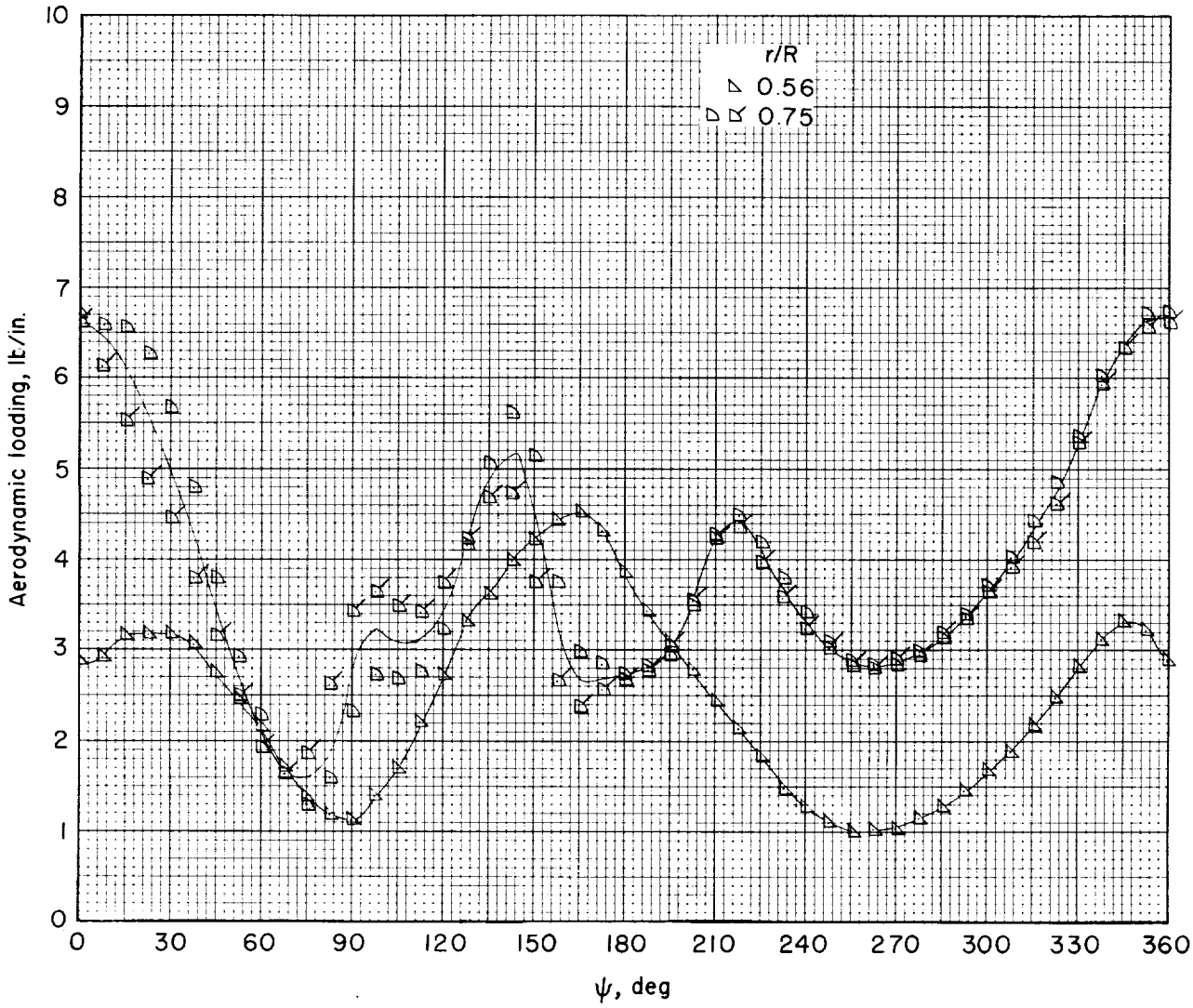

(f) Concluded.

Figure 9.- Concluded.

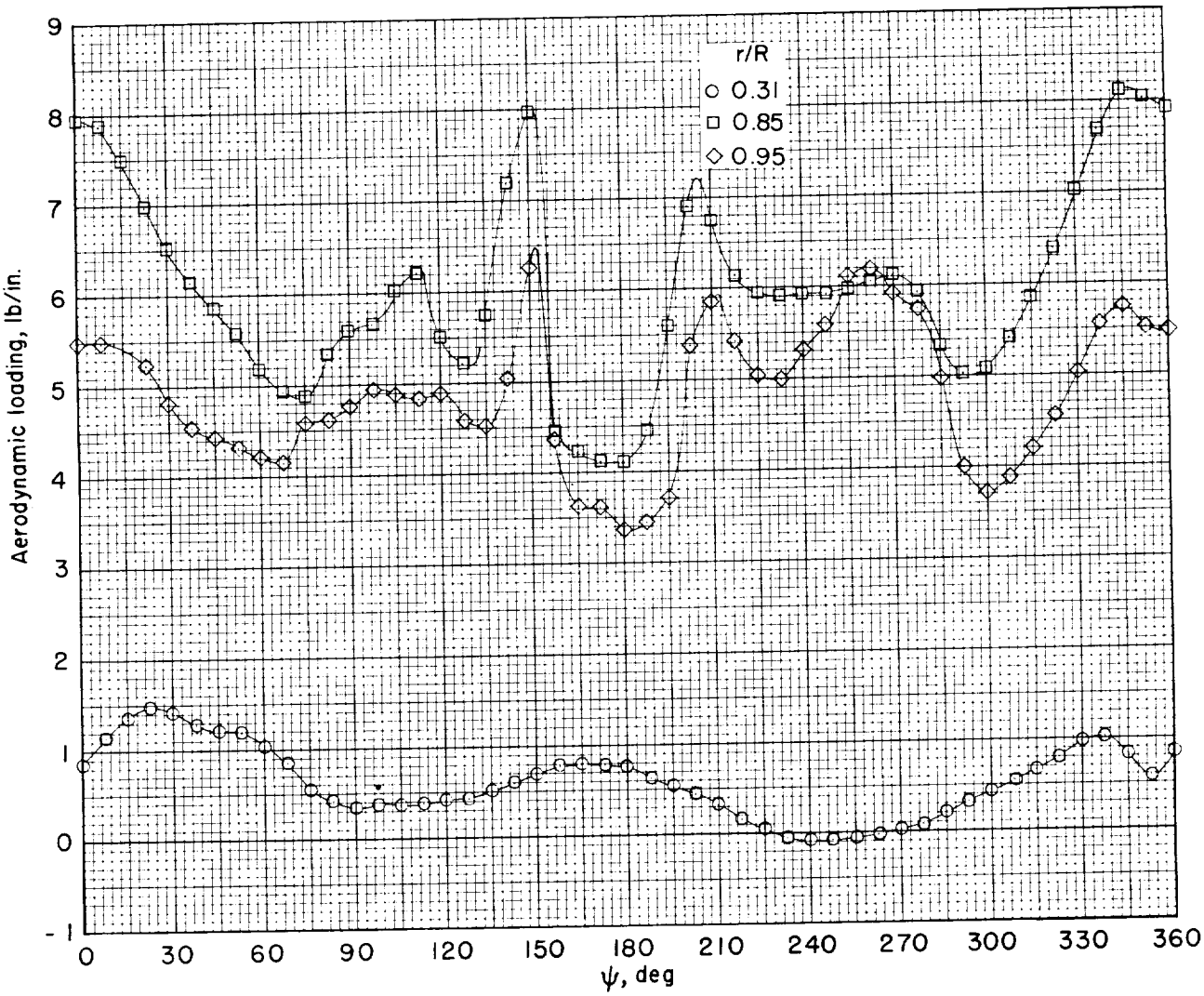

(a) Disk loading = 6 lb/sq ft; L_0 = 234.9 lb.

Figure 10.- Variation of section aerodynamic loading with azimuth at various spanwise stations for rear rotor of nonoverlapped rotor system for special conditions. x/R = 2.03. μ = 0.19.

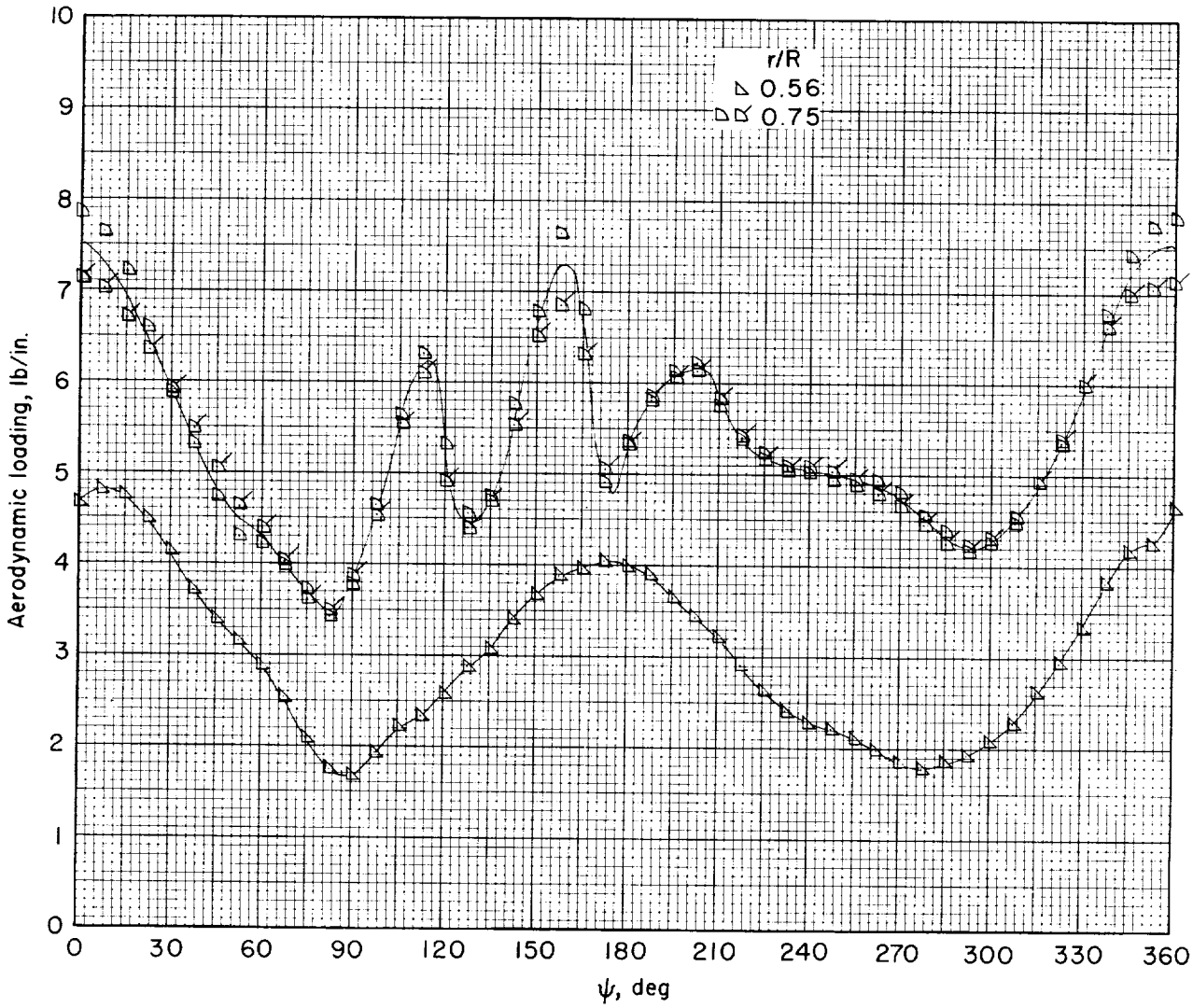

(a) Concluded.

Figure 10.- Continued.

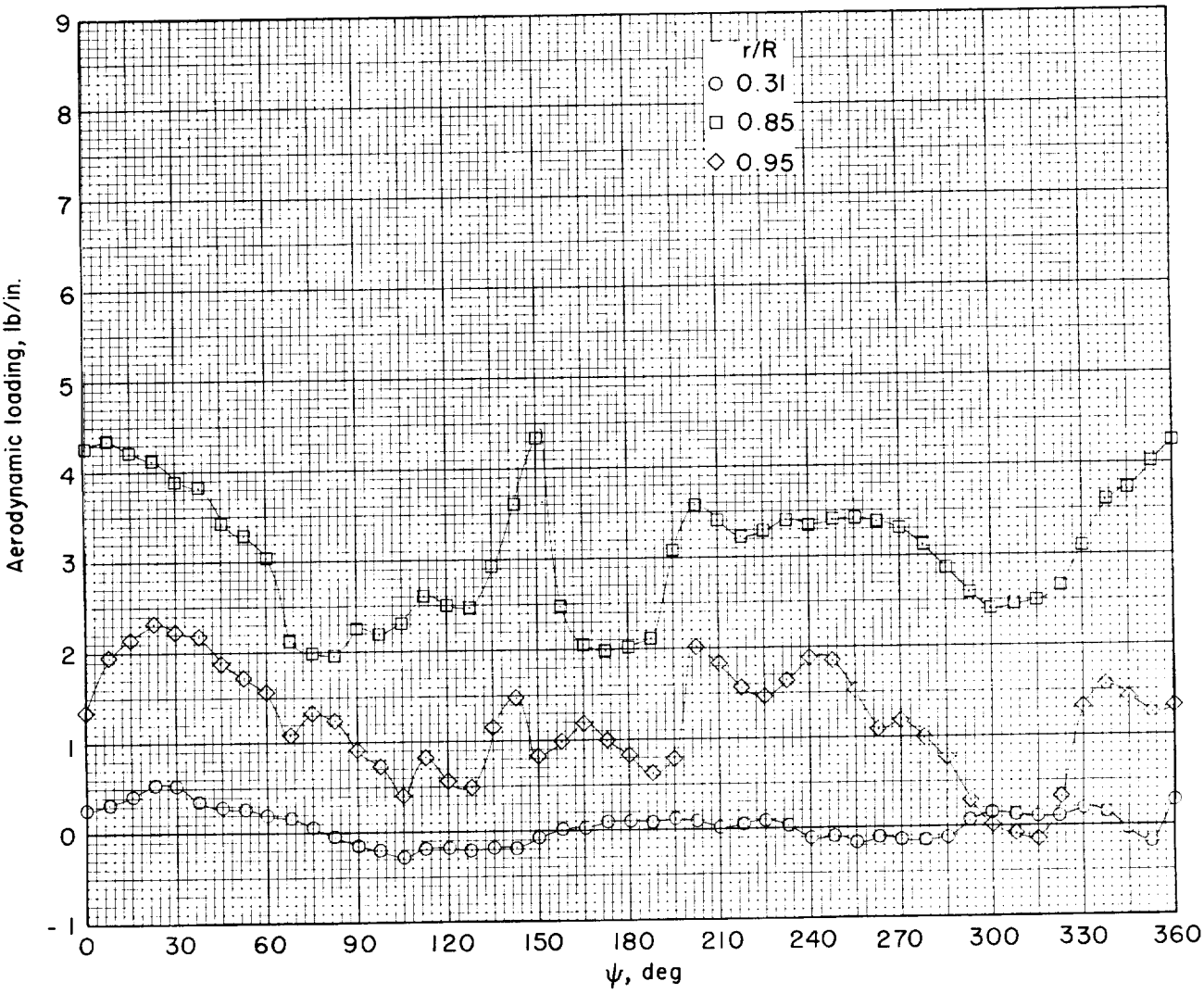

(b) Disk loading = 3 lb/sq ft; L_O = 100.5 lb.

Figure 10.- Continued.

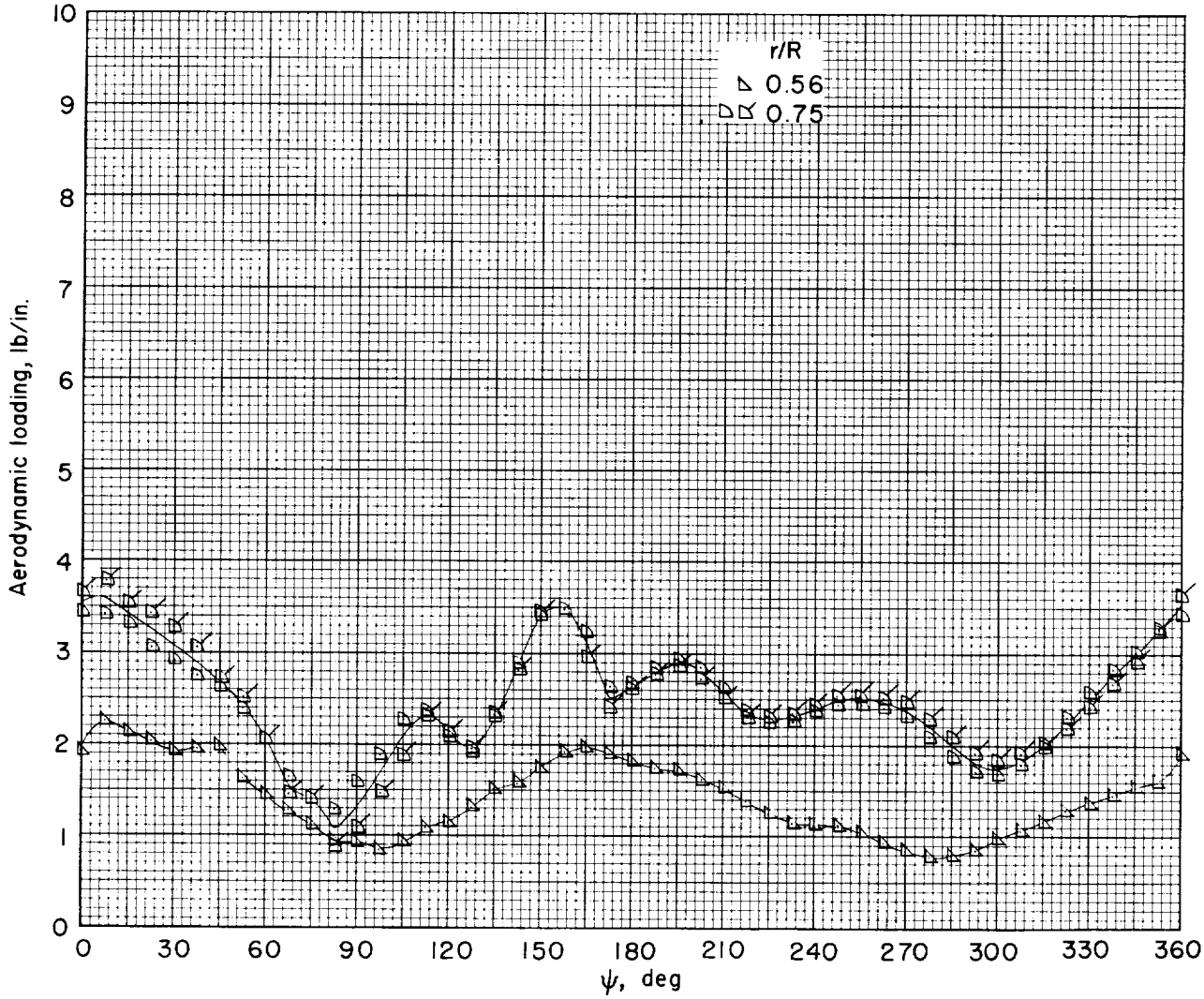

(b) Concluded.

Figure 10.- Continued.

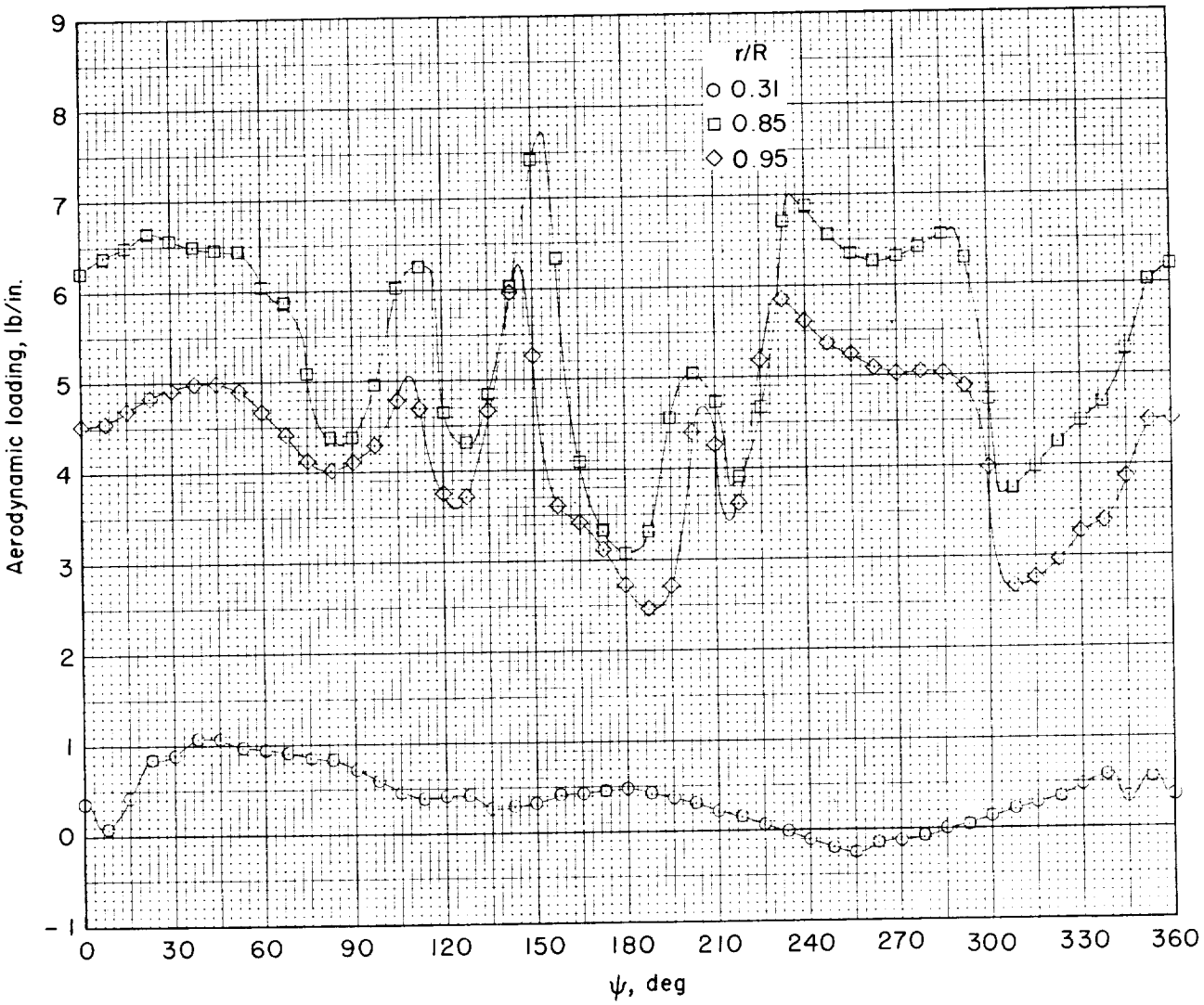

(c) Yaw angle = 10°; L_0 = 192.3 lb.

Figure 10.- Continued.

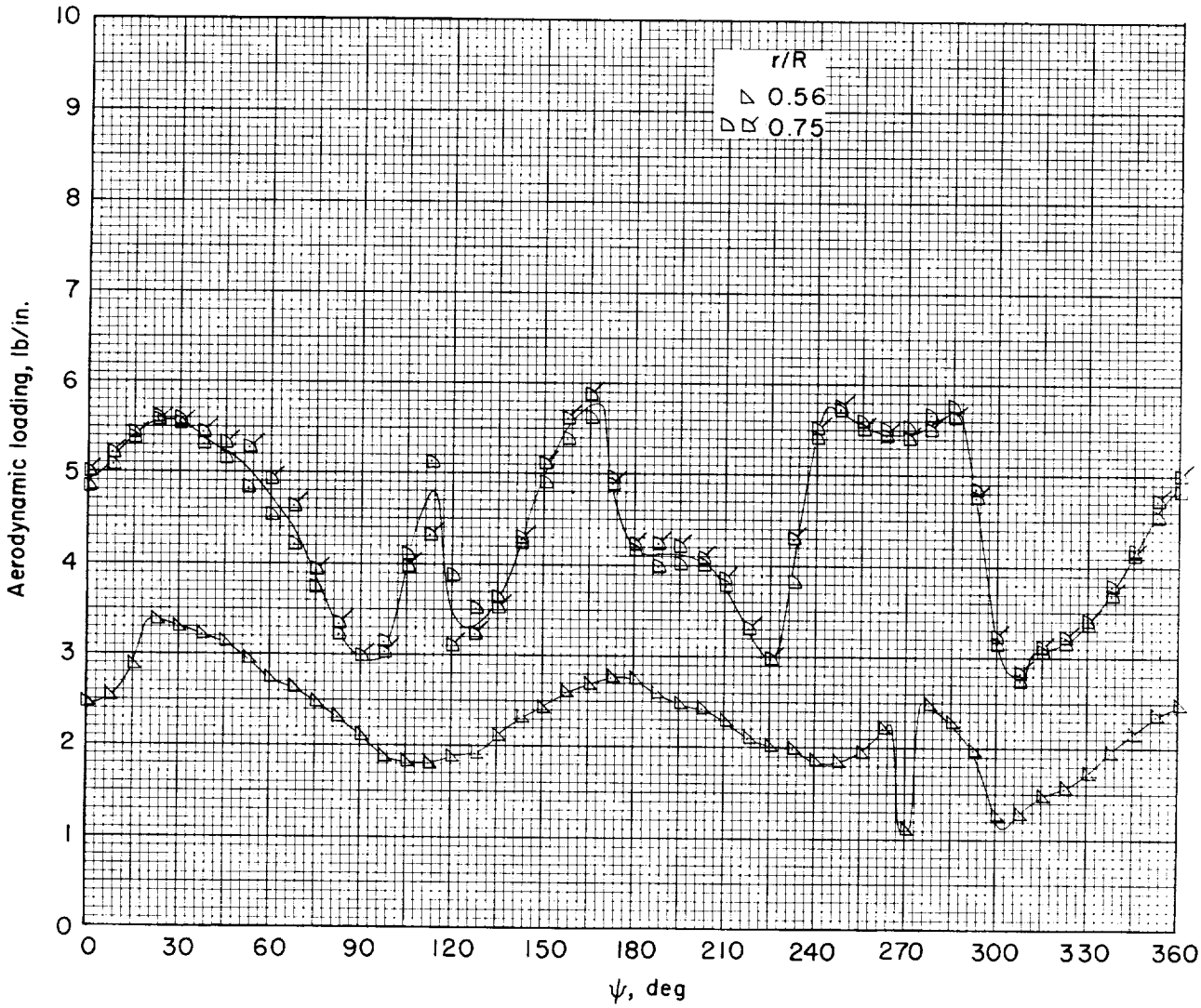

(c) Concluded.

Figure 10.- Concluded.

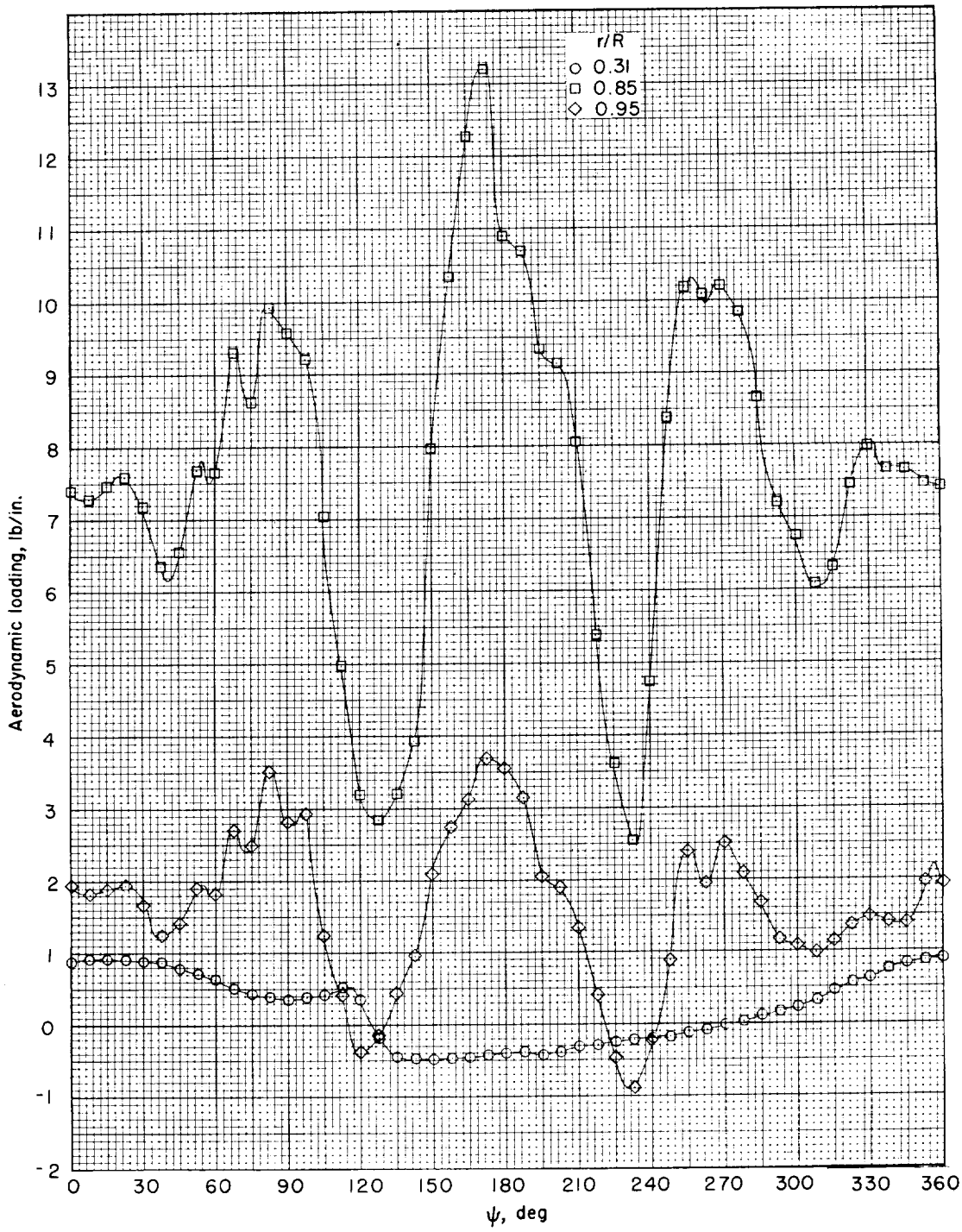

(a) $\mu = 0.075$.

Figure 11.- Variation of section aerodynamic loading with azimuth at various spanwise stations for rear rotor of overlapped rotor system. x/R = 1.23.

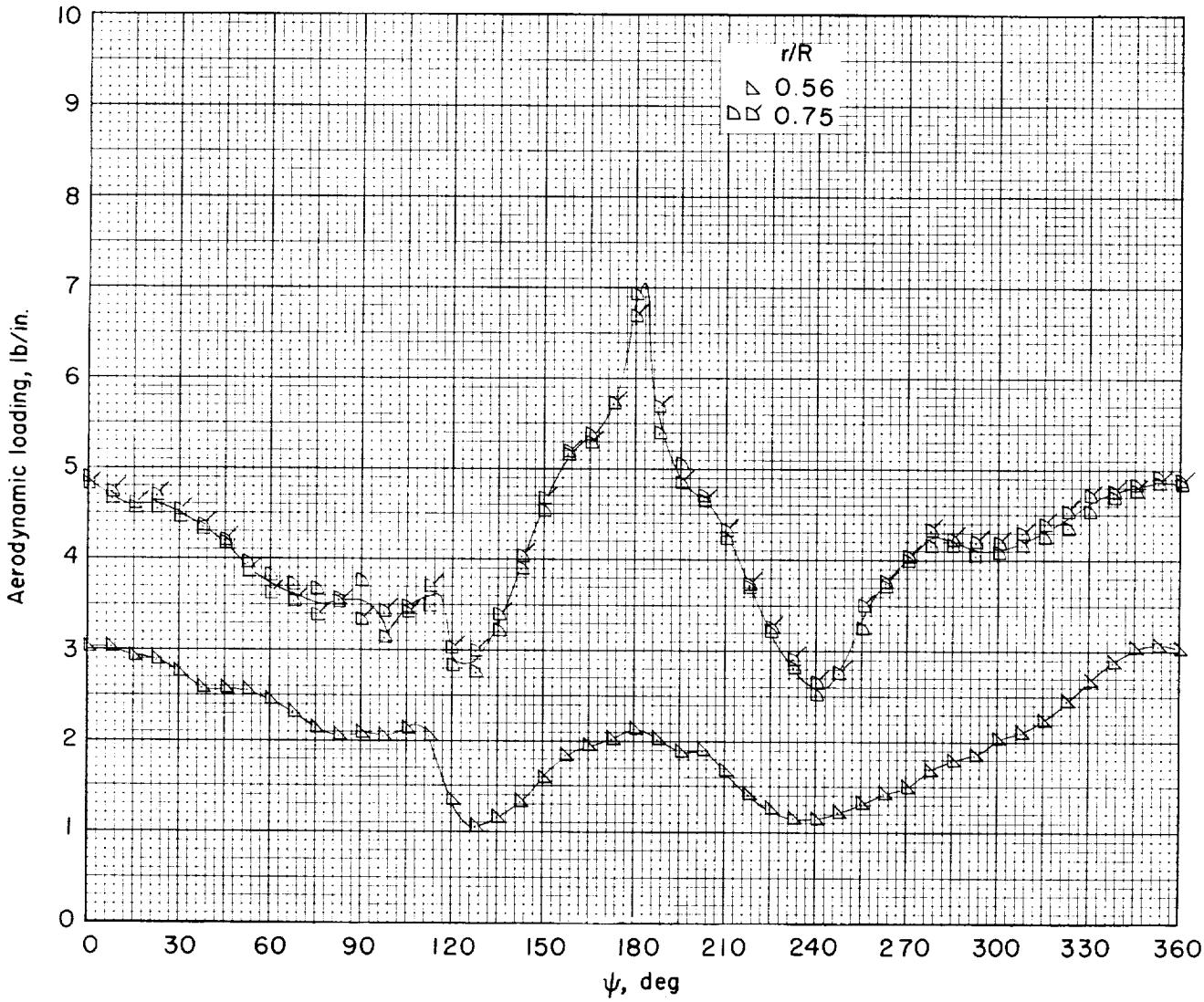

(a) Concluded.

Figure 11.- Continued.

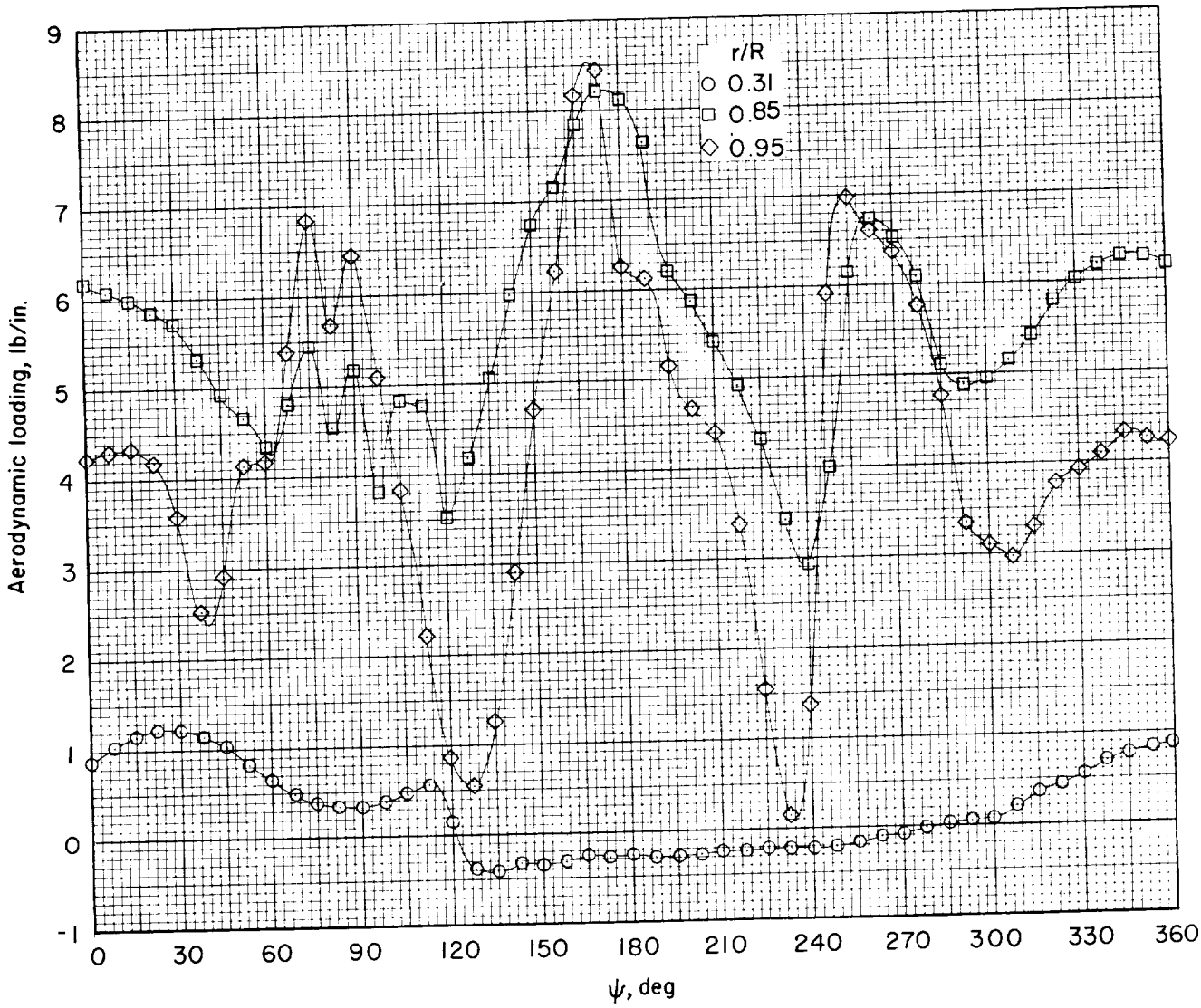

(b) $\mu = 0.10$.

Figure 11.- Continued.

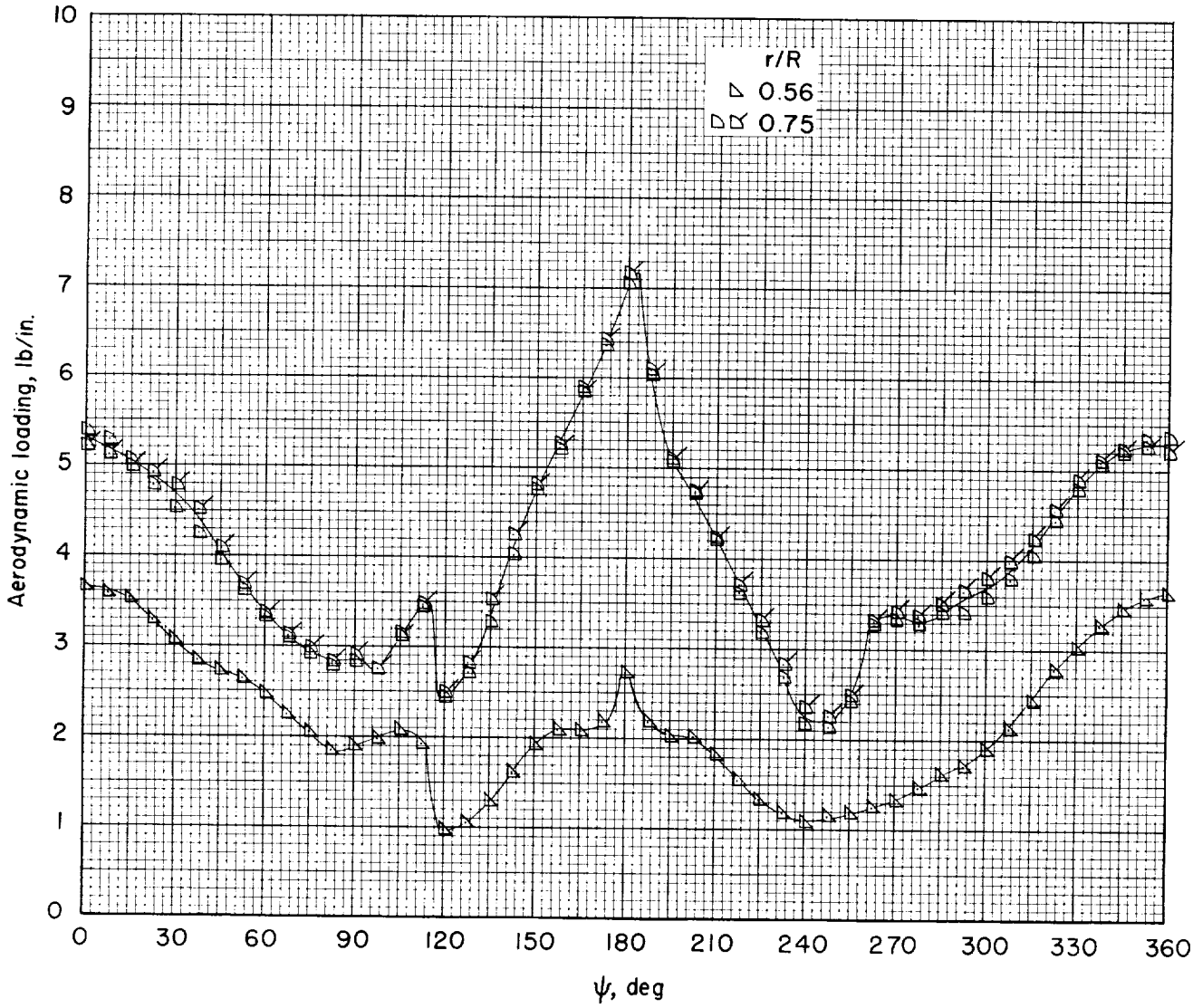

(b) Concluded.

Figure 11.- Continued.

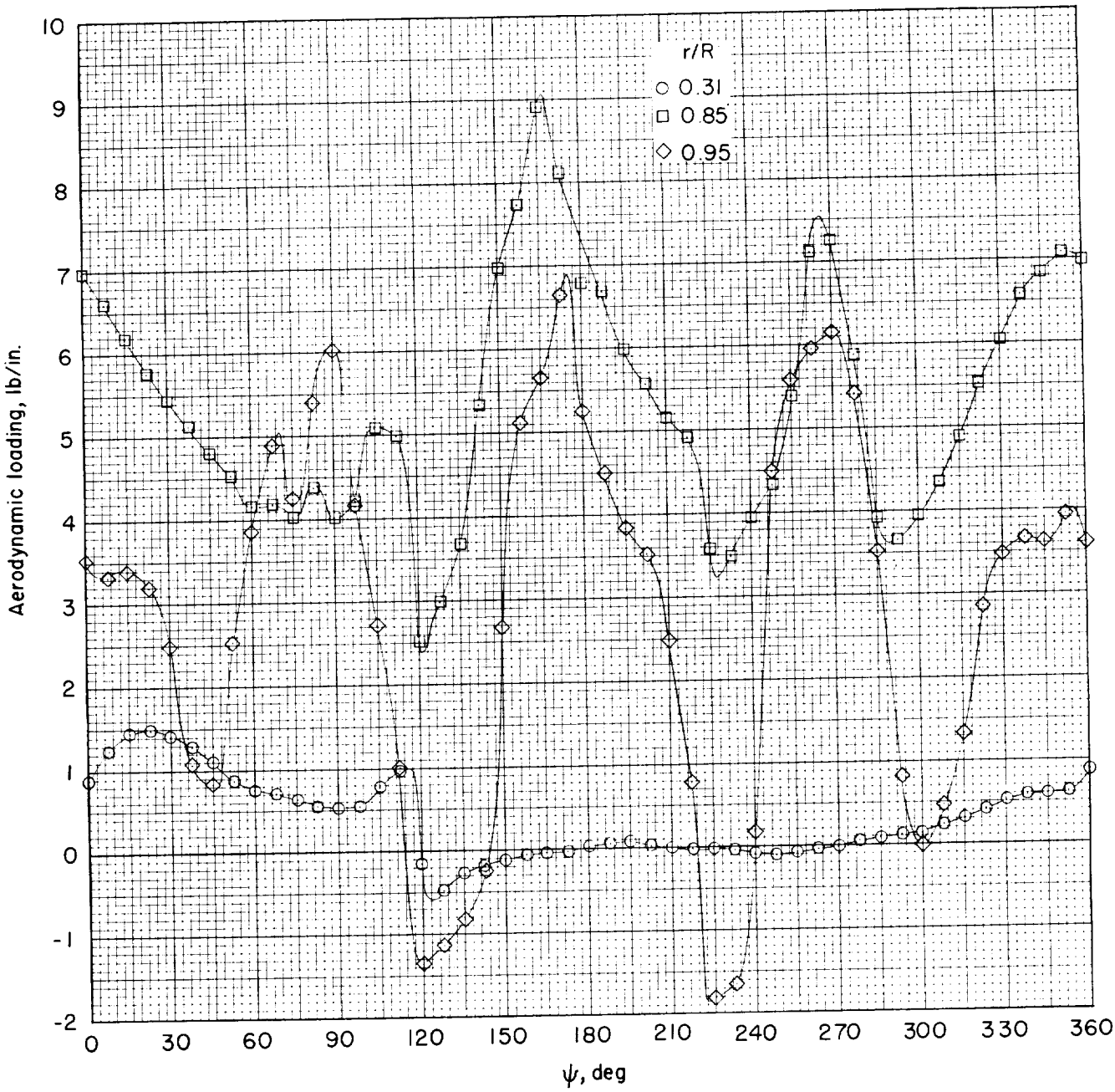

(c) $\mu = 0.14$.

Figure 11.- Continued.

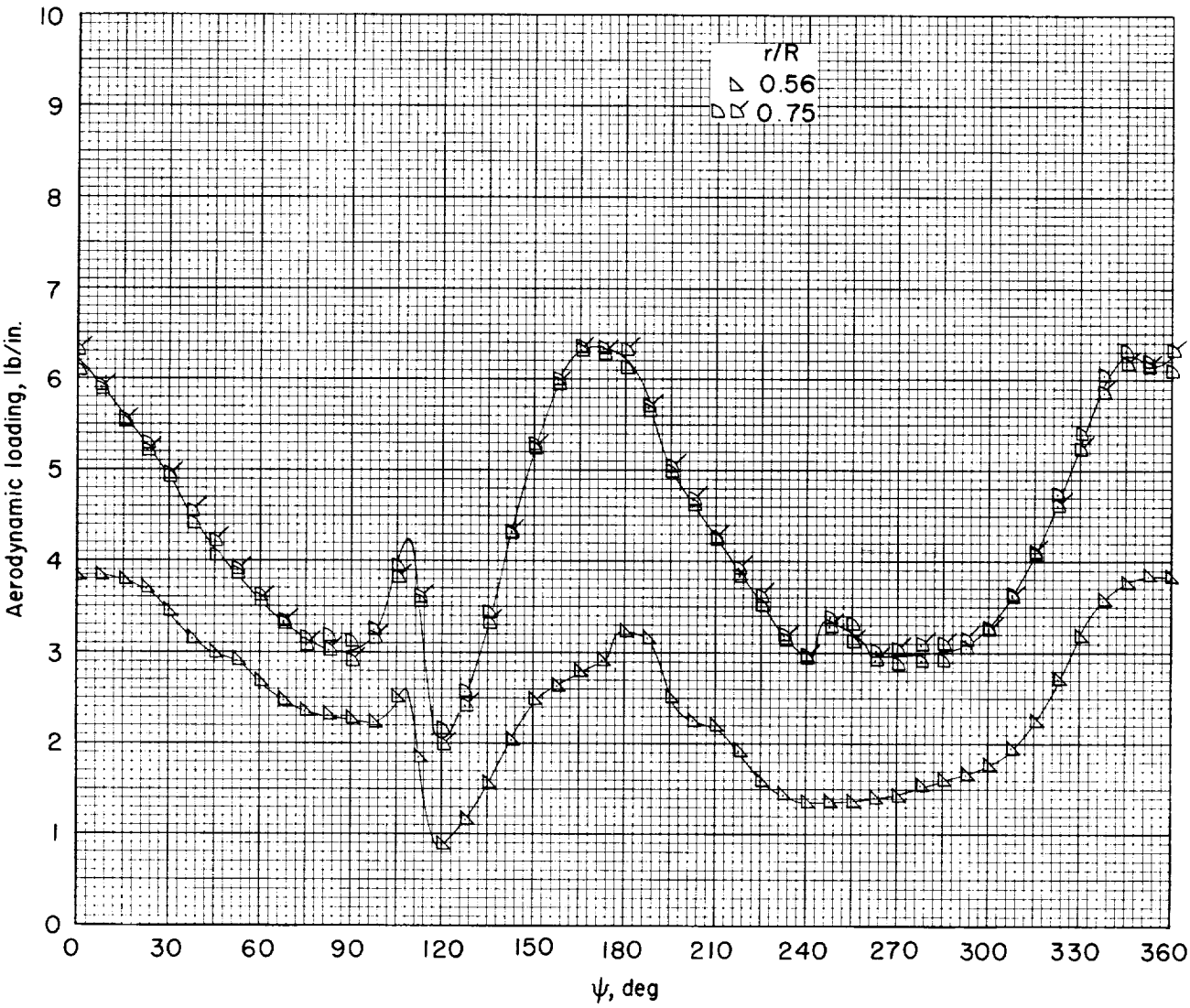

(c) Concluded.

Figure 11.- Continued.

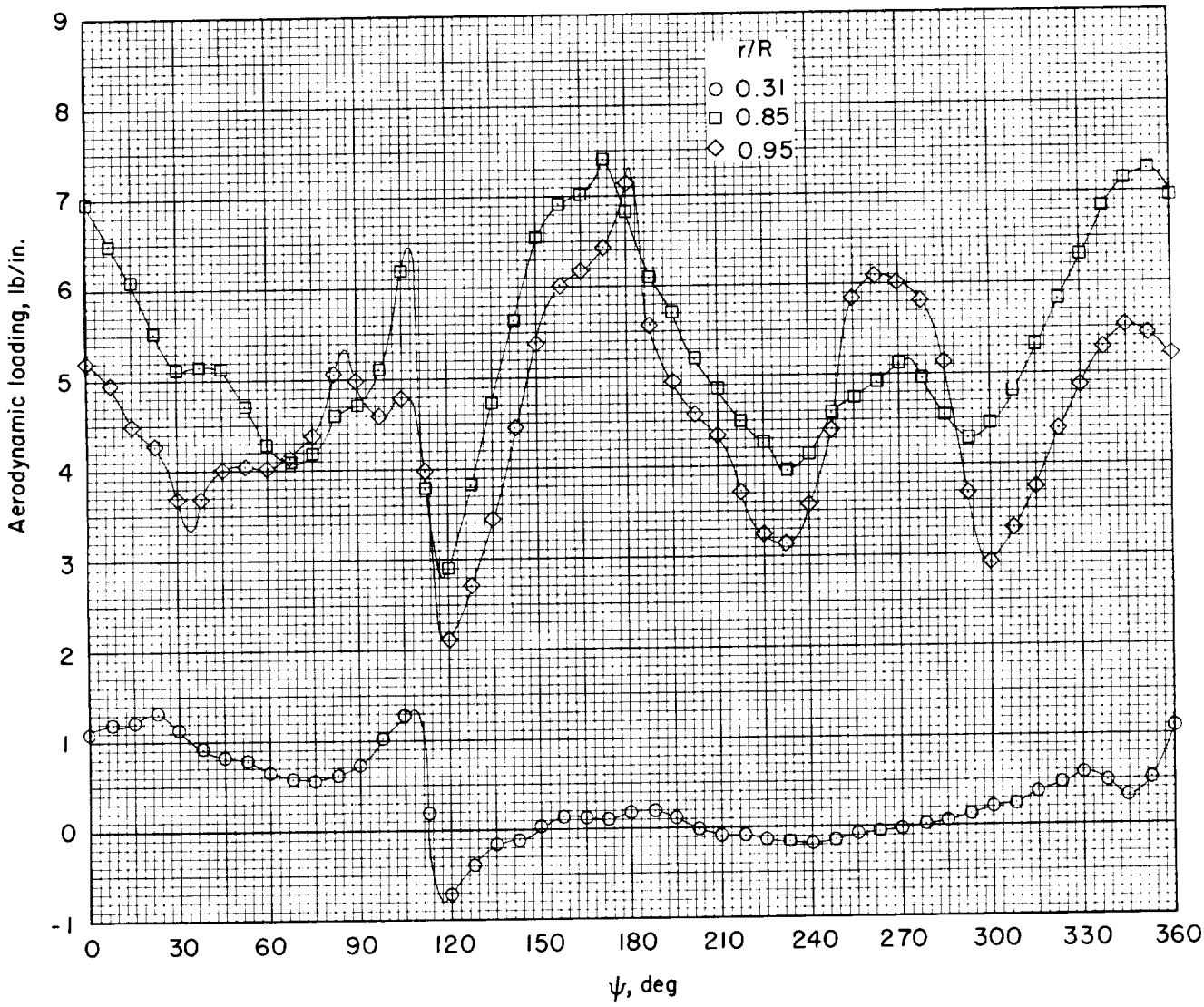

(d) $\mu = 0.19$.

Figure 11.- Continued.

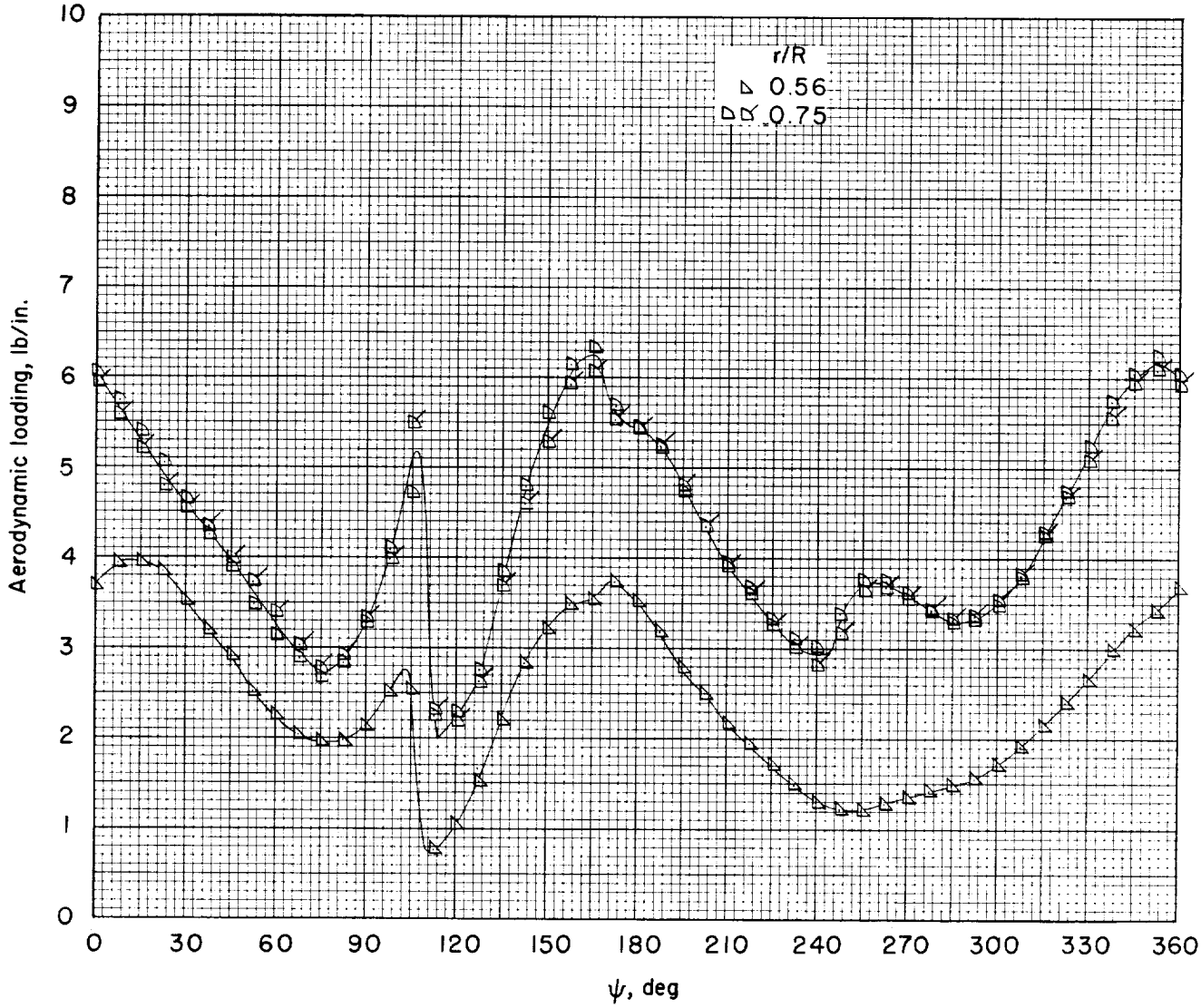

(d) Concluded.

Figure 11.- Continued.

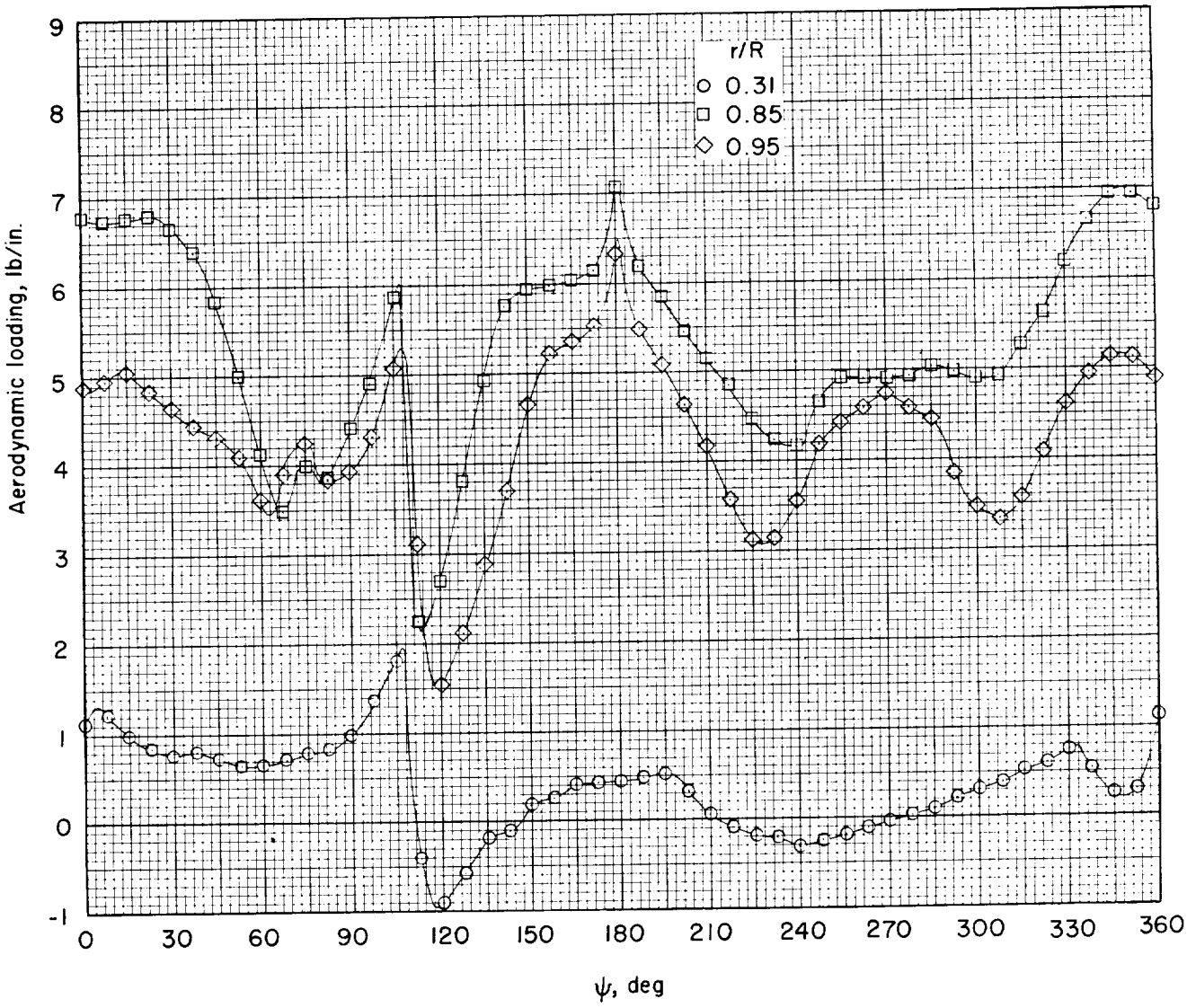

(e) $\mu = 0.24$.

Figure 11.- Continued.

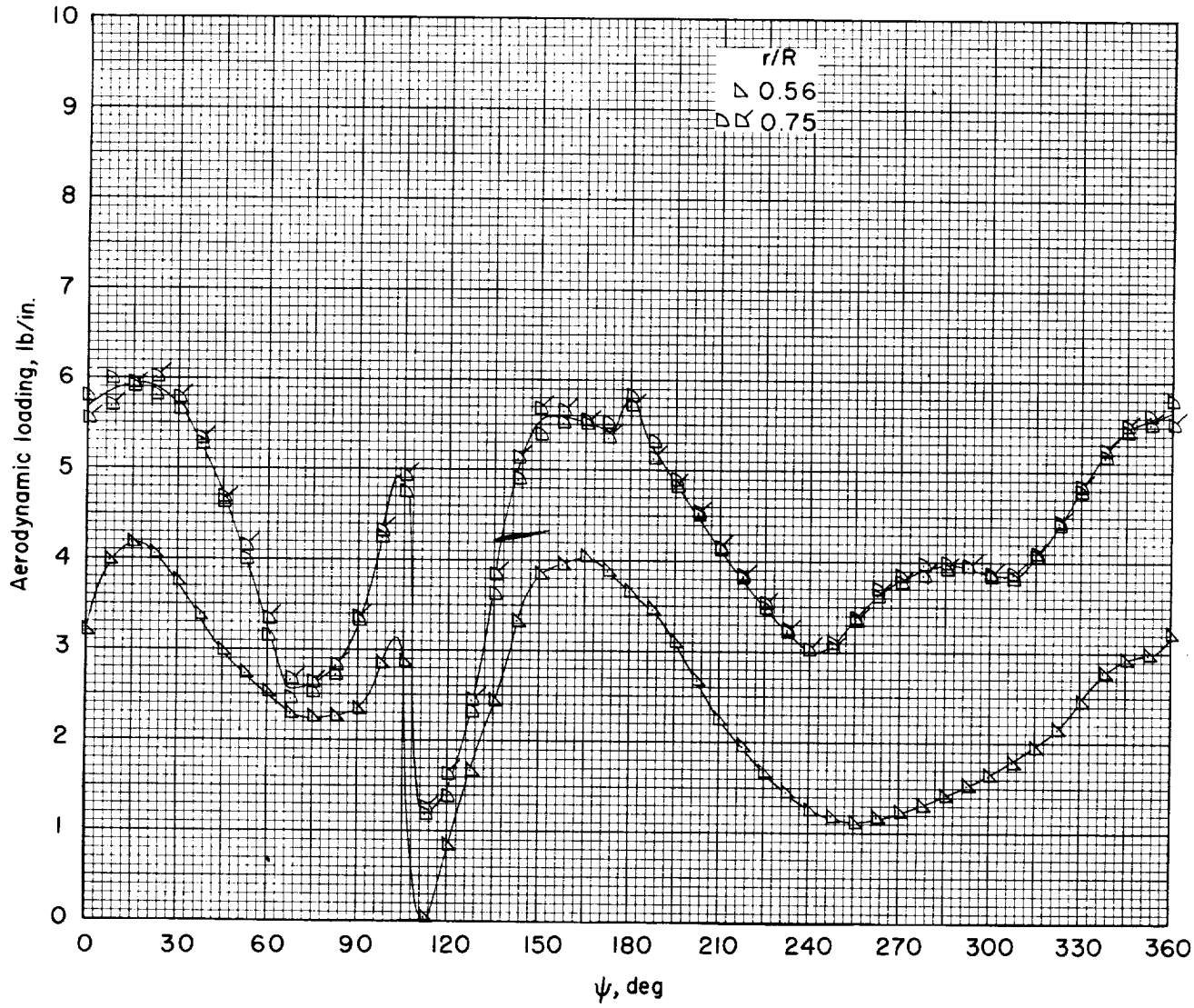

(e) Concluded.

Figure 11.- Continued.

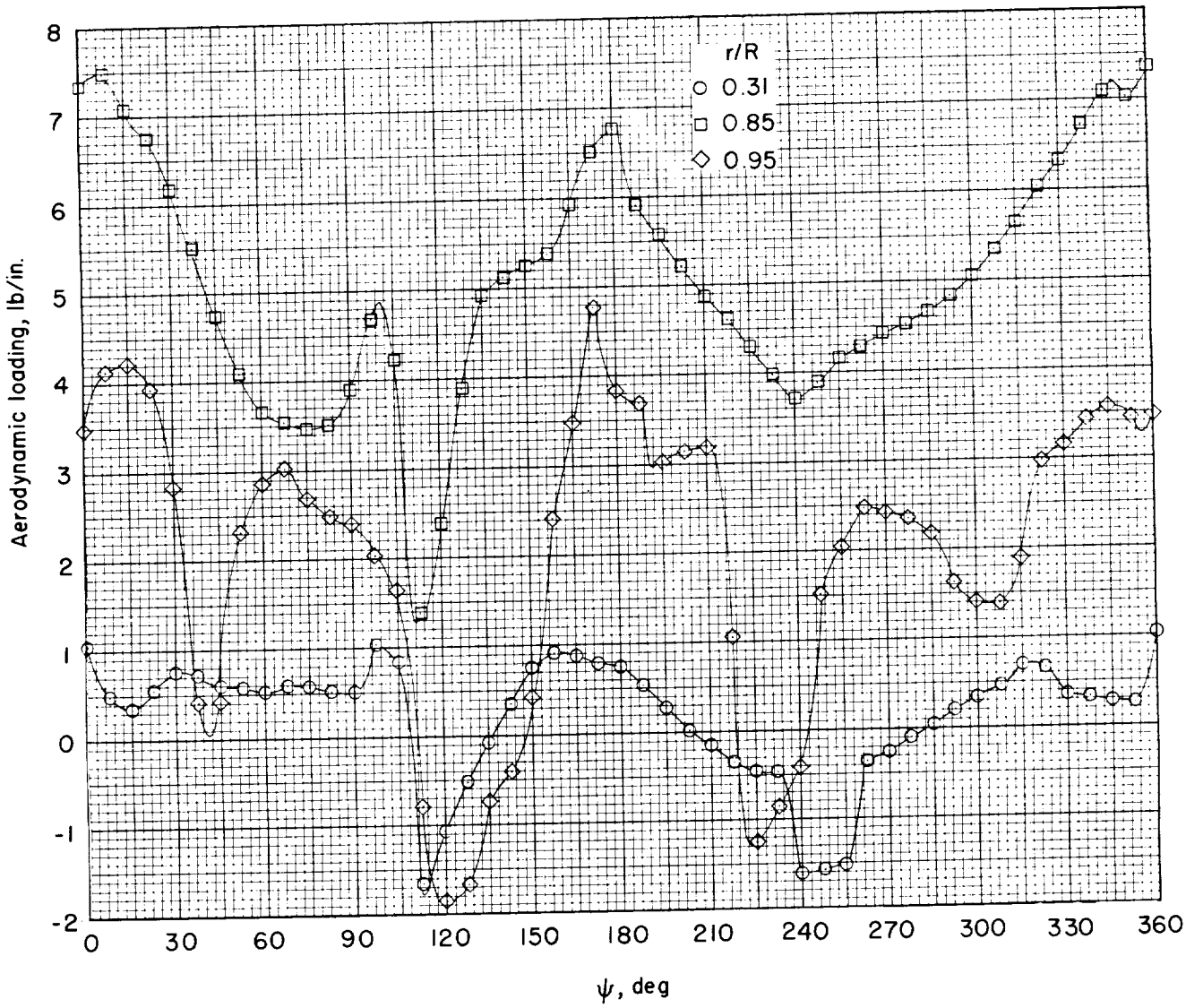

(f) $\mu = 0.28$.

Figure 11.- Continued.

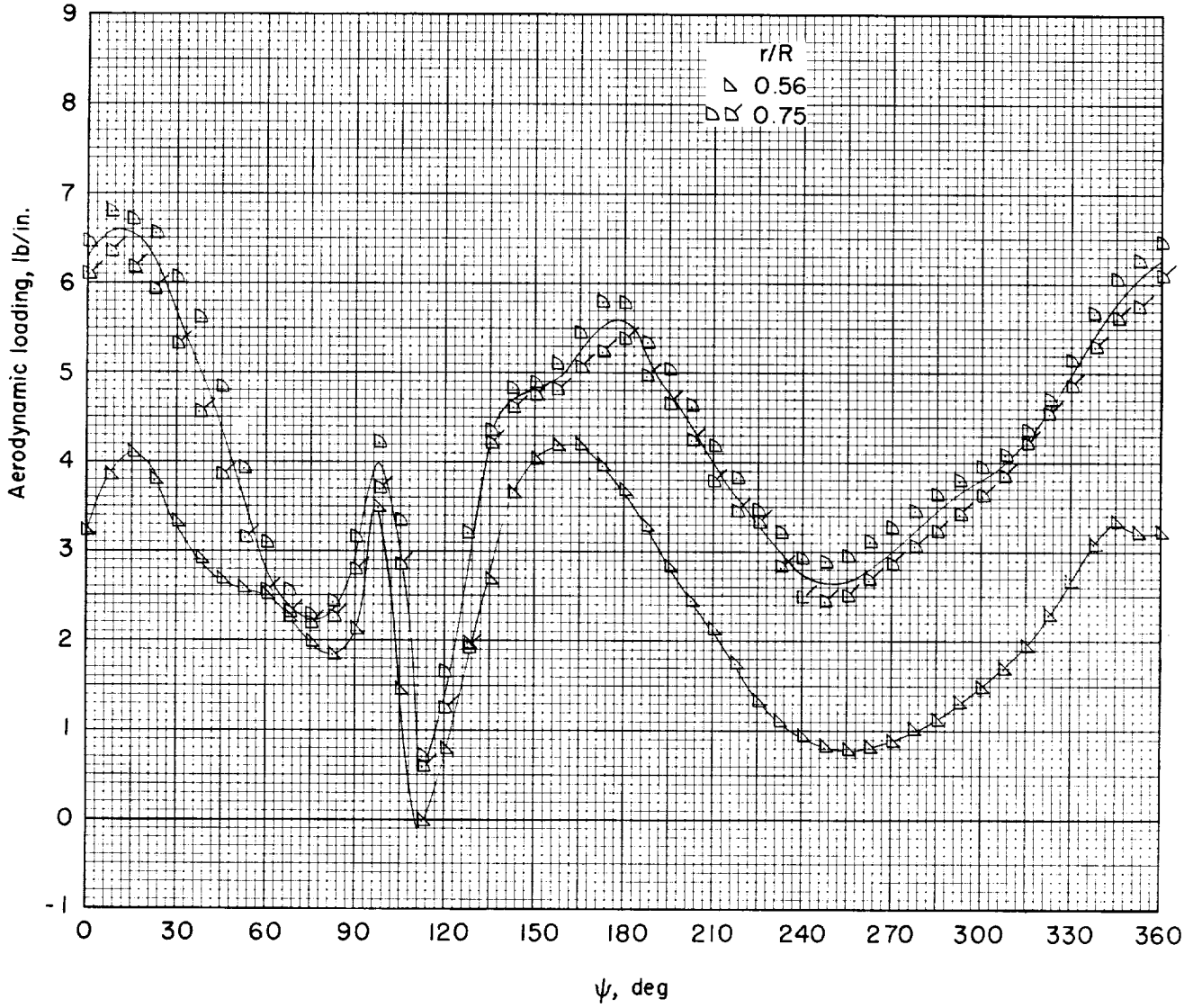

(f) Concluded.

Figure 11.- Concluded.

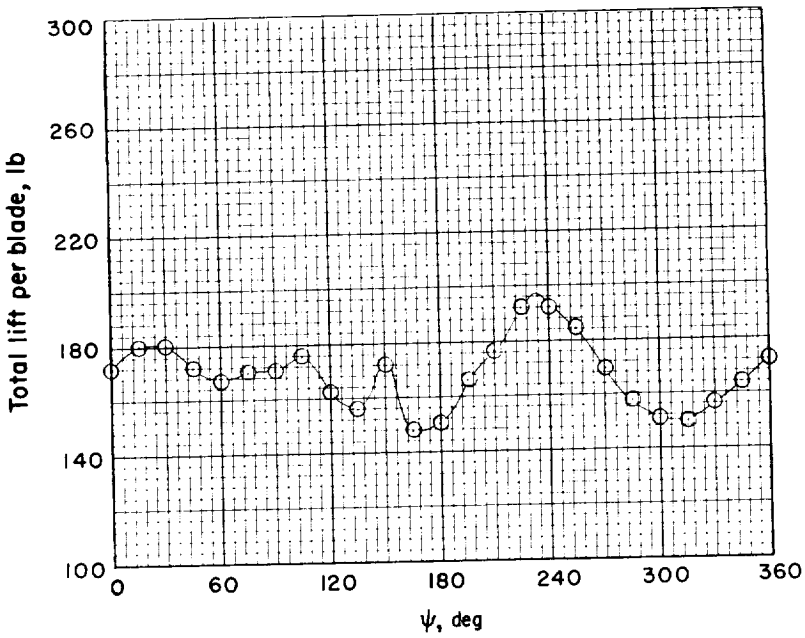

(a) L_0 = 168.4 lb.

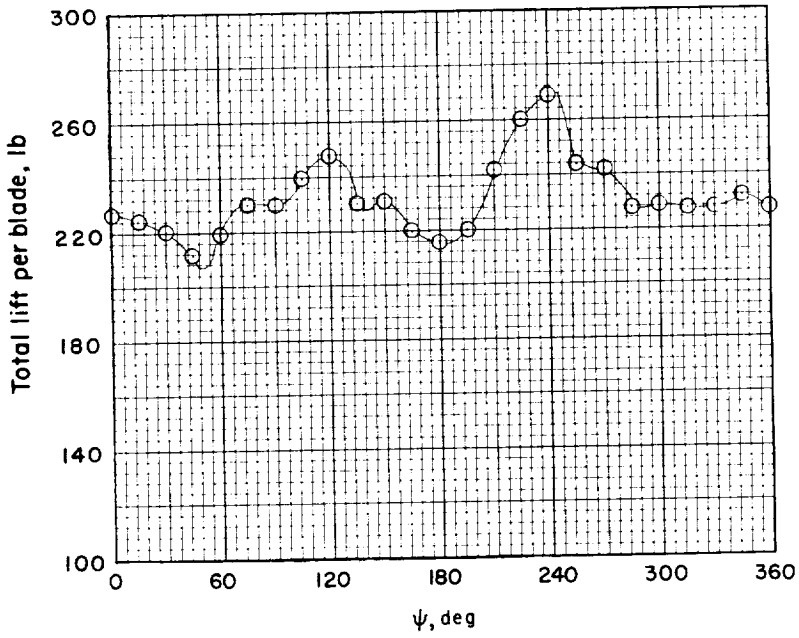

(b) L_0 = 232.0 lb.

Figure 12.- Variation of total blade lift with azimuth for rear rotor of nonoverlapped rotor system in hovering. x/R = 2.03.

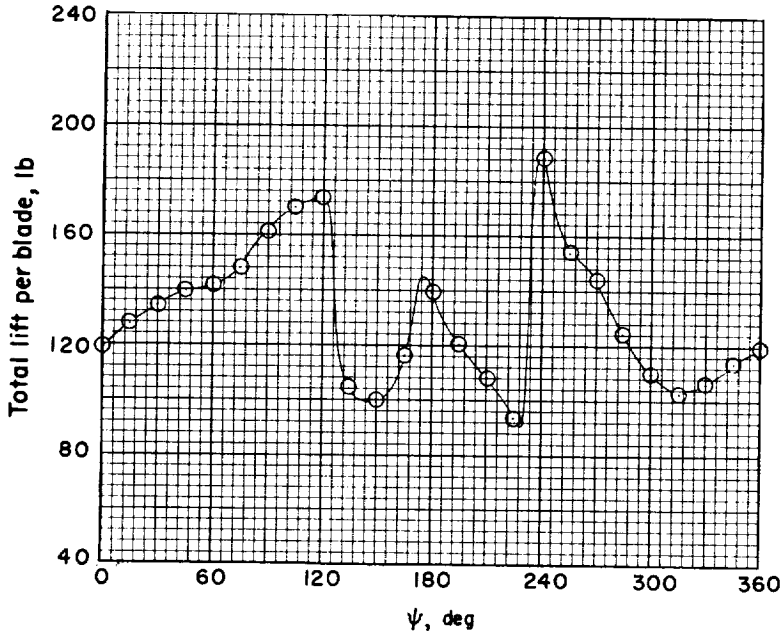

(a) L_0 = 131.2 lb.

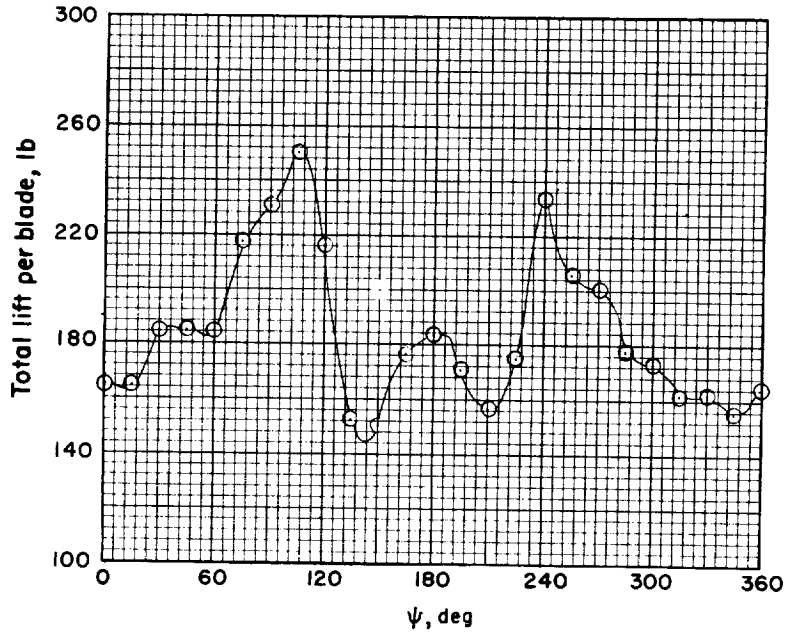

(b) L_0 = 185.1 lb.

Figure 13.- Variation of total blade lift with azimuth for rear rotor of overlapped rotor system in hovering. x/R = 1.23.

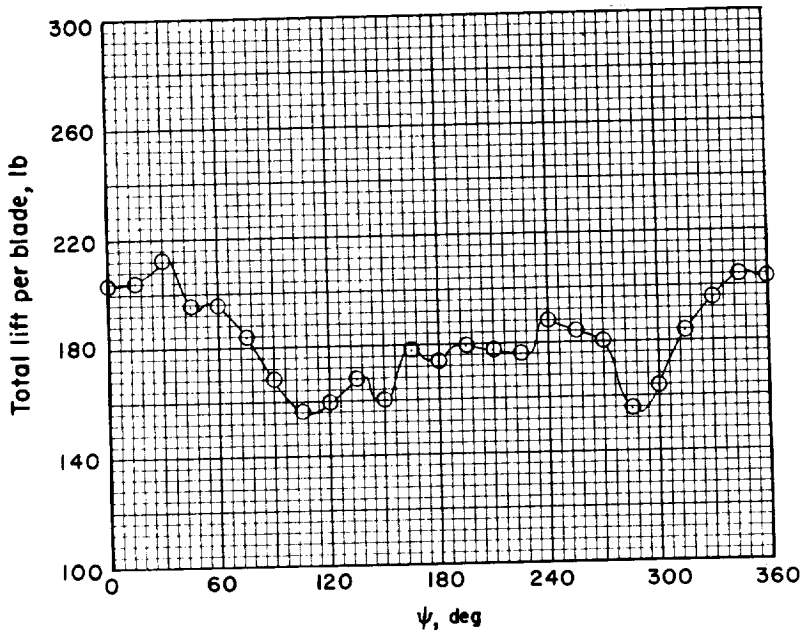

(a) $\mu = 0.075$.

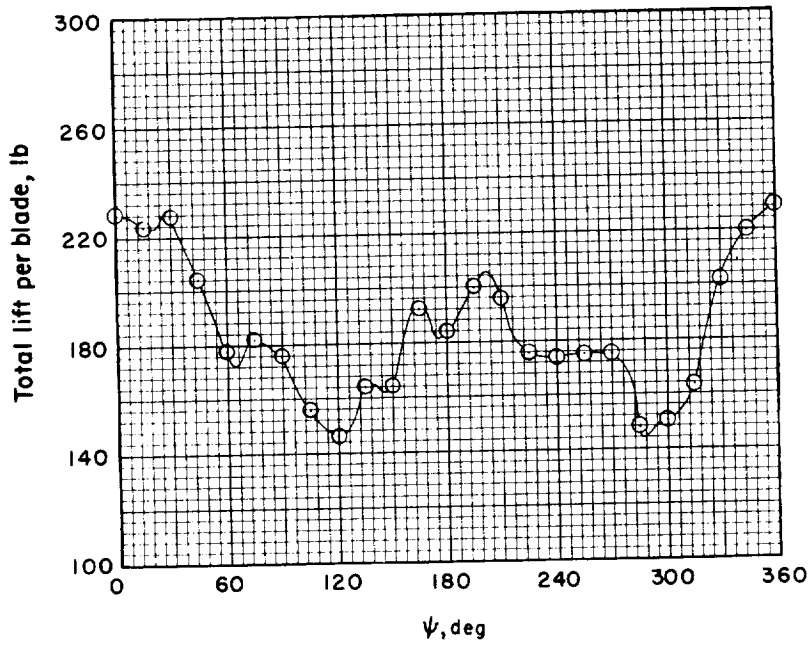

(b) $\mu = 0.10$.

Figure 14.- Variation of total blade lift with azimuth for rear rotor of nonoverlapped rotor system. $x/R = 2.03$.

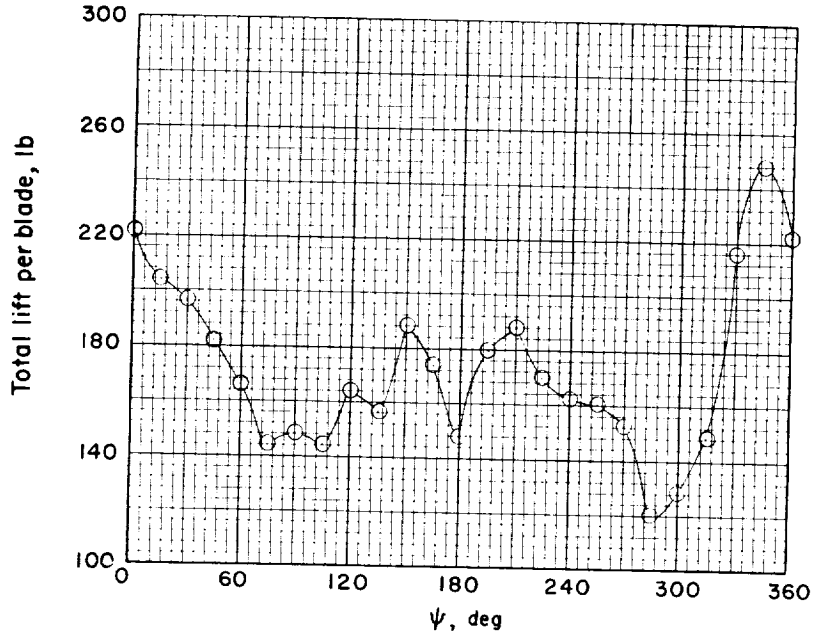

(c) $\mu = 0.14$.

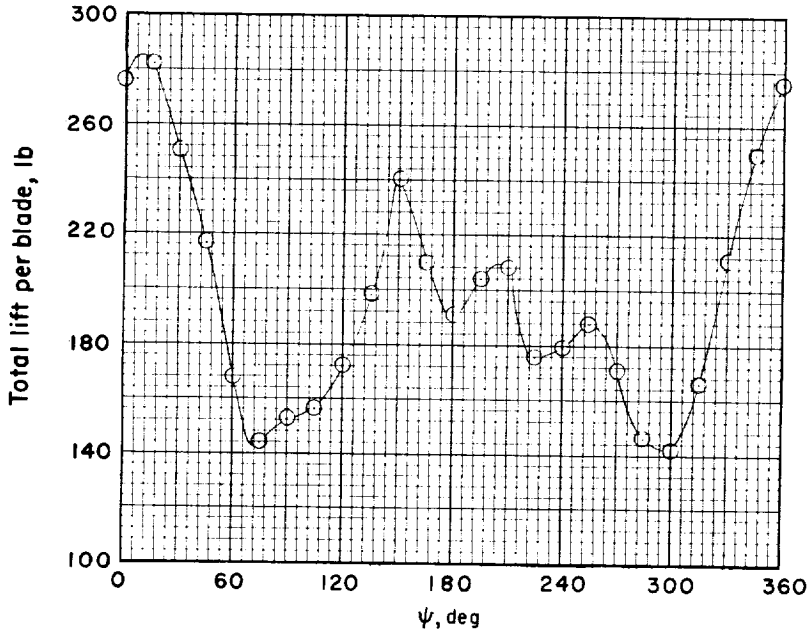

(d) $\mu = 0.19$.

Figure 14.- Continued.

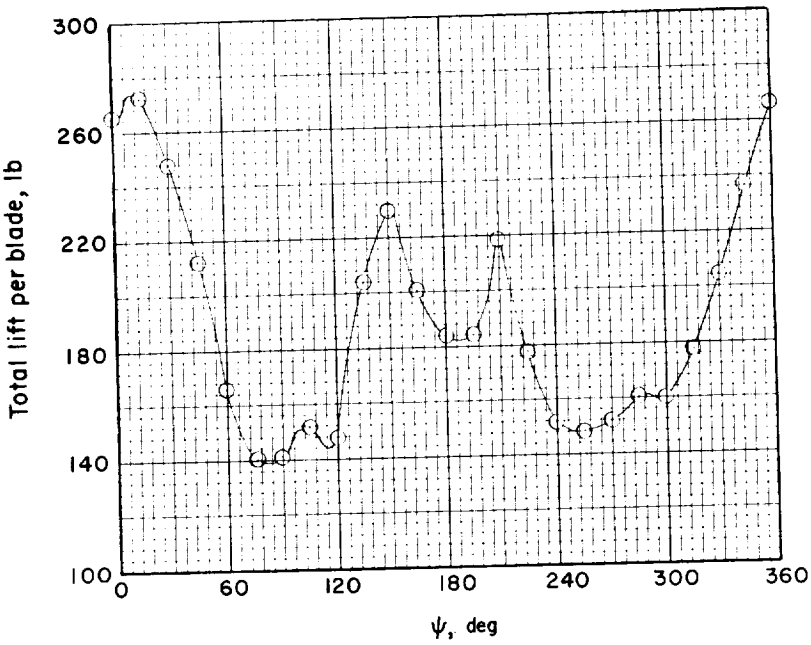

(e) $\mu = 0.24$.

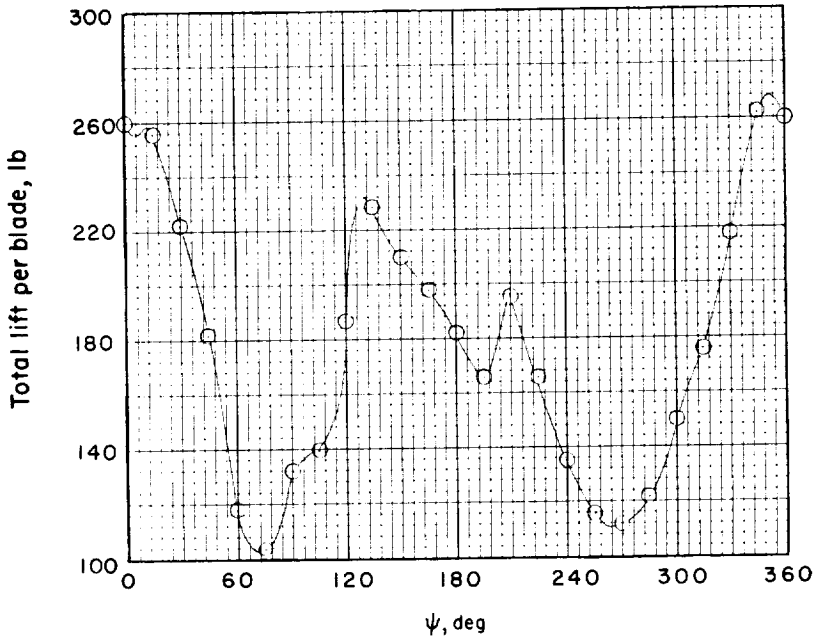

(f) $\mu = 0.28$.

Figure 14.- Concluded.

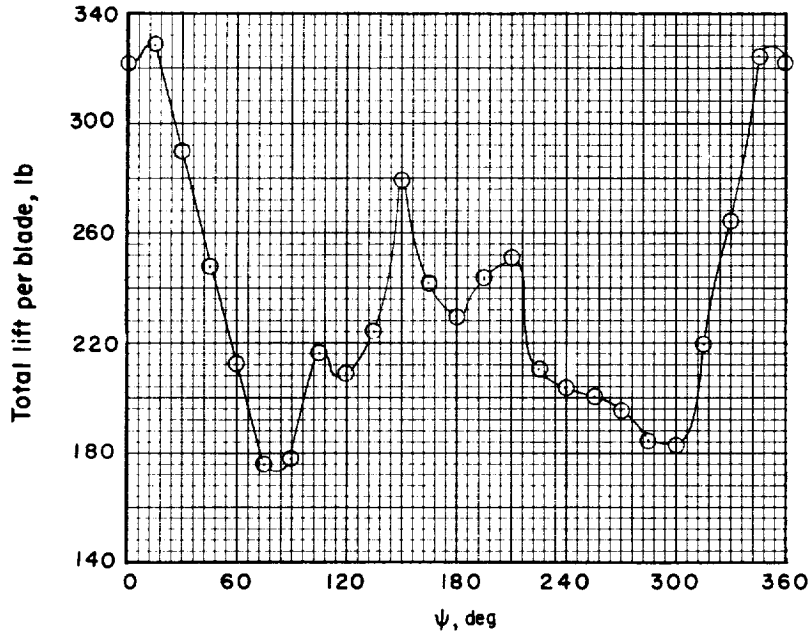

(a) Disk loading = 6 lb/sq ft; L_0 = 234.9 lb.

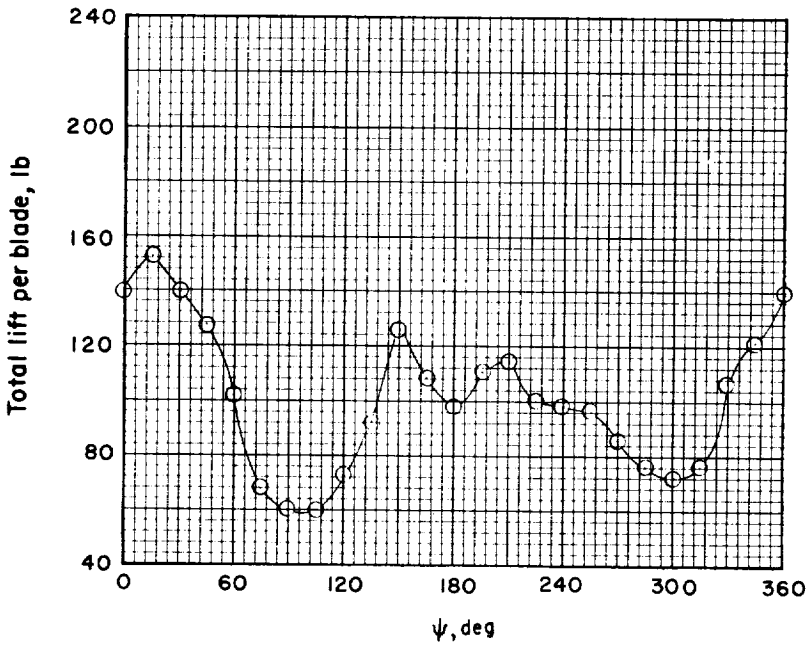

(b) Disk loading = 3 lb/sq ft; L_0 = 100.5 lb.

Figure 15.- Variation of total blade lift with azimuth for rear rotor of nonoverlapped rotor system for special conditions. μ = 0.19; x/R = 2.03.

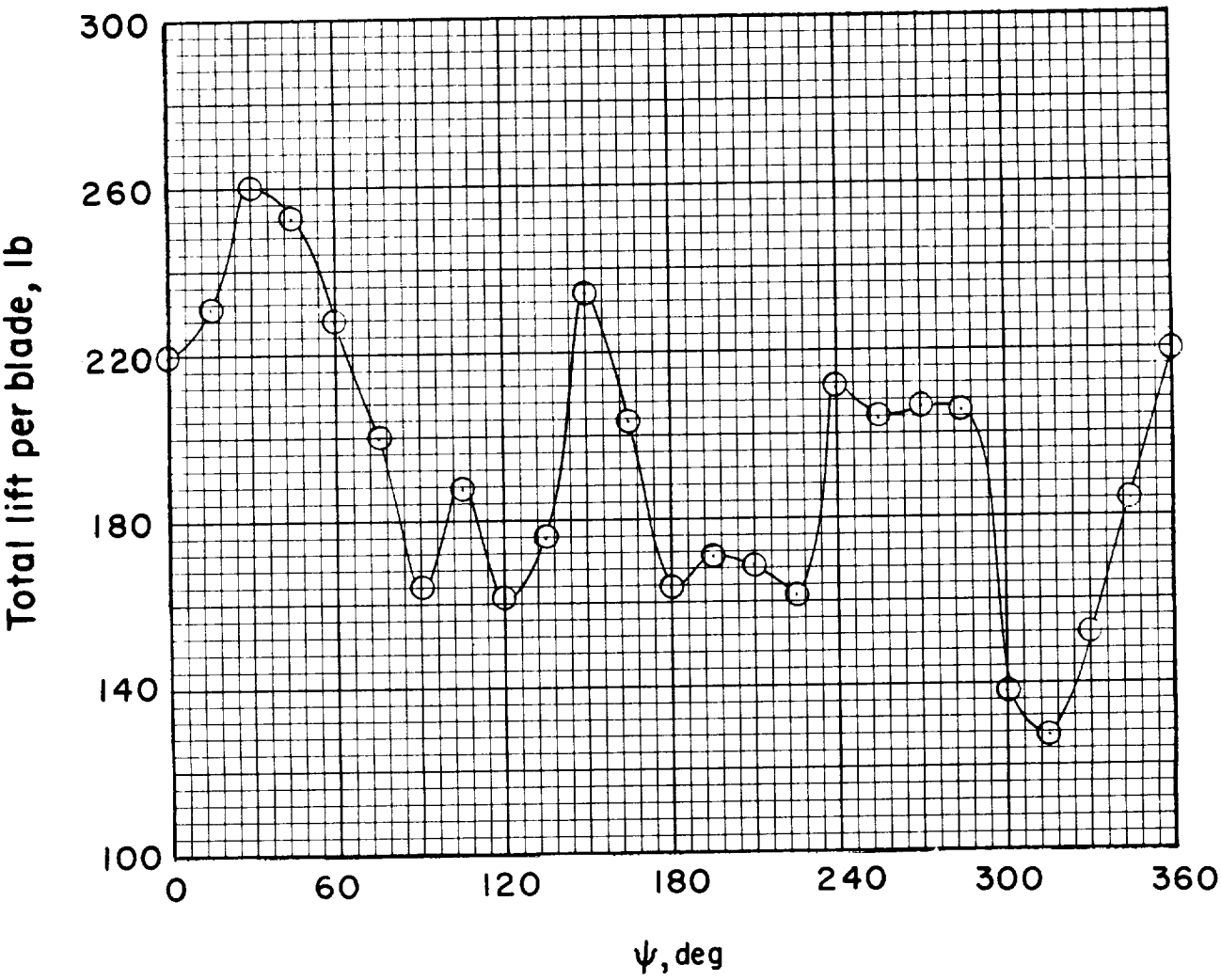

(c) Yaw angle = 10°; L_0 = 192.3 lb.

Figure 15.- Concluded.

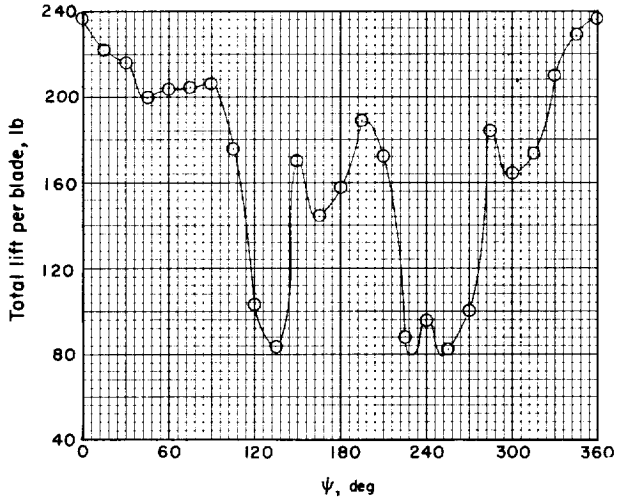

(a) $\mu = 0.075$.

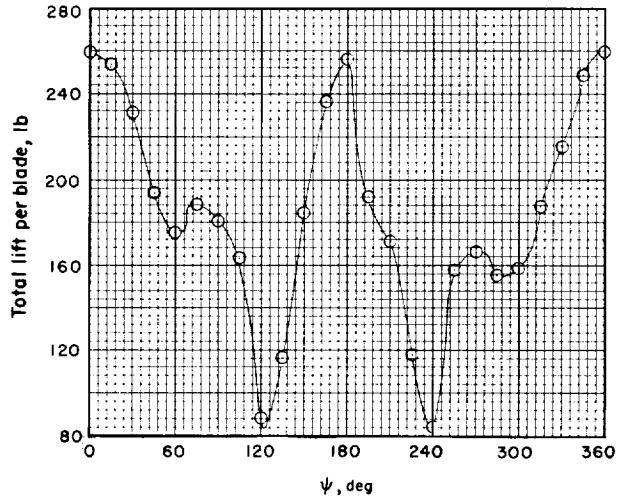

(b) $\mu = 0.10$.

Figure 16.- Variation of total blade lift with azimuth for rear rotor of overlapped rotor system. $x/R = 1.23$.

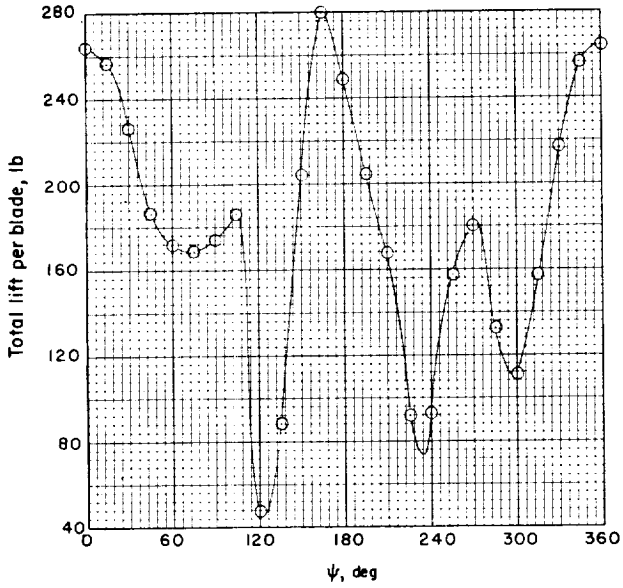

(c) $\mu = 0.14$.

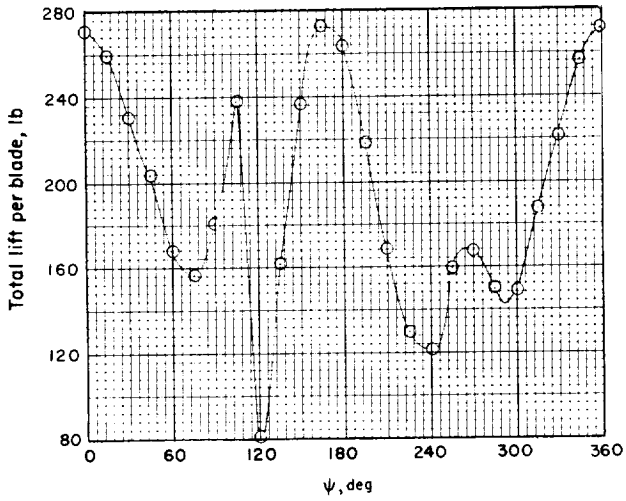

(d) $\mu = 0.19$.

Figure 16.- Continued.

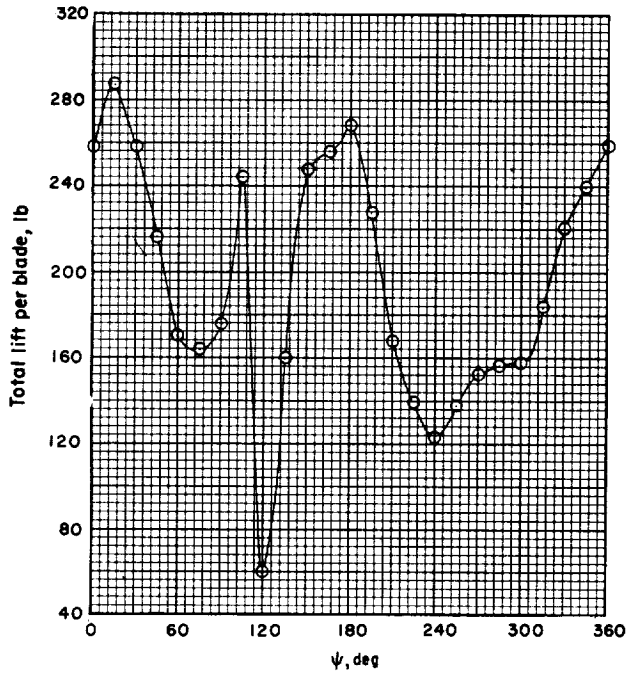

(e) $\mu = 0.24$.

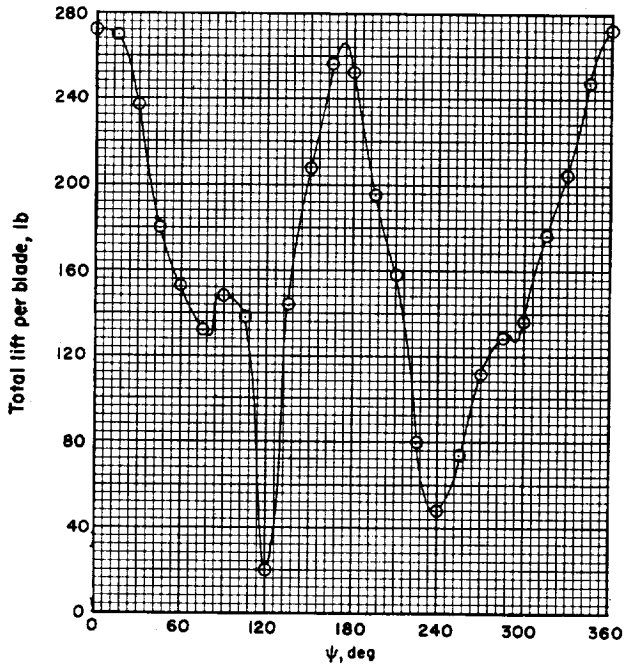

(f) $\mu = 0.28$.

Figure 16.- Concluded.

NASA-Langley, 1963 L-3522